Investigation of Structure-Function-Relationships of Membrane-Anchored Proteins with the Help of Fourier Transform Infrared Attenuated Total Reflection (FTIR ATR) Spectroscopy

DISSERTATION

zur Erlangung des
akademischen Grades

Doktor der Naturwissenschaften

eingereicht von

Mag. Gerald Reiter

Institut für Physikalische Chemie
Fakultät für Naturwissenschaften und Mathematik
der Universität Wien

Wien, Juli 2001

Do not all fix´d Bodies when heated beyond a certain degree, emit Light and shine, and is not this Emission performed by the vibrating Motions of their parts?...
Isaac Newton, *Opicks, or a Treatise of the Reflections, Refractions, Inflections and Colours of Light*, 2nd ed. (1718) Query 8.

An dieser Stelle seien all jene Personen erwähnt, welche die Erstellung dieser Dissertation ermöglicht bzw. gefördert haben. Zuallererst Prof. Urs Peter Fringeli, der mir nicht nur in seinen Vorlesungen, sondern auch in anregenden Diskussionen erste und weiterführende Einblicke in das Gebiet der biophysikalischen Chemie im allgemeinen und in die FTIR ATR-Spektroskopie im speziellen vermittelt hat. Weiters Dr. Dieter Baurecht, der nicht nur mit großem persönlichen Einsatz das Computer-Netzwerk installiert und gewartet, sondern auch bei der computerunterstützten Messdatengewinnung, -verarbeitung und -interpretation maßgeblich geholfen hat. Ich danke auch den anderen Mitgliedern unserer Arbeitsgruppe, die wie die beiden erstgenannten mit ihrer freundlichen Art wesentlich zum angenehmen Arbeitsklima beigetragen und so optimale Arbeitsbedingungen geschaffen haben, unter ihnen Michael „Mike“ Schwarzott und Monira „Mo“ Siam, mit denen mich viele gemeinsame Experimente und fruchtbare Gespräche verbinden. Außerdem sei Prof. Roux, Dr. Angrand und Dr. Bortolato (ICBMC, Universität Claude Bernard, Lyon, Frankreich) für die unermüdliche Unterstützung bei der Isolation der membrangebundenen alkalischen Phosphatase gedankt, sowie als Institutionen dem Österreichischen Austauschdienst (ÖAD), welcher meine Frankreichaufenthalte ermöglicht hat, und der Österreichischen Nationalbank sowie der Universität Wien selbst, die mich mit Forschungsstipendien unterstützt haben.
Ein ganz besonderer Dank gebührt meinen Eltern, die mich während meiner Studienzeit in jeder Hinsicht unterstützten und dem Abschluss dieser Dissertation genauso entgegenfieberten wie ich selbst.

Zusammenfassung

In der vorliegenden Dissertation wurden Struktur-Funktions-Untersuchungen an membrangebundenen Proteinen mit Hilfe von Fourier Transform Infrarot abgeschwächter Totalreflexions (FTIR ATR)-Spektroskopie durchgeführt. Die Proteine wurden auf planaren Modellmembranen immobilisiert, wobei ein Germaniumkristall sowohl als Träger als auch als internes Reflexionselement (IRE) diente. Jeder Präparationsschritt wurde mittels FTIR ATR-Spektroskopie (wenn möglich *in situ*) überwacht und danach eine quantitative Analyse ausgeführt, um die Oberflächenkonzentration und die Orientierung der untersuchten Moleküle zu bestimmen. Die Single Beam Sample Reference (SBSR)-Technik kam zur Anwendung, um eine bessere Hintergrund-Kompensation als bei der konventionellen Einstrahltechnik zu erreichen. Zeitaufgelöste modulierte Anregungs (Modulated Excitation, ME)-Spektroskopie kann die selektive Antwort eines Systems aus einem großen, nicht stimulierten Hintergrundsignal herausfiltern; der temperaturabhängige Übergang α-Helix ↔ β-Faltblatt von Poly-L-Lysin und das temperaturabhängige Falten/Entfalten des Enzyms RNAse A dienten als Beispiele, um die Möglichkeiten dieser Art von Spektroskopie in bezug auf Proteinsysteme aufzuzeigen.

Die Alkalische Phosphatase (AP) gehört zu einer breiten Gruppe von Enzymen (EC 3.1.3.1), welche *in vivo* die unspezifische Hydrolyse von Phosphatmonoestern in alkalischer Umgebung katalysieren. Die Bedeutung der AP in der Pathologie und Klinischen Chemie liegt in der Änderung der Aktivität dieses Enzyms bei manchen Krankheiten begründet. Alkalische Phosphatasen sind Membranproteine, die alle über den Lipidteil eines Glycosylphosphatidylinositol (GPI)-Ankers an die äußere Schicht der Plasmamembran gekoppelt sind. Mit Hilfe der FTIR ATR-Spektroskopie sollte der Effekt dieses Ankers auf die Bindung der AP an Modellmembranen und auf die Aktivität des immobilisierten Enzyms aufgeklärt werden. Nach der Extraktion und Aufreinigung der GPI-AP aus Rinderdarm-Schleimhaut und einer Dialyse zur Entfernung des bei der Extraktion verwendeten Tensids β-Oktylglukosid (β-OG) wurde die Wechselwirkung dieses Enzyms mit zwei Modellmembran-Systemen spektroskopisch untersucht. Erstens mit einem Langmuir-Blodgett(LB)-Film aus Dipalmitoylphosphatidsäure (DPPA), gefolgt von der Adsorption von Palmitoyl-Oleoyl-Phosphatidylcholin (POPC) an das GPI-AP/DPPA-System, um eine Doppelschicht-ähnliche Struktur zu schaffen. Zweitens mit einem DPPA/POPC-Bilayer mit DPPA als innerer und POPC als äußerer Schicht. Das Enzym adsorbierte ziemlich langsam (die Sättigung erfolgte innerhalb von 8 Stunden), was die Abwesenheit von begünstigenden elektrostatischen Wechselwirkungen wie bei der mitochondrialen Creatinkinase anzeigt. Die für das immobilisierte Enzym abgeschätzte Belegungsdichte war ca. 45% im Falle der Adsorption an DPPA und ca. 5% im Falle der Adsorption an die DPPA/POPC-Doppelschicht; dies zeigt, dass die äußere POPC-Schicht die An- bzw. Einlagerung des Enzyms in den Bilayer stark behindert. Die Immobilisate waren in jedem Experiment zumindest drei Tage lang gleichbleibend katalytisch aktiv. Dieselben Untersuchungen wurden auch mit der entsprechenden, kommerziell erhältlichen AP *ohne Anker* aus Rinderdarm-Schleimhaut durchgeführt, was zu denselben Ergebnissen führte. Dies lässt

darauf schließen, dass der GPI-Anker keinen Einfluss auf die Wechselwirkung der AP mit den untersuchten Lipid-Modellmembranen ausübt. Diese Fakten wurden mit den Resultaten einer Studie verglichen, welche die Bindung der Alkalischen Phosphatase an POPC-Liposomen untersuchte und in der die Anzahl der gebundenen Enzym-Moleküle ausschließlich mit Hilfe von Aktivitätsmessungen abgeschätzt wurde: Im Falle der GPI-AP wurde eine Belegungsdichte von ca. 3% bestimmt, was gut mit den 5% beim Adsorptionsversuch mit der DPPA/POPC-Doppelschicht übereinstimmt, aber im Falle der AP ohne Anker wurde im Gegensatz zu den Doppelschicht-Untersuchungen keine Aktivität bei den Liposomen-Experimenten gefunden. Der Grund des Fehlens der Aktivität mag vielfältig sein, und es kann nicht ausgeschlossen werden, dass *inaktives* Enzym an die Liposomen gebunden hat.

In vivo sind mitochondriale Creatinkinasen eine Gruppe von Isoenzymen (EC 2.7.3.2), die sich im Intermembranraum befinden und einen Energiepuffer in Zellen bereitstellen, indem sie die Transphosphorylierung vom Phosphocreatin (PCr) zu ADP katalysieren, wobei ATP erzeugt wird (oder umgekehrt). Mi-CK wurde an negativ geladenen planaren Doppelschichten immobilisiert, die einerseits aus DPPA als innerer und aus Cardiolipinen (CL) als äußerer Schicht mittels LB/Vesikel-Methode, andererseits aus reinem DPPA mittels LB-Methode hergestellt wurden. Die für das immobilisierte Enzym abgeschätzte Belegungsdichte war zumindest 50%. Der beobachtete schnelle Adsorptionsprozess (Sättigung innerhalb von 30 min) beruht größtenteils auf den elektrostatischen Wechselwirkungen zwischen den Lysin- und Arginin-reichen Proteinoberflächen und den negativ geladenen Kopfgruppen des CL oder DPPA. Der H-D-Austausch des immobilisierten Proteins zeigte, dass ca. 30 % der Amid-Protonen für das Lösungsmittel schwer zugänglich sind, was gut mit dem aus Röntgenbeugungsdaten ermittelten α-Helix-Anteil von 33% überstimmt. Schließlich zeigen FTIR ATR-Differenzspektren die Beteiligung der Aminosäuren Arg, Asp, Glu und Tyr von Mi-CK bei der Bindung des Substrates MgADP.

Mit beiden Enzymen, AP und Mi-CK, ist es gelungen, gut definierte und stabile Protein-Lipid-Systeme herzustellen. Die gleichzeitige Anwendung von FTIR ATR-Messungen mit Methoden zur Bestimmung der enzymatischen Aktivität sowie die Anwendung der selektiven ME-Spektroskopie sollten weitere Einblicke in den Wechselwirkungs-mechanismus zwischen verschiedenen Arten von Membranproteinen und ihren Lipidmatrizen liefern.

Abstract

In this study polarized Fourier Transform IR Attenuated Total Reflection (FTIR ATR) spectroscopy was used for investigations of structure-function-relationships of membrane-bound proteins. The proteins have been immobilized on supported model membranes with a germanium trapezoid acting as internal reflection element (IRE) and as solid support. Each preparation step was monitored by FTIR ATR spectroscopy (*in situ*, if possible), and quantitative analysis was carried out in order to determine the surface concentration and the orientation of the molecules of interest. Single beam sample reference (SBSR) technique was used to achieve more stable background compensation than with the conventional single beam technique. Time resolved modulated excitation (ME) spectroscopy is able to detect the selective response of a system separately from a large unstimulated background; as examples, the temperature-dependent α helix to β pleated sheet conversion of poly-L-lysine and the reversible unfolding/folding of RNAse A are given to demonstrate the applicability of this technique to protein systems.

The alkaline phosphatase (AP) belongs to a wide group of enzymes (EC 3.1.3.1) which catalyze *in vivo* the non-specific hydrolysis of phosphate monoesters in an alkaline environment. The significance of AP in pathology and clinical chemistry is due to its disease-related changes in activity. APs are membrane proteins which are all attached to the outer leaflet of the plasma membrane by the lipid moiety of a glycosylphosphatidylinositol (GPI) anchor. The aim was to investigate the effect of this anchor on the enzyme binding to membrane model systems and on the activity of the immobilized enzyme with the help of FTIR ATR spectroscopy. After the extraction and purification of GPI-AP from bovine intestinal mucosa and after dialysis in order to remove the tenside β-octylglucoside used in the preceding steps, the interaction of the enzyme with two model membrane systems was spectroscopically investigated. Firstly, with a dipalmitoylphosphatidic acid (DPPA) Langmuir-Blodgett (LB) layer, followed by adsorbing palmitoyl oleoyl phosphatidylcholine (POPC) to the GPI-AP/DPPA assembly in order to constitute a bilayer-like system. Secondly, with a DPPA/POPC bilayer with DPPA as inner and POPC as outer leaflet. The enzyme adsorption was quite slow (saturation within 8 hours) indicating the absence of enhancing electrostatic interactions as observed with mitochondrial creatine kinase. The density of coverage estimated for the immobilized enzyme was ca. 45% in case of adsorption to DPPA and ca. 5 % in case of adsorption to the DPPA/POPC bilayer showing that the POPC outer layer prevents enzyme binding to a large extent. The immobilisate was catalytically active in each experiment, and the activity was remained for at least three days. The same investigations have also been carried out with the corresponding commercially available AP from bovine intestinal mucosa *without anchor* showing the same results. This indicates that the GPI motif shows no effect on the interaction of alkaline phosphatase with the investigated lipid model membranes. These facts were compared with the results of a binding study of alkaline phosphatase to POPC liposomes where the number of bound enzyme molecules were estimated only with the help of activity measurements: In the case of GPI-AP, a surface coverage of ca. 3 % was estimated being in good accordance with the 5 % in the case of DPPA/POPC bilayer adsorption, but in the case

of anchorless AP, no activity was found in the liposome experiments in contrast to the DPPA/POPC bilayer investigations. This lack of activity remains a point of discussion, but it cannot be excluded that *inactive* enzyme had been attached to the liposomes.

In vivo mitochondrial creatine kinases (Mi-CK) are a group of isoenzymes (EC 2.7.3.2) located in the intermembrane space performing an energy buffering in cells by transphosphorylation from phosphocreatine (PCr) to ADP producing ATP (or vice versa). Mi-CK was immobilized on negatively charged supported bilayers made from DPPA as inner and cardiolipins (CL) as outer leaflet built up by the LB/vesicle method, or made from pure DPPA built up by the LB method. The density of coverage estimated for the immobilized enzyme was found to be at least 50%. The observed fast adsorption process (saturation within about 30 min) is predominantly due to electrostatic interactions between the lysine and arginine rich surfaces of the protein and the negatively charged headgroups of CL or DPPA. The H-D-exchange of immobilized protein showed that about 30% of amide protons are weakly accessible for the solvent being in agreement with 33% α-helices observed by X-ray diffraction. Finally, FTIR ATR difference spectra reveal the involvement of the amino-acids Arg, Asp, Glu and Tyr of Mi-CK in the binding of the substrate MgADP.

With both enzymes, AP and Mi-CK, it was possible to build up well-defined and stable protein-lipid-assemblies. The simultaneous application of FTIR ATR measurements with methods for determining the enzymatic activity and the application of selective ME spectroscopy could give further insights into the mechanism of interactions between different types of membrane proteins and their lipid matrices.

Contents

1 Introduction

1.1 Oriented membrane assemblies

Biological model membranes in the form of planar supported bilayer assemblies are of special interest for attenuated total reflection spectroscopy (ATR), since the internal reflection element (IRE) may act as both, the solid support and the wave guide. This set up enables membrane spectroscopy from the part of the solid support, and simultaneous control of the membrane environment from the opposite part. Moreover, the supported membrane is located in the most intense region of the electric field of the evanescent wave which favors the fraction of light absorbed by the membrane with respect to unwanted absorptions of the background (e.g. buffer solution). Oriented regions of the assembly, which should be expected because of intrinsic ordering of lipid bilayers, may be detected and analyzed in a straightforward way by the use of polarized incident light.

Several methods have been described in the literature to prepare symmetric or asymmetric lipid bilayers. Among them the three most important one should be noted: (i) The Langmuir-Schaefer method, adapted for model membrane studies by Tamm and McConnell [1]. A hydrophilic plate was coated by a Langmuir-Blodgett (LB) monolayer of a phospholipid. The hydrophobic surface of the supported monolayer was then contacted with the corresponding hydrophobic surface of a compressed monolayer at the air water interface of a film balance. Immersing this plate in vertical direction into the subphase results in the supported bilayer in the aqueous environment of the subphase. (ii) A different way to get supported bilayers was described by Brian and McConnell [2]. A dispersion of small unilamellar lipid vesicles is brought into contact with the hydrophobic surface of a solid support, leading to a spontaneous spreading of the vesicles on the solid. (iii) The best characterized procedure leading to supported bilayers is the so called LB/vesicle method [3], [4], [5],[6]. As in the first case, the ATR plate (IRE) is coated by a LB lipid monolayer pointing with the hydrocarbon chains towards the air. This plate is now mounted in an ATR flow-through cell where it is contacted by an aqueous solution of lipid vesicles. Since a hydrophobic surface exhibits a large surface energy when in contact with liquid water, a spontaneous oriented adsorption of lipid molecules from the vesicles to the LB monolayer takes place leading to a stable bilayer membrane. Adsorption may be monitored *in situ* by IR ATR spectroscopy.

So far a variety of experiments with different types of supported lipid membranes have been reported for the interaction with proteins, peptides and drugs. First use was made by studying the interaction of local anesthetics (LA) of the tertiary amine type with a dipalmitoylphosphatidic acid (DPPA)/palmitoyl-oleoyl-phosphatidylcholine (POPC) lipid bilayer where POPC was facing the liquid environment [7]. In order to probe the degree of penetration of the LA dibucaine (DIBU) into the lipid bilayer, as well as the influence on hydrocarbon chain ordering in the membrane, a supported bilayer was used, consisting of DPPA as inner monolayer and dimyristoyl-phosphatidylcholine with deuterated hydrocarbon chains (DMPC-d54) as outer layer facing the aqueous environment [8,9]. In another application, a supported DPPA/POPC bilayer served by

itself as a support for natural membrane fragments enriched with the Na+/K+-ATPase (sodium-potassium pump)[10]. The orientation of the peptide melittin in a POPC/POPG (POPG: Palmitoyl-oleoyl-phosphatidylglycerol) was studied by means of FTIR ATR spectroscopy using polarized incident light [11]. This study revealed that the structure of melittin as well as its orientation with respect to the membrane critically depends on the degree of hydration. A similar behavior was observed with the antibiotic alamethicin which was incorporated into dipalmitoyl-phosphatidylcholine (DPPC) multibilayers [12]. Obviously, the structures of oligopeptides are very sensitive to the environment. As a consequence, fully hydrated membrane assemblies must be considered as the most adequate models for ATR spectroscopy. In this respect, it is of great importance to have a good characterization of the supported bilayer from different points of view. In addition to FTIR studies (refs [3]-[6]) valuable information on the nano-structure was obtained by combined application of FTIR and atomic force microscopy (AFM) [13] since nano- and ultra-structure of a sample are of utmost importance for a reliable interpretation of polarized spectra. A further critical point when working with supported bilayers is the lateral mobility of lipid molecules in the inner (LB) monolayer. Fluorescence recovery after photo bleaching (FRAP) has revealed that the lateral mobility of natural phospholipids is preserved [5] giving good evidence for a significant water layer between the solid support (IRE) and the immobilized membrane.

1.2 Enzyme-membrane assemblies

There are several ways of how membrane proteins are attached to a lipid bilayer. Two proteins with respect to their interactions with model membranes have been investigated. The preparation and characterization of two enzyme-membrane assemblies are discussed. These are the mitochondrial creatine kinase (CK) interacting with cardiolipin (CL), and the alkaline phosphatase (AP) interacting with POPC.

1.2.1 Alkaline phosphatase

The alkaline phosphatase (AP) (EC 3.1.3.1; alkaline phosphomonoesterase) is a dimeric metallo enzyme that contains two ions of zinc and one ion of magnesium in each active site region (one site per monomer) and one glycosyl-phosphatidylinositol (GPI) molecule covalently bound to each subunit. AP belongs to a wide group of enzymes which catalyze the non-specific hydrolysis of phosphate monoesters in an alkaline environment[14,15,16]. APs are widely distributed and it has been found in both eucaryotes and procaryotes.

The *Escherichia coli* alkaline phosphatase is the most investigated enzyme. This protein is a dimeric metallo enzyme that contains two ions of Zn^{2+} and one Mg^{2+} in each active site region (one site per monomer). For catalytic activity, only two ions of Zn^{2+} are required[17]. The X-ray diffraction data on the *E. coli* AP (Fig. 1) indicated that the phosphate substrate is coordinated to both Zn^{2+} [18]. This enzyme has been the object of several spectroscopic studies such as NMR[17,19,20,21], FTIR [22] and phosphorescence [23]. In contrast to the *E. coli* AP, very little is known on the secondary structure of mammalian APs and no X-ray diffraction data on the eukaryotic enzymes are available. Sequence comparisons between the mammalian APs and the *E. coli* AP show 25-30% similarity; the comparison of the amino acid sequence of bovine intestinal AP

with the sequence of *E. coli* AP was outlined in [24]. The eukaryotic enzymes possess highly variable loops and major insertions with no equivalent in the *E. coli* AP structure[25,26]. Although there are significant differences between the two types of AP, mammalian APs are also dimeric metalloproteins that contain two to four ions of zinc and one to two ions of magnesium per dimer.

In mammals, AP is a highly polymorphic enzyme. At least four structural genes encoding AP have been cloned, sequenced and mapped to human chromosomes [27]. On the one hand, there is the tissue-nonspecific alkaline phosphatase (TNAP) gene, expressed in osteoblasts, hepatocytes, kidney, early placenta and other cells; on the other hand, three tissue-specific APs (TSAP) are known, as there are the placental, intestinal and germ-cell isoenzymes. APs are membrane proteins which are all attached to the outer leaflet of the plasma membrane or to the topologically equivalent lumenal face of secretory granules by the lipid moiety of a glycosylphosphatidylinositol (GPI) anchor [28,29,30]. The hydrophobic hydrocarbon chains of this lipid moiety are responsible for anchoring the enzyme in the lipid bilayer. Nascent proteins that are destined to be anchored to the plasma membrane by a GPI moiety contain two signal peptides to direct processing in the endoplasmatic reticulum (ER). They possess a typical hydrophobic NH_2-terminal signal peptide that, after directing the protein to a specific site in the ER via an intricate mechanism involving several protein components, is cleaved by NH_2-terminal signal peptidase [31]. Unique to nascent GPI tailed proteins is a hydrophobic COOH-terminal signal peptide that in some way directs them to a putative transamidase that cleaves the peptide and concomitantly adds the GPI moiety. Amino acid requirements adjacent to the site of cleavage and GPI attachment in the COOH-terminal signal peptide are described in [32]. Reviews of proposed mechanisms of GPI addition have been presented in [33,34,35,36]. A favored line of investigation of GPI proteins concerns research on the mechanism of their release by specific anchor-cleaving activities e.g. phospholipases C [37,38]. The process is interesting regarding not only the effects evoked by the released proteins but also regarding the fact that the anchor molecules liberated can potentially act as signals for a broad spectrum of metabolic pathways [39,40,41,42,43,44].

GPI anchors appear to be ubiquitous among eukaryotes. They have been implicated in protective functions in the parasitic protozoa and, in mammalian cells, in intracellular protein targeting, potocytosis and signal transduction. The chemical structure of the GPI anchor (Fig. 2), which is covalently linked to the carboxy-terminus of the enzyme, was determined in the case of human placental AP [45], and the microheterogeneity of the hydrophobic and the hydrophilic part of the GPI anchor of AP from calf intestine was investigated in [46]. However, very little is known about the effects of the GPI anchor on the AP activity or conformation. AP is insoluble in aqueous buffer solution and needs addition of a detergent for solubilization. On the other hand structure and stability of the supported lipid bilayer are influenced, too. Detachment from the IRE was observed as soon as the detergent concentration was equal or higher than the critical micelle concentration (cmc). Obviously, the transfer of AP from solution to the lipid bilayer is much more critical than that of CK. *In situ* measurements of the formation and characterization of the membrane assembly consisting of an inner DPPA LB-layer with an adsorbed POPC layer and bound AP have been performed.
Evidence for GPI anchoring of intralumenal AP of the calf intestine is given in [47]. The binding of alkaline phosphatase from bovine intestinal mucosa with (referred to as „GPI-AP“ in sections 2.3.3 and 3.2) and without anchor (referred to as „AP“ in sections 2.3.3 and 3.2) to model membranes has been investigated.

1.2.1.1 The Significance of AP in Pathology and Clinical Chemistry

AP has been continously and extensively investigated for more than 70 years. Throughout that period, observations of the disease-related changes in AP activity in plasma provided a constant stimulus to explain the related pathology and extend the range of diagnostic applications. The basic mechanisms by which AP activity in plasma comes to reflect disease processes are now known in considerable detail. For example, increased osteoblastic activity is the source of the raised levels of the bone-derived isoform in bone disease; similarly, the initial change in hepatobiliary disease is an increased production of hepatic AP [48,49], probably as a result of accumulating bile acids due to localized or generalized cholestasis. Furthermore, congenital hypophosphatasia is characterized by a generalized deficiency of TNAP [50]. Last but not least, the ectopic and increased eutopic expression of certain AP genes in cancer not only has provided a new series of tumor markers, especially in germ-cell tumors [51] but, perhaps more important, has opened new opportunities for the study of changes in genetic regulation accompanying malignant transformation.

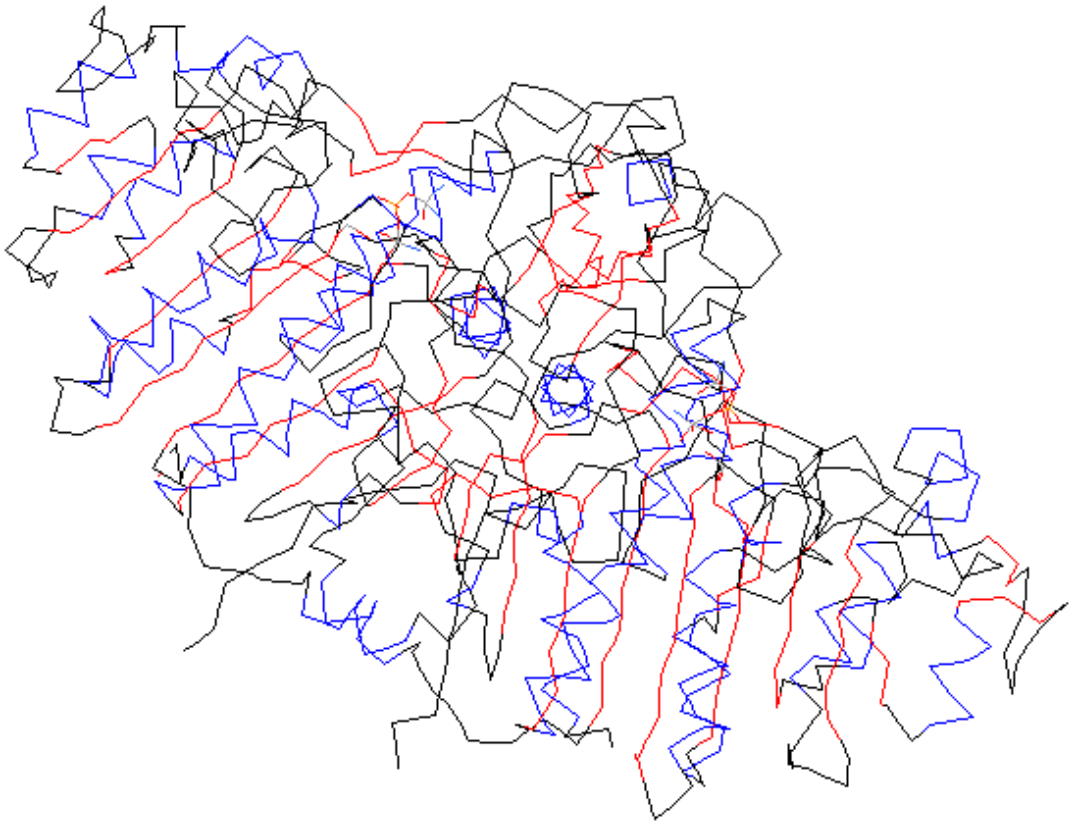

Fig. 1. Threedimensional structure (α-carbon trace) of the *E. coli* AP based on X-ray diffraction data [18]. *Colors*: α-helices, blue; ß-strands, red; aperiodic structures, black.

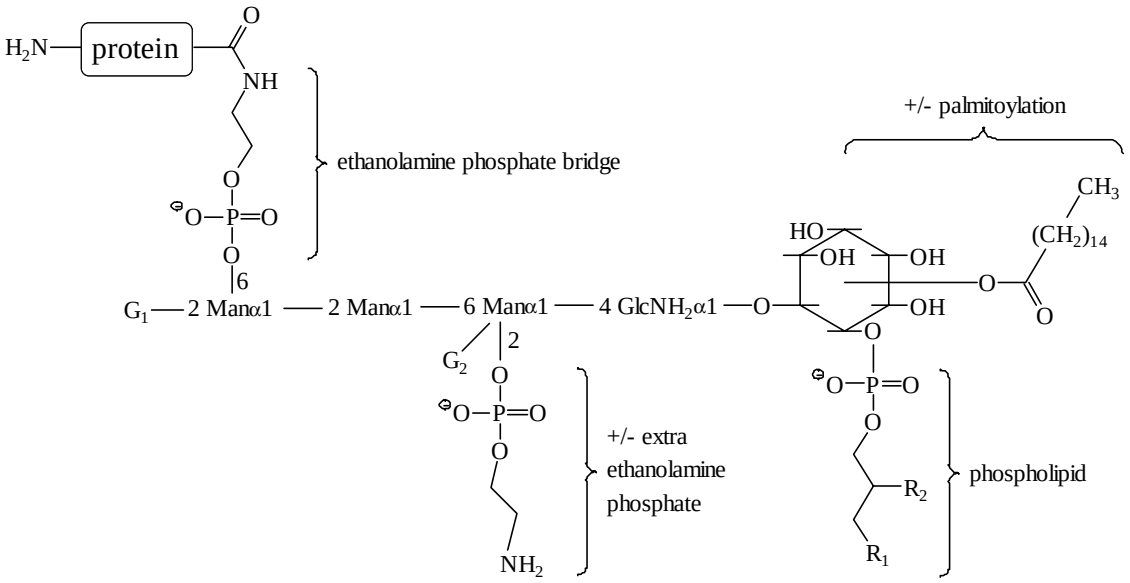

Fig. 2. Structure of the glycosyl phosphatidylinositol (GPI) anchor, reproduced after Ferguson [29]. The carboxy-terminus of the protein is linked to the inositol phospholipid via an ethanolamine phosphate bridge and sugars. G1, G2, sugar residues the composition of which depend on the organism; Man, mannose; $GlcNH_2$, N-acetylglucosamine.

1.2.1.2 Aim of Investigation

- establishment of supported model membrane systems by incorporation of AP into a planar lipid bilayer for FTIR ATR spectroscopic and enzyme activity measurements; both of them are performed *in situ*, the latter on-line in a circulating system by means of p-nitrophenyl phosphate as substrate

- in future experiments selective detection of conformation changes at the active site of the enzyme under the influence of different pH values, substrates and different Zn^{2+}- and Mg^{2+}-concentrations with the help of ME spectroscopy (see 2.4)

The results of these investigations can lead to

- a better understanding of the factors which are responsible for the disease-related changes in AP-activity in plasma

- the development and optimization of clinical assays in medical diagnostics

- the development and optimization of biosensors based upon immobilized enzymes

1.2.2 Mitochondrial creatine kinase

In vivo mitochondrial creatine kinase (Mi-CK) is found in the intermembrane space, attached to the inner mitochondrial membranes, which are rich of the negatively charged cardiolipin (CL) [52]. Mi-CK is known to bind effectively to the surface of negatively charged bilayers like CL [53]. Physiologically, the mitochondrial CK is important for the energy metabolism in cells of high and fluctuating energy requirements: Through transphosphorylation from phosphocreatine (PCr) to ADP producing ATP (or vice versa) the enzyme realizes a temporal and spatial energy buffering. The native form of the enzyme is octameric and highly ordered as revealed by x-ray diffraction (Fig. 3) [54]. Typical features are a large channel, connecting the top to the bottom face of the nearly cubic shaped octamer and the accumulation of positively charged residues (Lys and Arg) at these opposite faces. CK was found to adsorb spontaneously to negatively charged phospholipid membranes most probably by one of the positively charged surfaces. First kinetic results have been obtained by plasmon resonance and light scattering experiments [55]. *In situ* FTIR ATR spectroscopy with polarized light was used to monitor the formation of a membrane assembly consisting of a DPPA/CL bilayer membrane and the binding of CK to this membrane. Moreover, the interaction of CK with a DPPA/DPPA bilayer was investigated. Quantitative analysis resulted in a surface coverage of at least 50% by CK [56]. Furthermore, a flow-through system enabled the measurement of enzyme activity simultaneously with spectroscopic data acquisition. Structural changes in the lipid bilayer revealed a predominant electrostatic interaction at the membrane surface [57].

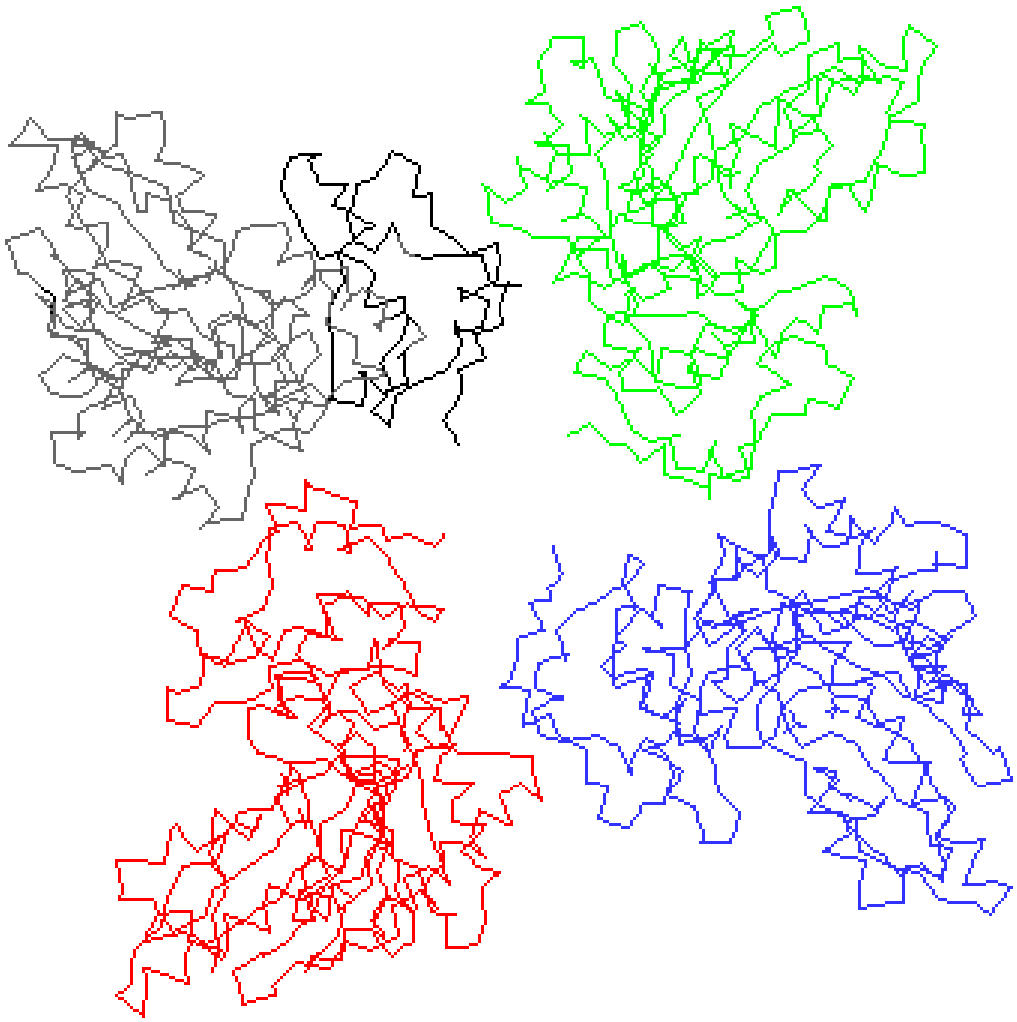

Fig. 3. Threedimensional structure (α-carbon trace) of chicken Mi_b-CK based on X-ray diffraction data [54]. Different colors denote different chains. Eight chains represent a biological unit.

1.2.3 Characteristic bands of proteins, phospholipids and β-octylglucoside

Typical amide group absorption bands of the protein backbone are located near 1650 cm^{-1} (amide I, I´, consisting of about 80% C=O stretching, ν(C=O), 10% C-N stretching, ν(C-N), and 10% N-H bending, δ(N-H)) [58], 1540 cm^{-1} (amide II, about 40-60% N-H bending δ(N-H), 18-40% C-N stretching, ν(C-N), and 10% C-C stretching, ν(C-C)) [58] and 1450 cm^{-1} (amide II´ which may be overlapped by HDO bending δ(HDO)).
The most prominent bands of phospholipids are located in the spectral range from 3000 to 2800 cm^{-1} and derive from vibrations of the hydrocarbon chain. Bands at 2959, 2917 and 2850 cm^{-1} are assigned to the asymmetric stretching of the methyl groups, $\nu_{as}(CH_3)$, to the asymmetric stretching of the methylene groups, $\nu_{as}(CH_2)$, and to the symmetric stretching of the methylene groups, $\nu_s(CH_2)$, respectively. The symmetric stretching of the methyl groups, $\nu_s(CH_3)$, at about 2873 cm^{-1} is not visible[59].
After the ν(CH) bands of the methyl group and the seven methylene groups of the octyl residue, the second most intense β-octylglucoside (β-OG) absorption bands result from the glucoside moiety (mainly C-O stretching, ν(C-O)) and are located around 1050 cm^{-1}.

1.2.4 The SBSR technique

A new ATR attachment enables the conversion of a single beam (SB) spectrometer into a pseudo double beam instrument in order to achieve more stable background compensation than with the conventional SB technique. This attachment converts convergent light entering the sample compartment into a parallel beam. The latter is focused to the entrance of a multiple internal reflection element (MIRE) by means of a cylindrical mirror thus producing a parallel ray propagation within the MIRE (wave guide). Placing now the sample at the lower half of the plate and the reference at the upper half and switching the beam by a chopper alternatively up and down leads to the so-called single beam sample reference (SBSR) technique [3], featuring two advantages over conventional SB technique: (i) elimination of water vapor incompensation, and (ii) compensation of drifts resulting from the instrument or the sample/reference, respectively. In this thesis a SBSR ATR attachment is presented which makes use of a computer controlled lift in order to move the upper or lower half of the MIRE into the parallel beam. This set up leads to a better base line than the chopper version used earlier [3,4] since the FTIR spectrometer turned out to have inhomogeneous intensity within the cross-section of the IR beam. Subdividing this beam into an upper and lower half and calculating the ratio of the corresponding single channel spectra will therefore not result in a flat 100% line as should be expected for an ideal spectrometer.

1.2.5 Modulated excitation FTIR spectroscopy

Finally, an outlook to the application of more sophisticated dynamic techniques such as modulated excitation (ME) FTIR spectroscopy is given. External periodic stimulation of the membrane assembly may be accomplished via thermodynamic parameters such as temperature (T), concentration (c), electric field (E), light flux (Φ) etc. The power of ME-FTIR spectroscopy is based on the one hand on a significant enhancement of the selectivity of the measurement which is of great importance in the case of

macromolecule spectroscopy featuring heavily overlapped absorption bands. Selectivity is achieved by the fact that only molecules or molecular parts (e.g. functional groups) affected by the periodic external perturbation will result in a corresponding modulated absorbance spectrum. Phase sensitive detection (PSD) enables now a separation of modulated and non-modulated parts of the FTIR spectrum with a higher accuracy than achieved by conventional difference spectroscopy. Moreover, if the system response to a sinusoidal excitation with frequency ω contains not only the fundamental ω, but also the first harmonic (2ω) or even higher harmonics, one has unambiguous evidence for a nonlinear chemical system, which may originate in chemical reactions different from first order and/or cooperative phenomena. The latter are of special interest in processes where conformational changes of biological macromolecules are involved. If a time resolved data acquisition of the system response is possible, a kinetic analysis of the process may be performed on the basis of the frequency dependence of both, amplitudes and phases of modulated absorbances of the system response. This information is accessible by phase sensitive detection (PSD) of time resolved FTIR absorbance spectra via analog or digital procedures [60]. Variation of the modulation frequency ω results in independent data sets which facilitate the reconstruction of the reaction scheme. This is the main advantage of ME spectroscopy on relaxation (REL) spectroscopy. Although both, ME and REL techniques have the same physico-chemical information content, the read out of this information, however, is facilitated by ME, because more independent experimental data is available due to the additional degree of freedom given by the parameter 'modulation frequency' ω, while the number of unknown kinetic parameters included the reaction scheme are the same for ME and REL. After a theoretical introduction to ME spectroscopy, T-ME spectra of poly-L-lysine (PLL) will be shown. PLL may be converted reversibly from the α-helical to the antiparallel β-pleated sheet structure by T-modulation under adequate conditions. At least three so far unknown transient species have been detected and sequentially assigned based on their phase shift with respect to the T-stimulation [61]. Finally, results from a T-modulation experiment performed with RNAse A is shown. This enzyme undergoes a reversible unfolding/refolding process with a distinct transition temperature at T=64°. Time resolved temperature jump (T-jump) measurements revealed relaxation times in the range of τ_i = 5-10 s [62]. A corresponding T-ME experiment has been performed by switching the temperature between 59°C and 69°C with a period τ_{mod} = 25 s.

1.3 Theory

1.3.1 Introduction

Application of vibrational spectroscopy to the problem of structure determination of molecules of biological interest goes back to the early uses of infrared spectroscopy in the study of organic molecules [63]. It was realized quite early that relevant structural information about biological systems often requires study in aqueous solution, which forms the natural environment for most biologically important systems. However, this poses a problem if the conventional absorption technique is used, since the high absorption coefficient of water in wide regions of the mid and far infrared implies use of thin layers and high concentrations. As a consequence the application of special techniques for measurement of IR spectra of biological material has been a necessity in many cases.

In the past decade Fourier transform infrared (FTIR) spectrometers have replaced dispersive instruments because of their better performance in nearly all respects [64]. The problem of background compensation, for example, has been reduced significantly, enabling routine measurements to be made, even in aqueous environments. Therefore, a growing interest in infrared membrane spectroscopy has been observed from biophysical, biochemical and biomedical viewpoints [65], as well as from the aspect of biosensors [66].

Fig. 4 shows a schematic comparison of (a) the conventional transmission and (b) the internal reflection technique. The latter is achieved by placing the sample material in close contact with the optically transparent internal reflection element (IRE) of higher refractive index (e.g. a Ge or ZnSe plate) and working above the critical angle θ_c [68].

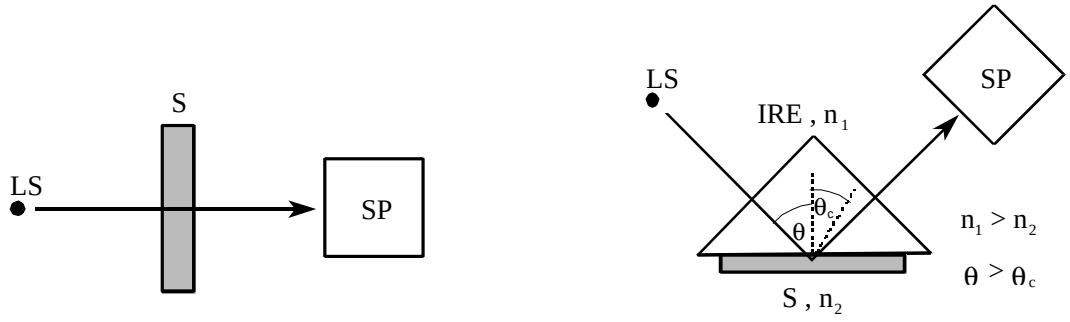

a. TRANSMISSION

b. INTERNAL REFLECTION

Fig. 4. Comparison of transmission (a) with internal reflection (b) technique. θ : angle of incidence, θ_c : critical angle, n_1,n_2 : refractive index of IRE and S, respectively. Abbreviations: LS, light source; S, sample; SP, spectrometer; IRE, internal reflection element (ATR crystal).

1.3.2 Quantitative ATR Spectroscopy

1.3.2.1 Evanescent wave and penetration depth

The relevant optical parameters are depicted by Fig. 5, which shows schematically the trace of a ray upon internal reflection at the membrane IRE interface. The goal of this analysis of FTIR ATR spectra is the calculation of the surface concentration and orientation of molecules in an adsorbed layer as well as the bulk concentration of dissolved substances in the aqueous environment. For that purpose some characteristic properties of internal reflection spectroscopy must be explained. Fig. 6 shows the IRE fixed coordinate system which is relevant for the description of optical and structural features of the system. Straightforward calculation of the propagation of a plane wave from medium 1 (IRE) into a nonabsorbing medium 2 under the conditions of total reflection [67] yields eqn. (1)

$$E_{x,y,z,2}(z) = E_{x,y,z,2}(0)\exp(-z/d_p) \qquad (1)$$

It follows that all electric field components of the so-called evanescent wave decrease exponentially with distance z from the interface. d_p denotes the penetration depth, which according to eqn. (2) is in the order of the wavelength of the light in the medium 1. The relative field components at the interface 1-2, $E^r_{x,y,z,2}(0) = E^r_{0x,0y,0z,2}$ may be calculated by Fresnel's equations ([4,67,68], eqn.(9)).

$$d_p = \frac{\lambda/n_1}{2\pi\left(\sin^2\theta - \left(\frac{n_3}{n_1}\right)^2\right)^{\frac{1}{2}}} \qquad (2)$$

$\lambda_1 = \lambda/n1$ denotes the wavelength in medium 1, and λ is the vacuum wavelength. θ is the angle of incidence. According to Eq. (2) the penetration depth d_P amounts to the order of magnitude of the wavelength λ of the infrared radiation. This fact allows IR absorption measurements of thin layers, provided optical contact between rarer medium (sample) and ATR plate may be established, e.g., by direct deposition of mono- or multilayers. In that case $z \approx 0$ which brings about, as Eq. (1) shows, the best possible interaction of the sample with the evanescent wave. Furthermore, under this condition

$$\left(\frac{A_{sample}}{A_{H_2O}}\right)_{ATR} >> \left(\frac{A_{sample}}{A_{H_2O}}\right)_{transmission}.$$

This means that ATR measurements of aqueous systems are less impeded by water absorption than transmission experiments. Since the thickness of a membrane assembly is in the range of 50 Å to 150 Å, i.e. only about 1 % of the penetration depth, the electric field in the rarer medium is predominantly determined by the bulk medium 3. Therefore, the refractive index n_3 is used instead of n_2, see Fig. 5. This is the basic assumption for the thin layer approximation introduced by Harrick [68]. As a consequence the electric field in the membrane (thin medium 2) is then assumed to be determined by the

boundary conditions valid for a thin dielectric film in the electric field of the evanescent wave generated by the bulk media 1 and 3 [4,68].

1.3.2.2 Effective thickness d_e

The concept of effective thickness has been introduced by Harrick [68]. The quantity d_e indicates the thickness of a sample that would result in the same absorbance in a hypothetical transmission experiment, as obtained with the genuine ATR experiment. This concept enables application of Lambert-Beer's law on ATR spectra according to eqn. (3).

$$T = 10^{-\varepsilon c d_e} = 10^{-A} \qquad (3)$$

where $A = \varepsilon c d_e$ denotes the absorbance per internal reflection. For an isotropic layer extended from $z = z_i$ to $z = z_f$ one obtains [4]:

$$d_e^{iso} = \frac{1}{\cos\theta}\frac{n_2}{n_1}\frac{d_p}{2}E_{02}^{r\,2}\left(\exp\left(-\frac{2z_i}{d_p}\right)-\exp\left(-\frac{2z_f}{d_p}\right)\right) \qquad (4)$$

According to eqn. (4) d_e turns out to be wavelength dependent via d_p, see eqn. (2). As a consequence, ATR spectra of bulk media generally show increasing intensity with increasing wavelength. However, if the thickness of the layer $d = z_f - z_i$ is small compared to d_p then eqn. (4) reduces to eqn. (5) which is independent of the wavelength.

$$d_e^{iso} = \frac{1}{\cos\theta}\frac{n_2}{n_1} d\, E_{02}^{r\,2} \qquad (5)$$

A further case often encountered is the bulk sample extended from $z_i = 0$ to $z_f = \infty$ resulting in eqn. (6).

$$d_e^{iso} = \frac{1}{\cos\theta}\frac{n_2}{n_1}\frac{d_p}{2}E_{02}^{r\,2} \qquad (6)$$

$E_{02}^{r\,2}$ denotes the square of the electric field strength in medium 2 which is proportional to the light intensity. For polarized incident light it follows

$$E_{02,\parallel}^{r\,2} = E_{02,x}^{r\,2} + E_{02,z}^{r\,2} \quad \text{and} \quad E_{02,\perp}^{r\,2} = E_{02,y}^{r\,2} \qquad (7)$$

Introducing eqn. (7) into eqn. (4) results in

$$d_{e\parallel}^{iso} = d_{ex}^{iso} + d_{ez}^{iso} \quad \text{and} \quad d_{e\perp}^{iso} = d_{ey}^{iso} \qquad (8)$$

It should be concluded from eqns. (7) and (8) that straightforward application of Lambert-Beer's law to ATR spectra of isotropic samples needs measurements with either parallel or perpendicular polarized incident light. The effective thickness for unpolarized incident light $d_{e,up}^{iso}$ turns out to be a linear combination of $d_{e\parallel}^{iso}$ and of $d_{e\perp}^{iso}$. The coefficients depend on the polarizing properties of the optical components in the spectrometer [4] which must be determined for each instrument.

1.3.2.3 Relative Electric Field Components

Electric field components of the evanescent wave may be calculated by means of Fresnel's equations [67,68]. For a 'nonabsorbing' thin film (Harrick´s weak absorber approximation), e.g. a membrane assembly as depicted in Fig. 5 (medium 2), one obtains the following expressions [4,68]:

$$E_{0x,2}^{r} = \frac{E_{0x,2}}{E_{0\parallel,1}} = \frac{2\cos\theta\left(\sin^2\theta - n_{31}^2\right)^{1/2}}{\left(1-n_{31}^2\right)^{1/2}\left[\left(1+n_{31}^2\right)\sin^2\theta - n_{31}^2\right]^{1/2}} \qquad (9)$$

$$E_{0z,2}^{r} = \frac{E_{0z,2}}{E_{0\parallel,1}} = \frac{2\cos\theta\sin\theta\, n_{32}^2}{\left(1-n_{31}^2\right)^{1/2}\left[\left(1+n_{31}^2\right)\sin^2\theta - n_{31}^2\right]^{1/2}}$$

$$E_{0y,2}^{r} = \frac{E_{0y,2}}{E_{0\parallel,1}} = \frac{2\cos\theta}{\left(1-n_{31}^2\right)^{1/2}}$$

The meaning of n_{ik} is the ratio of the refractive indices of media i and k, respectively, i.e. $n_{ik} = n_i/n_k$. According to the thin film approximation by Harrick [68] the corresponding field components of the bulk environment (medium 3) are obtained by replacing index 2 by index 3. This affects only the z-component in accordance with electrostatic boundary conditions.

For intermediate layer thickness, i.e. $d \approx d_p$ the electric field components (eqn. (9)) must be modified, either by accurate treatment of a layered system [67], or by the application of an approximation described by eqn. (10)which is based on the interpolation between the results obtained for a thin layer ($d << d_p$) and a bulk medium ($d >> d_p$)[69]. The results obtained by this approximation deviate less than 5% from those got by the much more complicated accurate calculation. Eqn. (10) holds for all field components (x-, y-, and z-direction).

$$E_{02}^{r}(d) = E_{02}^{r}(\text{thin layer}) + \left(1-e^{-d/d_p}\right)\left(E_{02}^{r}(\text{bulk}) - E_{02}^{r}(\text{thin layer})\right) \qquad (10)$$

1.3.2.4 Validity of Effective Thickness Concept

Since the effective thickness concept enables the application of Lambert-Beer's law to ATR data, experimental validation may be performed easily by comparing spectra of the same sample measured by both, ATR and transmission (T).

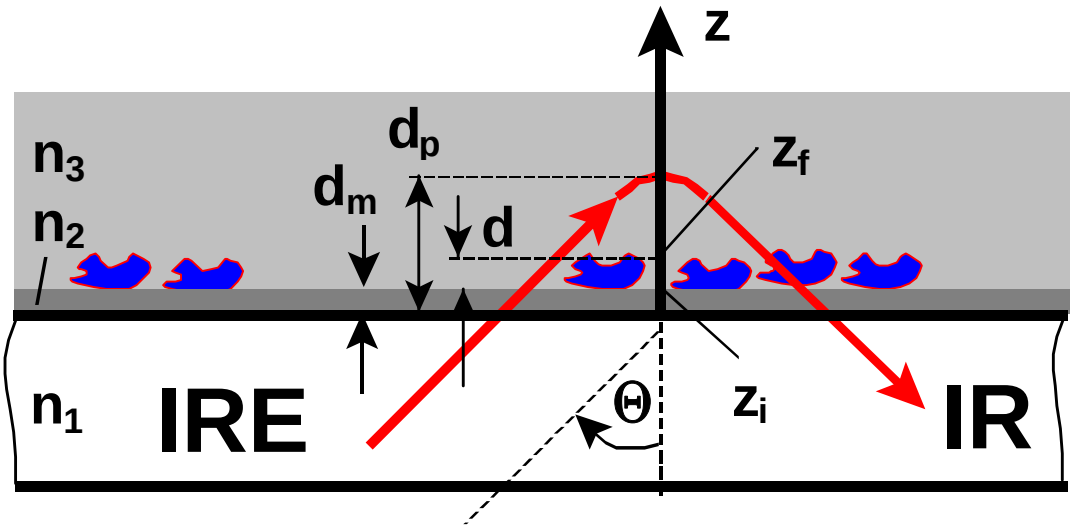

Fig. 5. Penetration depth dp of the evanescent wave. The internally reflected light propagates within the IRE (index 1) with an angle of incidence θ . It penetrates the membrane (index 2) of thickness $d_m \approx 50$ Å and the adsorbed enzyme (adlayer of thickness d, ranging from $z = z_i$ to $z = z_f$) and enters the aqueous environment (index 3). The strength of the electric field decreases exponentially with distance z from the 1-2 interface, see eqn (1). The refractive indices of the media are denoted by n_1, n_2, and n_3.

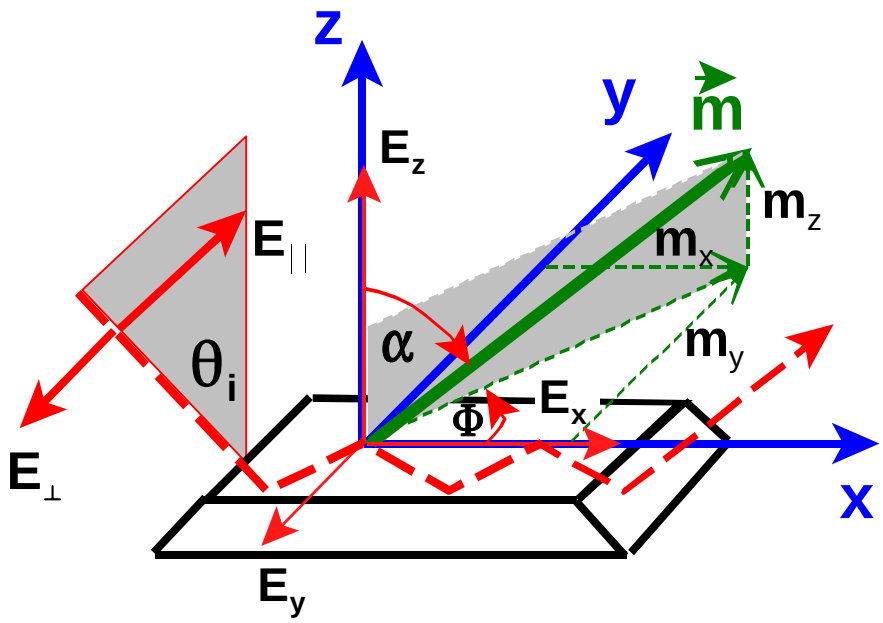

Fig. 6. ATR set up. Optical and structural features are related to the IRE fixed coordinate system x,y,z. $E_{\parallel}$ and $E_{\perp}$ denote the parallel and perpendicular polarized components of the light incident to the IRE under the angle θ. $E_{\parallel}$ results in the E_x and E_z components of the evanescent field, while $E_{\perp}$ results in the E_y component. $\vec{m}$ denotes the unit vector in direction of the transition dipole moment vector of a given vibrational mode, and m_x, m_y, m_z are the corresponding components in the IRE coordinate system. $\vec{m}$ goes off at an angle α with respect to the z-axis and the projection of $\vec{m}$ to the xy-plane goes off at an angle ϕ with respect to the x-axis.

As long as the results do not differ significantly from each other the analytical approach described above is considered to be justified. ATR and T measurements with aqueous solutions of Na_2SO_4 have shown that at 1 molar concentration Lambert-Beer's law is still fulfilled for the very intense SO_4^{2-} stretching band at 1100 cm^{-1}. Even for the strong H2O bending (δ(H2O)) band of liquid water at 1640 cm^{-1} the integral molar absorption coefficients determined by ATR with a germanium MIRE at an angle of incidence of $\theta = 45°$ was found to be equal to T-data within the experimental error [4]. However, a few percents of deviation were found when peak values of the absorbance were used to determine the molar absorption coefficient. The latter indicates the onset of band distortion, a phenomenon well known in ATR spectroscopy under extreme conditions [68]. This finding is in accordance with calculations by Harrick using Fresnel's equations with complex refractive indices [68]. For Ge in contact with liquid water and $\theta = 45°$ the analysis resulted in an upper limit of the absorption coefficient $\alpha_{max} \approx 1000$ cm^{-1}. The concept of effective thickness as described above may be considered to be valid for $\alpha < \alpha_{max}$. For organic compounds this condition is generally fulfilled. In case of δ(H2O) of liquid water, however, the absorption coefficient [4] results in $\alpha = \varepsilon(1640\ cm^{-1})\cdot c = 1.82\cdot 10^4\ cm^2\cdot mol^{-1}\cdot 5.56\cdot 10^{-2}\ mol\cdot cm^{-3} = 1011.9\ cm^{-1}$, which indicates that the limit of validity of the approach is reached, in complete accordance with experimental data mentioned above.

1.3.2.5 Oriented Samples

Considering a transition dipole moment $\vec{M}$ associated with a vibrational mode of a given molecule and the electric field $\vec{E}$, responsible for vibrational excitation, the intensity of light absorption depends on the mutual orientation of these vectors according to

$$\Delta I \infty \left(\vec{E}\cdot\vec{M}\right)^2 = \left|\vec{E}\right|^2\cdot\left|\vec{M}\right|^2\cdot\cos^2\left(\vec{E},\vec{M}\right) = \left(E_x M_x + E_y M_y + E_z M_z\right)^2 \qquad (11)$$

Eqn. (11) forms the basis of orientation measurements. M_x, M_y, and M_z denote the components of the transition dipole moment in the IRE fixed coordinate system shown in Fig. 6. It is usual to work with dimensionless relative intensities instead of absolute intensities in order to get rid of physical and molecular constants, e.g. the magnitude of the transition moment. Introducing the so-called dichroic ratio, the absorbance ratio obtained from spectra measured with parallel and perpendicular polarized incident light, i.e.

$$R = \frac{A_\parallel}{A_\perp} = \frac{d_{e,\parallel}}{d_{e,\perp}} = \frac{\int A_\parallel d\tilde{\nu}}{\int A_\perp d\tilde{\nu}} \qquad (12)$$

In order to get information on the direction of the transition dipole moment $\vec{M}$, the scalar product notation using vector components (see eqn. (11)) will be used. Taking into account that in the evanescent field pp light is represented by x- and z-components, and vp light by the y-component one obtains for the dichroic ratio:

$$R = \frac{A_{\parallel}}{A_{\perp}} = \frac{d_{e,\parallel}}{d_{e,\perp}} = \frac{E_x^2 m_x^2 + E_z^2 m_z^2 - 2E_x E_z m_x m_z}{E_y^2 m_y^2} \qquad (13)$$

m_x, m_y, and m_z are the unit vector components of $\vec{M}$. Eqn. (13) holds for a single crystalline sample. In a complex non crystalline molecule there are generally many possibilities of molecular arrangements, conformational changes and fluctuations. The experimentally available quantity R is therefore an ensemble mean represented by:

$$R = \frac{A_{\parallel}}{A_{\perp}} = \frac{d_{e,\parallel}}{d_{e,\perp}} = \frac{E_x^2 \langle m_x^2 \rangle + E_z^2 \langle m_z^2 \rangle - 2E_x E_z \langle m_x m_z \rangle}{E_y^2 \langle m_y^2 \rangle} \qquad (14)$$

Uniaxial orientation along the z-axis is often encountered in membrane spectroscopy. In this case

$\langle m_x m_z \rangle = 0$, resulting in

$$R = \frac{A_{\parallel}}{A_{\perp}} = \frac{d_{e,\parallel}}{d_{e,\perp}} = \frac{E_x^2 \langle m_x^2 \rangle + E_z^2 \langle m_z^2 \rangle}{E_y^2 \langle m_y^2 \rangle} \qquad (15)$$

The unit vector components as presented in Fig. 6 are determined by the angles α and Φ

$$\begin{aligned} m_x &= \sin\alpha \cos\Phi \\ m_y &= \sin\alpha \sin\Phi \\ m_z &= \cos\alpha \end{aligned} \qquad (16)$$

with corresponding mean squares

$$\langle m_x^2 \rangle = \langle \sin^2 \alpha \cos^2 \Phi \rangle = \frac{1}{2}\left(1 - \langle \cos^2 \alpha \rangle\right)$$

$$\langle m_y^2 \rangle = \langle \sin^2 \alpha \sin^2 \Phi \rangle = \frac{1}{2}\left(1 - \langle \cos^2 \alpha \rangle\right)$$

$$\langle m_z^2 \rangle = \langle \cos^2 \alpha \rangle$$

It should be noted that for an isotropic arrangement of transition moments the ensemble mean of any component of eqn. (16) result in 1/3. As a consequence eqn. (15) results in

$$R^{iso} = \frac{E_x^2 + E_z^2}{E_y^2} \qquad (17)$$

which, according to eqn. (9) differs from unity. $R^{iso} = 1$ holds only for transmission spectroscopy.

Introducing eqn. (16) into eqn. (15) results in

$$R = \frac{E_x^{\,2}}{E_y^{\,2}} + 2\frac{E_z^{\,2}}{E_y^{\,2}}\frac{\langle\cos^2\alpha\rangle}{1-\langle\cos^2\alpha\rangle} \qquad (18)$$

Solving eqn. (18) for $\langle\cos^2\alpha\rangle$ results in

$$\langle\cos^2\alpha\rangle = \frac{\left(R - \frac{E_x^{\,2}}{E_y^{\,2}}\right)\frac{E_y^{\,2}}{E_z^{\,2}}}{2 + \left(R - \frac{E_x^{\,2}}{E_y^{\,2}}\right)\frac{E_y^{\,2}}{E_z^{\,2}}} \qquad (19)$$

This quantity is directly related to the segmental order parameter S_{seg}, which corresponds to the bond order parameter encountered in nuclear magnetic resonance (NMR) spectroscopy.

$$S_{seg} = \frac{3}{2}\langle\cos^2\alpha\rangle - \frac{1}{2} \qquad (20)$$

Perfect alignment along the z-axis would result in $\langle\cos^2\alpha\rangle = 1$, and $S_{seg} = 1$, respectively. On the other hand, an isotropic arrangement of transition moments would result in the ensemble mean $\langle\cos^2\alpha\rangle = 1/3$, corresponding to $S_{seg} = 0$. Finally, isotropic arrangement of the transition moments in the x,y-plane, i.e. $\alpha = 90°$ would result in $S_{seg} = -1/2$.

Both $\langle\cos^2\alpha\rangle$ and S_{seg} are experimentally accessible by polarized light measurements.

1.3.2.6 Effective Thickness of Oriented Samples and Surface Concentration

Axial effective thicknesses of isotropic samples as introduced by eqns. (4) and (8) must now be weighted by the corresponding ensemble mean of the unit vector components of the transition moment, resulting in

$$d_{ex} = 3\langle m_x^{\,2}\rangle d_{ex}^{iso} = \frac{3}{2}\left(1 - \langle\cos^2\alpha\rangle\right)d_{ex}^{iso} \qquad (21)$$

$$d_{ey} = 3\langle m_y^{\,2}\rangle d_{ey}^{iso} = \frac{3}{2}\left(1 - \langle\cos^2\alpha\rangle\right)d_{ey}^{iso}$$

$$d_{ez} = 3\langle m_z^{\,2}\rangle d_{ez}^{iso} = 3\langle\cos^2\alpha\rangle d_{ez}^{iso}$$

In analogy to eqn. (8) one obtains for the effective thickness with parallel polarized incident light

$$d_{e\parallel} = d_{ex} + d_{ez} \quad \text{and} \quad d_{e\perp} = d_{ey} \qquad (22)$$

The surface concentration Γ of a species in a layer of thickness d is considered as projection of the volume concentration c to the surface of the IRE. It follows from eqns. (3) and (21)

$$\Gamma = c \cdot d = \frac{A_{\parallel} \cdot d}{\varepsilon \cdot d_{e\parallel}} = \frac{\int A_{\parallel} d\tilde{\nu} \cdot d}{\int \varepsilon d\tilde{\nu} \cdot d_{e\parallel}} = \frac{A_{\perp} \cdot d}{\varepsilon \cdot d_{e\perp}} = \frac{\int A_{\perp} d\tilde{\nu} \cdot d}{\int \varepsilon d\tilde{\nu} \cdot d_{e\perp}} \qquad (23)$$

$A_{\parallel}$ and $A_{\perp}$ denote the absorbances measured with parallel and perpendicular polarized incident light, respectively. ε is the molar absorption coefficient. It should be noted that eqn. (23) holds for integrated absorbance, too, provided that integrated molar absorption coefficients are used. With N active total reflections (see 1.3.2.7) and ν equal functional groups of a molecule, eq. (23) yields

$$\Gamma = c \cdot d = \frac{A_{\parallel} \cdot d}{\nu \cdot N \cdot \varepsilon \cdot d_{e\parallel}} = \frac{\int A_{\parallel} d\tilde{\nu} \cdot d}{\nu \cdot N \cdot \int \varepsilon d\tilde{\nu} \cdot d_{e\parallel}} = \frac{A_{\perp} \cdot d}{\nu \cdot N \cdot \varepsilon \cdot d_{e\perp}} \qquad (24)$$

$$= \frac{\int A_{\perp} d\tilde{\nu} \cdot d}{\nu \cdot N \cdot \int \varepsilon d\tilde{\nu} \cdot d_{e\perp}}$$

1.3.2.7 Number of active total reflections

The number of reflections is calculated from simple geometrical considerations. If an IRE is uesd as depicted in Fig. 6, the beam advances a distance („skip distance“) of $t \cdot \tan\theta$ for each reflection (t: plate thickness; θ: angle of incidence). If the coated plate length is l, the total number of reflections for a single pass in the plate is given by

$$N = l/(t \cdot \tan\theta) \qquad (25)$$

However, if a flowthrough cell like in Fig. 7 is used, instead of l an average length $\bar{l}$ of the sealed compartment has to be calculated because the sample is only in there. The compartment can be supposed to consist of a rectangle with length L and width W and two semicircles with radius r. This results in

$$\bar{l} = L + 2 \cdot \frac{1}{\pi} \int_0^{\pi} r \sin x dx = L - 2 \cdot \frac{1}{\pi} r \cos x \Big|_0^{\pi} = L + \frac{4r}{\pi} \qquad (26)$$

and $N = \bar{l}/(t \cdot \tan\theta)$

From the point of view of background compensation, the number of internal reflections should be as small as possible. From an optimization criterion given in [4] it is concluded that 20-40 internal reflections are optimum for an angle of incidence θ of 45° and germanium as IRE.

1.3.3 Time resolved modulated excitation (ME) spectroscopy

1.3.3.1 External ME of Lipids, Peptides and Proteins

Change of any external thermodynamic parameter generally exerts a specific influence on the state of a system. The system response will be a relaxation from the original state (e.g. an equilibrium) to a new equilibrium state. In case of a periodic change (modulation) of the parameter, the system response will also be periodic, i.e. those absorption bands of the spectrum which result from stimulated molecules or parts of them will be labelled by the same frequency. As a consequence, it will be possible to separate the modulated response of the system, which is correlated with the external stimulation from the stationary response, resulting from parts of the system that were not affected by modulated excitation (ME) and from the background. Moreover, if the kinetics of the stimulated process is in the same time range as the period of external stimulation, phase-lag and amplitude measurements of modulated absorbances give information on the reaction scheme and the kinetics of the stimulated process. Hydration modulation, e.g. was applied to determine the hydration sites of lecithins [70,71].

Temperature ME of poly-L-lysine was used to study induced periodic secondary structural changes as well as the sequence of transients [61]. The classical ATR set-up (see Fig. 19) facilitates the application of electric fields to membrane assemblies, since a Ge ATR plate, supporting the membrane, may be used as one electrode, and the back-wall of the cuvette as counter electrode. First use of electric field ME of immobilized acetylcholine esterase (AChE) was reported in ref. [72]. In the view of today, the interpretation of a field-dissociation effect (second Wien effect) of carboxylic acid residues of AChE must be qualified. Since Ge decomposes at slightly positive potentials, forming germinic acid, the periodic deprotonation and reprotonation of -COOH groups of AChE may be interpreted as a superposition of electric field and pH-effect. As a consequence, passivation of the Ge surfaces [73] is a prerequisite for electric field ME experiments. The problem of anodic decomposition of germanium does not exist in the case of electric field ME of liquid crystals [74,75].

Electronic ME of photochemical processes by modulated UV-/VIS-light enables access to a wide range of excitation frequencies. Light flux modulation in the kHz range, which may be easily performed by means of a mechanical chopper, enables kinetic analysis even in the µs region as shown in the case of the photooxidation of pyrocatechol by modulated electronic excitation IR and ESR spectroscopy [76].

1.3.3.2 Example: Temperature Modulated Excitation (T-ME) of Chemical Reactions

The principles of T-ME may be elucidated by considering the simple reversible chemical reaction between two species A_1 and A_2 where k_{12} and k_{21} denote the rate constants of forwards and backwards reaction.

$$A_1 \underset{k_{21}}{\overset{k_{12}}{\rightleftarrows}} A_2$$

If the sample is exposed to a periodic temperature stimulation according to

$$T(t) = T_i + \frac{\Delta T}{2}(1 - \cos \omega t) \qquad (27)$$

where Ti, ΔT and ω denote the initial temperature, the peak to peak temperature variation and the angular frequency, respectively. The influence of temperature on rate constants may be described by the Arrhenius equation. Since ΔT is small ($\leq 5°C$), the linearized form will be used in this context, leading to

$$k_{ik}(t) = k_{ik}(\overline{T}) + \frac{\Delta k_{ik}}{2}(1 - \cos \omega t) \quad \text{with} \quad \Delta k_{ik} = k_{ik}(T_i)\frac{E_{ik}}{RT_i^2}\Delta T \qquad (28)$$

k_{ik} denotes the rate constant from species i to species k and E_{ik} is the corresponding activation energy.
Introducing the reaction number ξ as the relevant concentration parameter for the description of turnover

$$[A_1] = [A_1]_0 - \xi, \; [A_2] = [A_2]_0 + \xi \qquad (29)$$

and inserting eqn. (29) into the rate equations for A_1 and A_2 results in the rate equation for ξ , eqn. (30). Since the peak to peak variation of the rate constants Δk_{12} and Δk_{21} are small compared to the mean values $\overline{k}_{12}$ and $\overline{k}_{21}$, the third term in parantheses of the coefficient of ξ in eqn. (30) may be neglected. The solution of the differential equation with constant coefficients is then given by eqn. (31) which describes the response of the reaction number. Insertion of eqn. (31) into eqn. (29) results in the time dependent behavior of the concentrations of species A_1 and A_2. It contains the relaxation from the initial state to the steady state which is reached for $t \geq 3\tau$, where τ denotes the relaxation time. In this simplest case of a reversible reaction τ is the inverse of the sum of the two rate constants, i.e. $\tau = (k_{12}+k_{21})^{-1}$. Modulation experiments are generally started after an initial period of 3τ where relaxation is completed to about 95%. The relevant steady state solution is then given by eqn. (32).

$$\dot{\xi} = -\left(\overline{k}_{12} + \overline{k}_{21} - \frac{1}{2}\left(\Delta k_{12} + \Delta k_{21}\right)\cos \omega t\right) \cdot \xi \qquad (30)$$

$$- \frac{1}{2}\left(\Delta k_{12}\left[A_1\right]_0 - \Delta k_{21}\left[A_2\right]_0\right)\cos \omega t$$

$$+ \overline{k}_{12}\left[A_1\right]_0 - \overline{k}_{21}\left[A_2\right]_0$$

It should be noted that the quantity $(k_{12} + k_{21})$ appears as inverse relaxation time τ in the exponentials of the general solution as well as in amplitude and phase angle of the steady state solution eqns. (32) and (33). This fact proves the equivalence of relaxation and modulation techniques.

$$\xi(t) = \frac{\bar{k}_{12}[A_1]_0 - \bar{k}_{21}[A_2]_0}{\bar{k}_{12} + \bar{k}_{21}}\left(1 - \exp\left(-\left(\bar{k}_{12} + \bar{k}_{21}\right)t\right)\right)$$

$$+ \frac{\left(\bar{k}_{12} + \bar{k}_{21}\right)\left(\Delta k_{12}[A_1]_0 - \Delta k_{21}[A_2]_0\right)}{2\left(\left(\bar{k}_{12} + \bar{k}_{21}\right)^2 + \omega^2\right)} \exp\left(-\left(\bar{k}_{12} + \bar{k}_{21}\right)t\right)$$

$$- \frac{1}{2}\left(\Delta k_{12}[A_1]_0 - \Delta k_{21}[A_2]_0\right) \sqrt{\frac{1}{1 + \left(\frac{\omega}{\bar{k}_{12} + \bar{k}_{21}}\right)^2}} \cos(\omega t + \Phi) \qquad (31)$$

for $t \to \infty$ one obtains the stationary solution

$$\xi(t) = -\frac{1}{2}\frac{\bar{k}_{12}[A_1]_0 - \bar{k}_{21}[A_2]_0}{\bar{k}_{12} + \bar{k}_{21}} \cdot \sqrt{\frac{\left(\Delta k_{12}[A_1]_0 - \Delta k_{21}[A_2]_0\right)^2}{1 + \left(\frac{\omega}{\bar{k}_{12} + \bar{k}_{21}}\right)^2}} \cos(\omega t + \Phi) \qquad (32)$$

with

$$\Phi = \arctan\left(-\frac{\omega}{\bar{k}_{12} + \bar{k}_{21}}\right) = \arctan(-\omega\tau) \qquad (33)$$

It follows from eqns. (32) and (33) that the product $\omega\tau$ is the relevant kinetic parameter in ME spectroscopy. For $\omega \to 0$ the system is expected to be able to respond immediately to the external stimulation. $\omega\tau = 1$ results in an amplitude damping by a factor of $\sqrt{2}$ (3 dB point), paralleled by a phase shift of Φ = -45°, whereas for $\omega \to \infty$ the amplitude approaches zero and the phase angle Φ = -90°. Consequently, the simple chemical reaction under consideration behaves just like an electronic RC low pass filter.

Of course, the amplitude and phase dependence on modulation frequency becomes more complex for more complicated chemical reaction schemes, however, any scheme features a characteristic amplitude/phase-frequency dependence. As soon as phase resolved ME experiments at different modulation frequencies are available, ME technique will enable a more detailed kinetic analysis of the system then step-excitation (SE) technique (relaxation technique) because of the additional experimental degree of freedom given by the modulation frequency ω.

2 Materials and Methods

2.1 Chemicals and Biochemicals

GPI-anchored AP was isolated and purified with the help of M. Angrand and M. Bortolato (Group Roux, ICBMC, University Claude Bernard, Lyon, France) [77], anchorless AP type VII-NL was purchased from Sigma (P-8647). The result was a 70 µg/ml enzyme solution stored at -18°C in Tris buffer (see below) with a tenside concentration of 5 mM β-octylglucoside (Octyl-ß-D-glucopyranosid, Fluka) in order to prevent oligomerisation and precipitation of the enzyme. Prior to immobilization experiments, the about 3.5 ml of the enzyme stock solution was dialysed in a cellulose bag (molecular weight cutoff ~ 18 kDa) versus Tris buffer for 48 h at 4°C, replacing 750 ml of buffer by a new one about every 12 hours. The dialysed solution being ready for adsorption had a protein content of about 50 µg/ml and a specific activity of 30 U/mg. Commercial anchorless AP was dissolved in Tris buffer to yield the same concentration as the GPI-anchored enzyme.
Mi-CK was provided by T. Wallimann and U. Schlattner (Institute for Cell Biology, ETH Zurich, Switzerland). Aliquots with a protein concentration of about 5 mg/ml were kept at -18°C. Prior to immobilization experiments, the stock solutions were thawed and then centrifuged at 15°C for 15 min with 6000g to separate higher aggregated protein from the octamer. Solution for the adsorption was prepared by diluting the supernatant with phosphate buffer (see below) to give the appropriate concentrations of about 0.5 mg/ml.
As solvents, ultrapure water (Elga) or D_2O from Aldrich was used. The buffer for AP experiments was 20 mM Tris pH 7.4 (or in D_2O pH* 7.0 ≡ pD 7.4) with 0.15 M NaCl, 50 µM $ZnCl_2$ and 0.1 mM $MgCl_2$). Tris(hydroxymetyl)-aminomethane and $MgCl_2$ were products from Fluka, NaCl and $ZnCl_2$ were purchased from Merck. If not otherwise stated, the substrate concentration for activity measurements of AP immobilized or in solution was 10 mM p-nitrophenyl phosphate (p-NPP, Fluka) in Tris buffer. The dye for determination of AP concentration in solution was Coomassie Brilliant Blue G 250 (Fluka) dissolved in 89 % *ortho*-phosphoric acid and 96% ethanol, both purchased from Merck. DPPA and POPC were bought from Fluka and Sigma, respectively.
In case of Mi-CK experiments, CL from beef hart was obtained from Sigma (Lot: 17H8392), phosphocreatine (PCr), ADP, and NADP were purchased from Fluka. As buffer 10 mM phosphate (Na_2HPO_4 and NaH_2PO_4 from Merck) pH 7.0 (or in D_2O pH* 6.6 ≡ pD 7.0) was used, with 50 mM NaCl and 1 mM β-mercaptoethanol (2-ME).
Chemicals and biochemicals were used without further purification.

2.2 SBSR spectroscopy

2.2.1 Introduction

Most FTIR spectrometers are working in the single beam (SB) mode. As a consequence a single channel reference spectrum has to be stored for later conversion of single channel sample spectra into transmittance and absorbance spectra. This technique favors inaccuracy due to drifts resulting from the instrument or from the sample as well as disturbance by atmospheric absorptions. In order to eliminate these unwanted effects to a great extent a new ATR attachment has been constructed, converting a single beam instrument into a pseudo-double beam instrument. The principle features of this attachment are depicted in Fig. 8.

As usually, a convergent IR beam enters the sample compartment. The focal point is now displaced by the planar mirrors M1 and M2 to the new position F, whereas the off-axis parabolic mirror M3 performs a conversion of the divergent beam into a parallel beam with fourfold reduced cross-section. This beam is focused to the entrance face of a trapezoidal IRE by a cylindrical mirror M4. Therefore, the ray propagation in the IRE is still parallel to the direction of light propagation (x-axis), enabling subdivision of the large IRE surfaces (x,y-plane) in perpendicular direction (y-axis) to the light propagation. One half of the IRE is then used for the sample (S) and the other one for the reference (R). Both, S and R, were encapsulated by flow-through cuvettes, independently accessible by liquid or gaseous flow-through. This principle is referred to as *Single Beam Sample Reference (SBSR)* technique. In a first version [3,4] a computer controlled chopper was used to direct the beam alternatively through the sample and reference (Fig. 7). Later on the chopper version has been replaced by the lift version shown in Fig. 8. The cell platform is moved alternatively up and down aligning the sample and reference cuvettes with the IR beam, respectively. The lift version has two significant advantages over the chopper version (i) as it makes use of the full beam of the spectrometer resulting in twice the single channel energy of the chopper version, and (ii) still more relevant for most applications, it compensates the inhomogeneous light flux inherent in most IR spectroscopic instruments.

Thus SBSR absorbance spectra are calculated from sample and reference single channel spectra which have been measured with very short mutual time delay.

2.2.2 SBSR spectra acquisition

The ATR plates applied for all experiments were 50 x 20 x 1 mm^3 Ge trapezoids. An angle of incidence of 45° resulted in 44 internal reflections. IR spectra were recorded with a Bruker IFS 25 FTIR spectrometer equipped with a gold grid polarizer on a KRS-5 substrate and a SBSR-ATR mirror attachment (angle of incidence θ = 45°). A mercurium-cadmium-telluride (MCT) detector was used. All spectra were scanned at 2 cm^{-1} resolution.

2.2.3 Sample manipulation

In the sample part of the SBSR delrin cell (sealed with Viton O-rings) the surfaces (immobilized lipids) were brought in contact with aqueous buffer solutions of sample (AP, Mi-CK) by help of a peristaltic pump and an ismaprene tubing system. Each sample was left in or pumped through the cell until equilibrium was reached. Then the system was washed with buffer. During all steps, the reference part of the sample cell sustained the same procedure with buffer. In order to get the H_2O and D_2O spectra of the proteins in the same SBSR experiment, the immobilized lipids had to be measured with D_2O buffer first, then with H_2O buffer; afterwards, the adsorption of the proteins from aqueous solution took place; the protein solution was then displaced by H_2O buffer that was finally exchanged by D_2O buffer.

2.2.4 Examples

2.2.4.1 HD exchange of creatine kinase

Fig. 9 shows the results of a series of HD exchange measurements performed in the SBSR mode with the enzyme creatine kinase (CK). The enzyme was adsorbed from H2O buffer to a DPPA/CL supported bilayer as described in ref. [56].

The conventional SB spectrum reflects the whole history of the sample, whereas the SBSR spectrum reflects the sample state when compared with a reference of the same age. Therefore, the SB spectrum contains the HDO produced by slight H2O contamination during the experiment in addition to the spectrum of CK. The former obscures the shape of ν(NH) and amide II' bands, which is an obvious disadvantage of the SB mode.

For HD exchange a D_2O buffer solution was circulated through the sample and reference cuvette of the ATR cell during three days. As a consequence slight contamination of D_2O by atmospheric H_2O could not be avoided in the course of this long-time experiment. The resulting HDO gave rise to absorption bands near 3400 cm^{-1} and near 1450 cm^{-1} interfering with NH stretching (ν(NH)) of non-exchanged amide protons, and with amide II' of deuterated amide groups of the protein, respectively. Since in sample and reference contamination by hydrogen is approximately the same due to equal treatment of the circulating D_2O buffer solutions, the HDO absorption bands (ν(OH) and δ(HDO)) will be compensated to a major extent, as demonstrated by Fig. 9, trace SBSR.

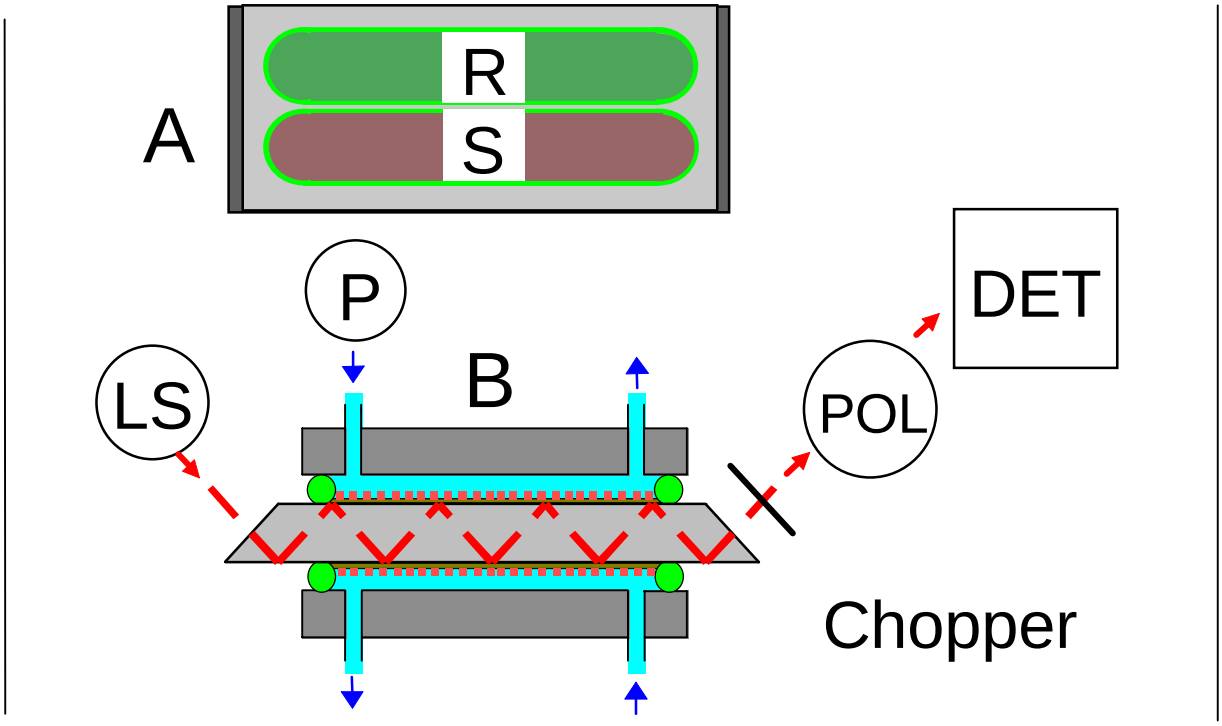

Fig. 7. Single beam sample reference (SBSR) arrangement for a flow through cuvette with two compartments. A) The Ge plate functioning as multiple internal reflection element (MIRE) and support for the membranes is divided into the sample (S) and the reference (R) compartment by the sealing of the cuvette by O-rings. B) A paralleled incident beam from the light source (LS) is focused on the entrance face of the Ge plate. Every reflection is accompanied by absorptions of the membrane and the bulk. A chopper divides the single beam into a sample S and a reference R beam before they pass a polarisator (POL) and impinge on the detector (DET). Solutions and buffers are moved through the compartments by the means of a peristaltic pump (P).

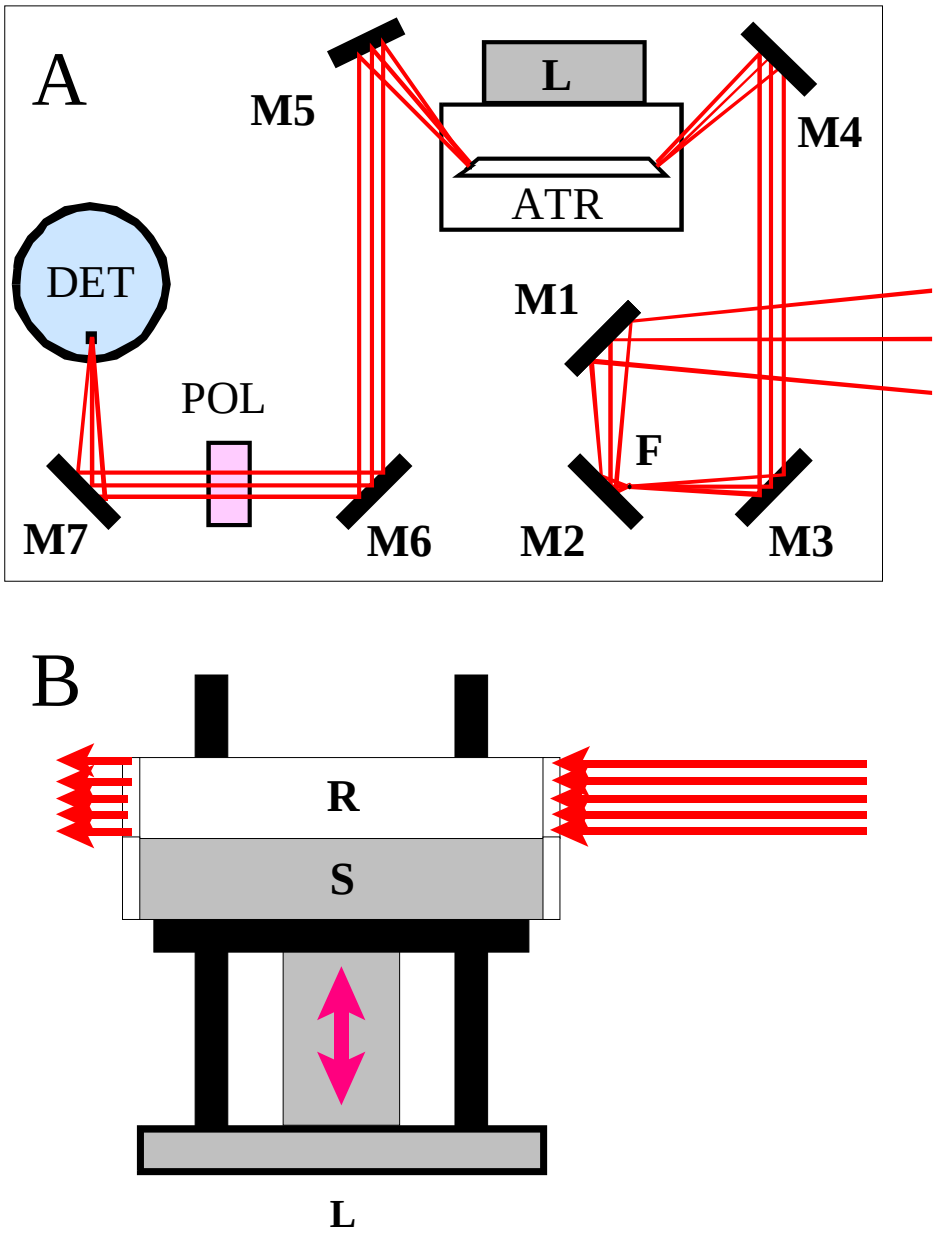

Fig. 8. Single Beam Sample Reference (SBSR) ATR attachment. (A) The focus in the sample compartment is displaced to the position F by the planar mirrors M1 and M2. The off-axis parabolic mirror M3 produces a parallel beam with a diameter of one centimeter, i.e. half of the height of the IRE. The cylindrical mirror M4 focuses the light to the entrance face of the IRE. M5 which has the same shape as M4 reconverts to parallel light passing via the planar mirror M6 through the polarizer POL and being focused to the detector DET by the off-axis parabolic mirror M7. (B) Alternative change from sample to reference and vice versa is performed by computer controlled lifting and lowering of the ATR cell body.

The SBSR trace represents predominately membrane bound CK in a partially deuterated state. The sample consisted of a DPPA/CL/CK assembly, and the reference of a DPPA/CL supported bilayer. Since a sequence of SBSR spectra consists of two independent sequences of single channel spectra, the collected data may by analyzed in the SB mode as well. Doing this by using the single channel spectrum of the sample channel measured in the SBSR mode before CK adsorption (DPPA/CL in D_2O environment in S and R) as reference and a corresponding single channel spectrum after about 12 hours of CK exposure to D_2O buffer as single channel sample spectrum. The resulting SB absorbance spectrum is also presented in Fig. 9, trace SB. Thus SBSR and SB spectra shown in Fig. 9 had exactly the same experimental conditions. To make best use of SBSR data, it is recommended to analyze the data by both modes, SBSR and SB since an unwanted synchronous breakdown of sample and reference assembly, e.g. by hydrolysis of a polymer matrix existing in S- and R-channel, or by equal loss of lipid molecules from a supported bilayer, would be obscured in the SBSR mode, but unambiguously detected in the SB mode.

2.2.4.2 Interaction of an endotoxin with a bilayer

Fig. 10 shows the interaction of an endotoxin (lipopolysaccharide, LPS) from *Pseudomonas aeruginosa* with a positively charged membrane consisting of DPPA (dipalmitoyl phosphatidic acid) as inner and a molar (1:1)-mixture of POPC (palmitoyl oleoyl phosphatidylcholine) and HDPyr (hexadecylpyridinium) as outer leaflet. The reference (R) spectra show the effect of buffer on the bilayer, the sample (S) spectra show the effect of LPS on the bilayer. The SBSR absorbance spectra represent the difference of the effect of LPS and the effect of buffer on the bilayer. There is a loss of ν(CH) (= loss of lipids) only by pumping the buffer over the membrane (R spectra), but at all LPS concentrations (S spectra), the loss of is greater, indicating a specific interaction of the endotoxin (SBSR spectra) with the bilayer.

2.2.4.3 SBSR compensation of a supported bilayer

Fig. 11 shows the spectroscopic compensation of the supported DPPA/(POPC:HDPyr) (1:1 x/x) bilayer by SBSR spectroscopy. In fact, this bilayer represented the basis for the experiment described in 2.2.4.2 and in Fig. 10. It is obvious that the reference (R) part and the sample (S) part of the SBSR cell should be both quite identical before a sample (like endotoxin) is brought in contact with the S part of the system. The SBSR spectrum (Fig. 11), which represents the difference between the S and the R part, can be taken as a proof for the good identicalness of the corresponding bilayers.

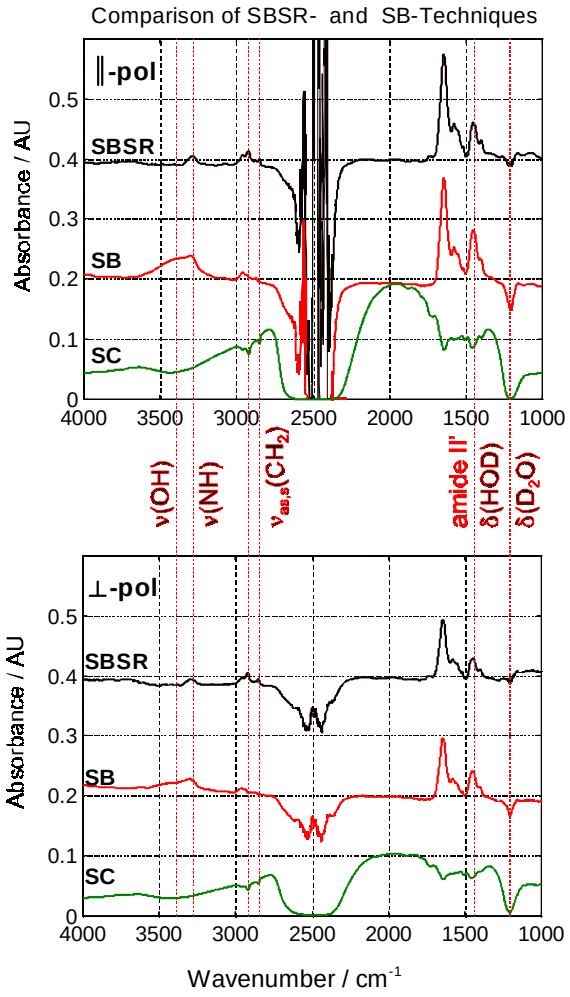

Fig. 9. Comparison of Single Beam Sample Reference (SBSR) pseudo-double beam technique with conventional single beam (SB) technique. Very low energy in the 2500 cm^{-1} and 1200 cm^{-1} region resulted from stretching ν(D2O) and bending δ(D2O) absorptions of liquid D_2O, respectively, as shown by a single channel (SC) spectrum. The supported bilayers in the sample and reference cuvettes consisted of a dipalmitoylphosphatidic acid (DPPA) LB monolayer and a cardiolipin (CL) adsorbed monolayer. Both membranes exhibited the same age, since the LB layer covered the whole width of the IRE, and CL adsorption from vesicles occurred synchronously by two independent equal circuits. In a second step creatine kinase (CK) was adsorbed from a circulating solution in the sample channel [56]. Therefore, the absorbance spectra shown in this figure reflect adsorbed CK as well as any other differences between S and R channel. Obviously, there are more detectable differences in the SB mode than in the SBSR mode, because SBSR reflects the actual difference between S and R, while SB shows the difference between the actual sample spectrum and a stored (older) reference spectrum. In this case, the partly different results obtained in the SBSR and SB mode result predominately from a slow uptake of H_2O vapor by the circulating D_2O solutions. This leads to overlapping of ν(NH) and amide II' of CK, as well as an overcompensation of D_2O absorption bands (~ 2500 cm^{-1} and 1200 cm^{-1}). It should be noted that the slight overcompensation of δ(D2O) at 1200 cm^{-1} is significant, since it reflects the reduced water content in the sample cuvette due to displacement by the CK layer. pp and vp absorbances are in accordance with eqns. (3) and (4), using z_i = 50 Å, z_f = 143 Å, $\varepsilon(\delta(D2O)) = 1.38 \cdot 10^4$ $cm^2 \cdot mol^{-1}$. Ge IRE, angle of incidence, $\theta = 51°$, number of active internal reflections, N = 36.7. The refractive indices were: $n_1 = 4.0$, $n_2 = 1.45$, and $n_3 = 1.30$, see Fig. 5.

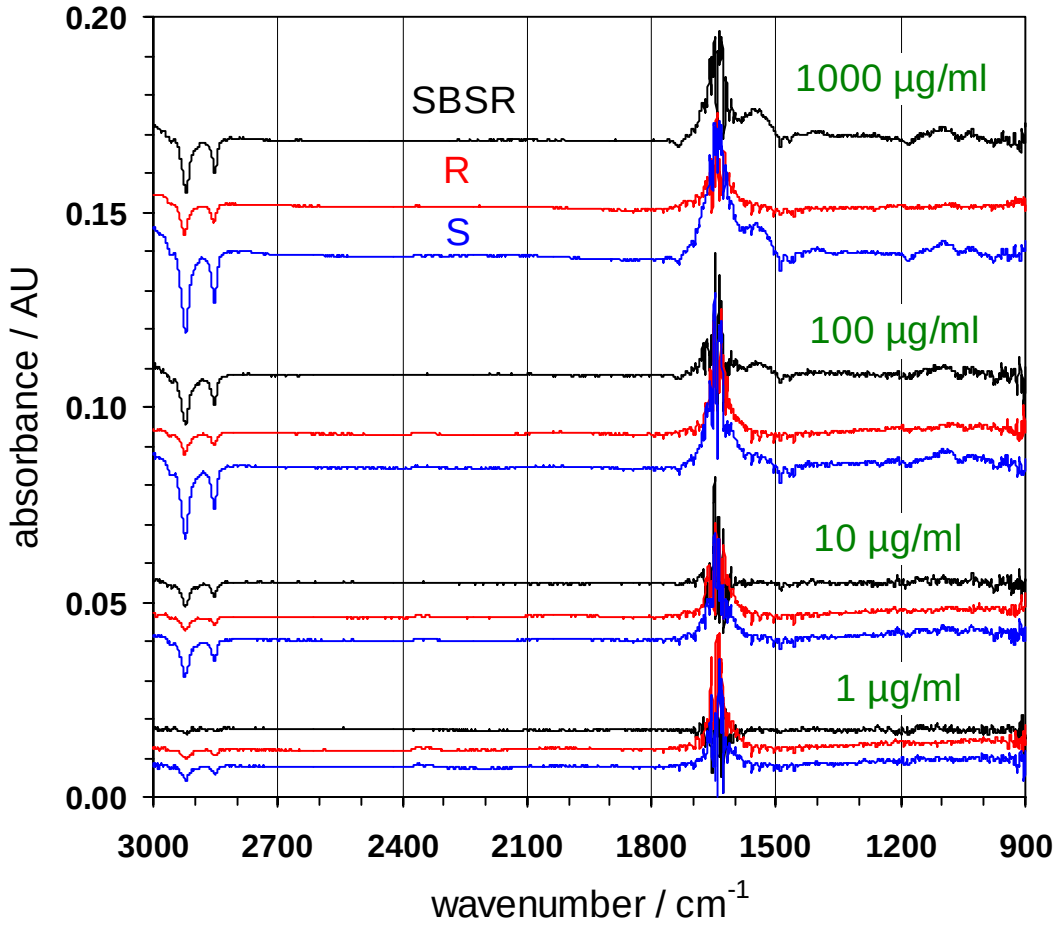

Fig. 10. IR ATR absorbance spectra of a DPPA/(POPC:HDPyr)(1:1 x/x) bilayer after treatment with different concentrations (1-1000 µg/ml) of LPS. ATR parallel (||) polarized light. Buffer: 20 mM phosphate buffer pH 7, 100 mM NaCl. Angle of light incidence $\theta = 45°$; number of active internal reflections N = 33; T = 25°C.
SBSR: SBSR absorbance spectra (S-R). Quasi-simultaneous difference of the effect of LPS and the effect of buffer on the bilayer. R: Reference part. Effect of buffer on the bilayer. S: Sample part: Effect of LPS on the bilayer. The ν(CH) region shows the loss of lipid caused by simultaneous pumping LPS (S) and buffer (R) solution over the bilayer, respectively. At all concentrations, the loss of ν(CH) is greater in the case of LPS. This leads to negative absorbances in the corresponding SBSR spectra.
DPPA, dipalmitoyl phosphatidic acid. POPC, palmitoyl oleoyl phosphatidylcholine. HDPyr, hexadecylpyridinium. LPS, lipopolysaccharide.

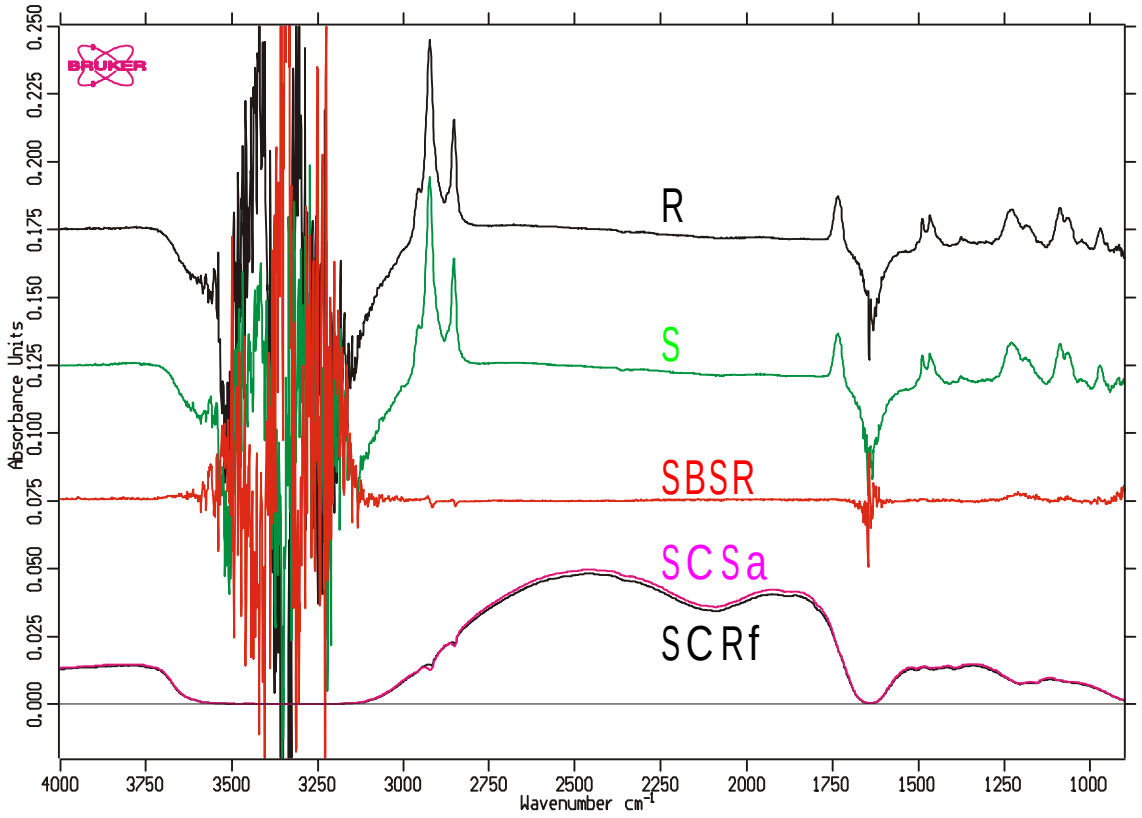

Fig. 11. Spectroscopic compensation of a supported DPPA/(POPC:HDPyr)(1:1 x/x) bilayer by SBSR spectroscopy. SCSa and SCRf: Parallel polarized IR ATR single channel spectra of a POPC:HDPyr (1:1)-monolayer adsorbed tail-to-tail to a DPPA Langmuir-Blodgett monolayer (SCSa) and of the corresponding DPPA Langmuir-Blodgett monolayer (SCRf) before POPC:HDPyr adsorption. Both spectra were taken from the sample compartment of the SBSR cell. R and S: Parallel polarized IR ATR SBSR absorbance spectra of the POPC:HDPyr (1:1)-monolayers adsorbed tail-to-tail to the DPPA monolayer of the sample (S) and to the DPPA monolayer of the reference (R) part of the SBSR cell. The SBSR absorbance spectrum (S-R) shows the difference between the S and R parts of the SBSR cell: The bilayer in the S and R part of the cell seems to be quite identical. Buffer: 20 mM phosphate buffer pH 7, 100 mM NaCl. Angle of light incidence $\theta = 45°$; number of active internal reflections N = 36.6; germanium ATR plate; temperature T = 25°C. For abbreviations see Fig. 10.

2.3 Preparation of supported protein model membrane assemblies

2.3.1 Clean Ge surface

Before a new experiment was begun, each side of the Ge ATR plate was polished by machine (Logitech PM5) with a pellon cloth by means of a 0.25 µm diamond paste, rotating at 30 rpm for 10 min. Subsequently, the plate was subjected to various cleaning procedures, using consecutively acetone, ultrapure water and ethanol, until there were no visible impurities left. Small particles originating from cleansing tissues used in the first cleaning steps were blown off by compressed air. In order to remove small traces of organic compounds, all glassware and ATR plates were finally cleaned 3 minutes by plasma (Harrick Sci. Corp.) before use. The Ge plate was considered to be clean if the $\nu(CH_2)$ bands at ~2920 and ~2850 cm^{-1} disappeared completely in the FTIR ATR spectrum (single beam mode).

2.3.2 Supported bilayers

Model bilayers for *in situ* ATR studies have been prepared according to the LB/vesicle method. The principle steps of this procedure are depicted in Fig. 18.

With the help of a film balance (Nima), the first lipid monolayer of a bilayer model membrane is transferred to the surface of a clean ATR Ge-plate by the Langmuir-Blodgett (LB) technique (Fig. 12) [78,79] at 23 ± 2°C, at a surface pressure of 30 ± 0.2 mN/m and at a withdrawing speed of 2 mm/min corresponding to an area transfer speed of 0.84 cm^2/min. As a result, the polar headgroups of this monolayer, also known as "LB-layer", are attached to the surface of the plate. After LB-layer transfer, see Fig. 18A, the monolayer coated IRE is mounted in an ATR flow through cuvette as depicted by Fig. 19. In all experiments DPPA was used because of its great monolayer stability. After spectroscopic examination of quantity and quality (ordering) of the LB DPPA monolayer a vesicle solution of any phospholipid is circulated through the cuvette. This set up enables direct monitoring of the state of lipid adsorption shown by Fig. 18B.

After about 30 min the state of Fig. 18C is reached. A special washing procedure turned out to be necessary in order to detach loosely bound vesicle fragments. This bilayer, with its polar headgroups oriented towards the aqueous environment, remains stable for several days, even under flowthrough conditions; for that reason, it represents a suitable system for carrying out interaction studies with membrane-active substances. For details, the reader is referred to refs. [4], [6] and [56]. A similar method for preparation of planar lipid matrices used for protein adhesion [80,81] to a solid support has been developed and optimized by Gertrud Puu et al.[82].

The DPPA/DPPA bilayer for CK binding studies was prepared by the LB method: Two layers of DPPA were transferred at 30 mN/m to the Ge avoiding air contact after preparation (see Fig. 20,I).

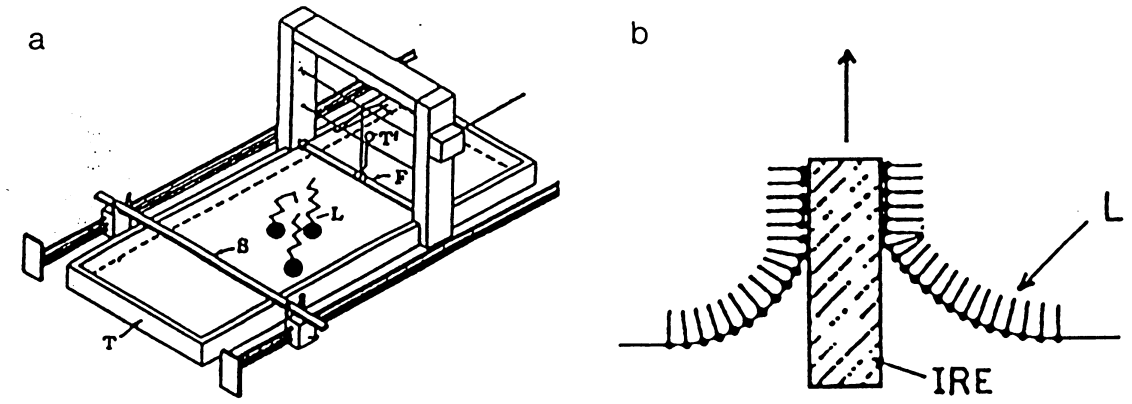

Fig. 12. (a) Film balance: T, trough filled with aqueous subphase; S, sweep for compression of lipid monolayer (L) spread at the air-water interface; F, float connected to torsion wire (T´) for film pressure measurement. (b) Transfer of a compressed lipid monolayer from the air-water interface to a solid substrate (internal reflection plate) by the Langmuir-Blodgett technique.

2.3.3 Membrane anchored alkaline phosphatase

Alkaline phosphatase (GPI-AP) is also a membrane bound enzyme. The binding mechanism of GPI-AP, however, is quite different from that of CK. Native GPI-AP forms a water insoluble dimer where each monomer has one covalently bound glycosyl phosphatidylinositol (GPI) phospholipid molecule. It is assumed that GPI-AP is anchored to a bilayer predominantly via the hydrocarbon chains of GPI, penetrating into the hydrophobic region of the bilayer. Consequently, the reconstitution of a membrane assembly with bound GPI-AP must be expected to be more delicate than with CK. Indeed, the detergent β-octylglucoside (β-OG) which was added in order to solubilize GPI-AP (GPI-AP tends to precipitate in aqueous buffer solutions and needs some detergent for solubilization) has lead to the fist problem, because it destroyed the POPC layer of a DPPA/POPC bilayer nearly completely. FTIR spectra revealed, however, that the spectra of GPI-AP and β-OG appeared at the place of POPC. In a second step it was possible to exchange β-OG by POPC using an aqueous buffer solution with POPC vesicles circulating through the ATR cuvette [56].

2.3.3.1 Isolation and Purification of GPI-AP

Isolation and purification of GPI-AP from bovine intestinal mucosa with the native anchor comprise several extraction and purification procedures in order to get a pure fraction of the enzyme, as there are

·) homogenisation of the bovine intestinal mucosa,

·) centrifugation steps in order to separate and get fractions which are enriched with enzyme

·) extraction of lipids which have to be separated from the enzyme

·) extraction of GPI-AP with the native anchor by a detergent (ß-OG, TX-100)

·) SDS-Polyacrylamide gel electrophoresis to verify the enrichment of GPI-AP with the native anchor in the fractions of the isolation and purification steps

·) affinity and ion exchange chromatography or use of an antibody column to get a very pure fraction of GPI-AP with the native anchor

·) enzyme activity measurements (p-nitrophenyl phosphate-method, see 2.3.3.2) in order to be sure that the catalytic properties of GPI-AP with the native anchor are not destroyed during the several isolation and purification steps and in order to detect the enrichment of the enzyme in the fractions during the purification procedures

·) determination of the protein concentration („Micro-Bradford-procedure“, see 2.3.3.3) to know the amount of protein of each fraction of isolation and purification

·) insertion of the enzyme into lipid vesicles (Liposomat-technique)

2.3.3.2 Enzymatic activity of AP

a Activity measurements of AP solutions

Enzymatic activity was determined from the rate of p-nitrophenol (p-NP) production by ester hydrolysis (Fig. 17) as detected by VIS spectroscopy at 420 nm [83] using a ZEISS diode array spectrometer. The activity of AP in solution was measured by mixing a definite volume V_P of protein solution (e.g. 0.1 ml) with V_S ml of substrate solution (e.g. 2 ml): 10 mM p-nitrophenylphosphate (p-NPP), 25 mM glycine, pH 10.4 (set with 1 M NaOH)). The absorbance was detected at 420 nm for one minute (7 measurements every 8.5 s) at 22°C, resulting in an absorbance difference ΔA/min. One enzymatic activity unit U is defined as the conversion of 1 µmol substrate (here: hydrolysis of p-NPP) per minute. The activity per ml protein solution is given by

$$\text{activity}[\text{U / ml}] = \frac{(\Delta A / \text{min}) \cdot (V_S + V_P)}{V_P \cdot \varepsilon_{p-NP} \cdot d} \qquad (34)$$

$\varepsilon_{p\text{-}NP}$ is the absorption coefficient of the product p-NP at 420 nm: $\varepsilon_{p\text{-}NP}$ = 18.5 cm^{-1} mM^{-1}, d is the thickness of the UV/VIS cuvette (in cm). If the activity (in U/ml) and the protein concentration c_P of a sample solution is known (in mg/ml) (see 2.3.3.3), the specific activity of the protein can be easily calculated:

$$\text{specific activity [U/mg]} = \text{activity [U/ml]} / c_P \text{ [mg/ml]} \qquad (35)$$

b In situ activity measurements

The *in situ* activity measurements were carried out by pumping the substrate solution (p-NPP) through a flow-through cuvette over the immobilisate and recording the time-dependent spectroscopic change produced by the enzymatic hydrolysis of the substrate with a.) the help of a UV/VIS spectrometer and b.) with FTIR ATR spectroscopy. A generalized scheme for carrying out *in situ* activity measurements is shown in Fig. 16.

2.3.3.3 Determination of the protein concentration

This was realized by a method based on Bradford [84] and modified by Read and Northcote [85]. This method takes advantage of the binding of the dye Coomassie Brilliant Blue G-250 to proteins; due to this binding the maximum of dye absorption shifts from 465 nm to 595 nm.

Stock solutions of dye were made with 0.25 g Coomassie Brilliant Blue G-250 in a mixture of 50 ml (= 87.5 g) 89 % H_3PO_4 and 25 ml (= 19.7 g) $EtOH_{abs}$. The dye is very soluble in this mixture and stable indefinitely at room temperature. To produce the dye-reagent solution before the measurements, 2.67 ml (= 4.67 g) 89 % H_3PO_4 and 1.33 ml (=1.05 g) $EtOH_{abs}$ were added to 1 ml stock solution, and this mixture was diluted with water to a total volume of 20 ml (sufficient for 16 samples). A calibration curve (Fig. 13) was made by adding 1.2 ml of dye-reagent solution to 0.8 ml of BSA (Sigma, A-7906) solutions in Tris buffer, containing 0, 2, 4, 8, 12, 16 and 20 µg BSA, respectively. After an incubation time of 10 min at room temperature, the absorbance at 595 nm was determined with a UV/VIS spectrometer. The samples with unknown protein concentrations were treated the same way; the concentrations were determined with the help of the calibration curve.

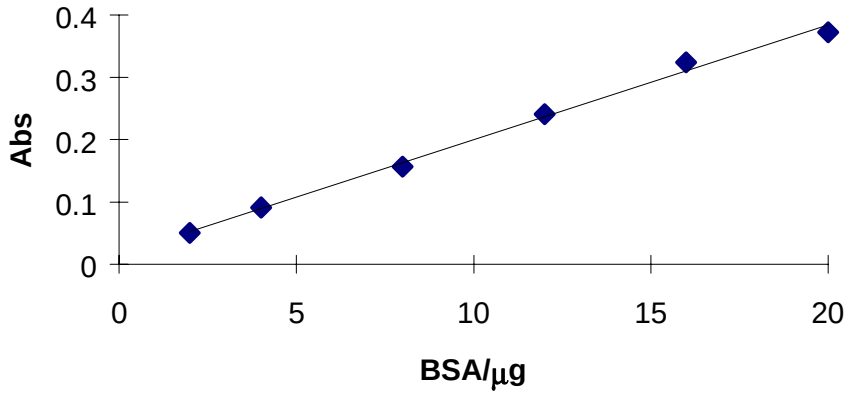

Fig. 13. Calibration curve obtained by the method of Read and Northcote [85] showing the absorbances of 2, 4, 8, 12, 16 and 20 µg BSA at 595 nm. If the total amount of the investigated enzyme is in that range, the enzyme concentration can be easily determined by interpolation.

2.3.3.4 Determination of the surface concentration Γ

In order to determine the surface concentrations of the GPI-AP or AP immobilisates in the FTIR ATR experiments, the following consideration was taken into account. The molecular weight of the AP monomer from bovine intestinal mucosa without anchor is 65 kDa (see 2.3.3.7). If a spherical shape and a specific protein volume of 0.72 ml/g is supposed and with 1 Da = $1.66 \cdot 10^{-27}$ kg, the bovine AP-monomer would have a radius of $r = 2.65 \cdot 10^{-7}$ cm (diameter $d = 5.30 \cdot 10^{-7}$ cm) and an area requirement of $r^2\pi = 2.21 \cdot 10^{-13}$ cm^2 in a densely packed monofilm. Therefore, an AP dimer would have an area requirement of $\cdot 4.42 \cdot 10^{-13}$ cm^2. This results in a maximal enzyme surface concentration Γ_{max} of the AP dimer of $3.76 \cdot 10^{-12}$ mol/cm^2 [= $(6.022 \cdot 10^{23}$ mol$^{-1} \cdot 4.42 \cdot 10^{-13}$ cm$^2)^{-1}$]. This Γ_{max} can be compared with the calculated Γ values of the FTIR ATR experiments. As an example, the determination of the enzyme surface concentration of the experiment depicted in Fig. 27, top, and described in section 2.3.3.5 with the help of the amide I´ band is given in detail. The refractive index of the Ge IRE $n_1 = 4.0$, of the thin film $n_2 = 1.45$ and of the D_2O bulk phase $n_3 = 1.33$. The angle of incidence $\theta = 45°$, the number of active internal reflections N = 36.6, the integrated absorbances between 1594 cm^{-1} and 1715 cm^{-1} are $A_{\parallel} = 3.375$ and $A_{\perp} = 2.078$, the peak maximum of the amide I´ band is at $\tilde{\nu} = 1645$ cm^{-1}. The integral absorption coefficient $\int \varepsilon d\tilde{\nu} = 2.74 \cdot 10^7$ cm/mol was taken from [10] and determined with the antibiotic peptide alamethicin [86]. The thickness of the protein layer is estimated to be the diameter of the protein $d = 5.30 \cdot 10^{-7}$ cm (see above), beginning at $z_i = 2.50 \cdot 10^{-7}$ cm (thickness of the DPPA monolayer lying between the IRE and the protein) and ending at $z_f = 7.8 \cdot 10^{-7}$ cm. The number of functional groups of the dimeric GPI-AP from bovine intestinal mucosa

$\nu = 1038$ (= 2·519, see 2.3.3.7). With these data one obtains with the thin film approximation the following surface concentration of the dimer: $\Gamma = 1.74 \cdot 10^{-12}$ mol/cm^2, corresponding to a surface coverage of 46 % [= 100·(1.74/3.76)].

2.3.3.5 Interaction of GPI-AP with a hydrophobic DPPA monolayer

First, the interaction of GPI-AP with a hydrophobic surface was investigated. With the help of a film balance, a monolayer consisting of dipalmitoyl phosphatidic acid (DPPA, Fig. 15,top) was transferred to the surface of a clean germanium (Ge) plate. GPI-AP solubilized with ß-octylglucoside (ß-OG) was directly adsorbed to the DPPA monofilm. In order to constitute a bilayer-like system, the GPI-AP/DPPA assembly was contacted with a palmitoyl oleoyl phosphatidylcholine (POPC) vesicle solution (Fig. 14, path 2: I,V,VI).

2.3.3.6 Interaction of GPI-AP with a DPPA/POPC bilayer

Second, the interaction of GPI-AP with a supported lipid bilayer was investigated. As model membrane, a DPPA/POPC bilayer was prepared using the Langmuir Blodgett (LB)/Vesicle Method[6]. After the transfer of DPPA mentioned above, the second layer consisting of POPC (Fig. 15,bottom) was produced by spontaneous adsorption to the hydrophobic DPPA monofilm from a vesicular solution. Finally, GPI-AP solubilized with ß-OG was directly adsorbed to the bilayer (Fig. 14, path 1: I - IV).
Both the formation of the GPI-AP/DPPA assembly and the adsorption of the enzyme to the DPPA/POPC bilayer were monitored by in situ FTIR ATR measurements.

2.3.3.7 Comparison with anchorless AP

In order to show the influence of the GPI anchor on enzyme adsorption and activity, the above experiments were also carried out with commercial anchorless AP type VII-NL (Sigma, P-8647) the primary amino-acid sequence of which was recently determined [25]. It consists of 519 amino-acid residues of which 52 are acidic (32 aspartic and 20 glutamic amino acids) and 56 are basic (21 lysine, 20 arginine and 15 histidine amino acids). Under denaturing conditions of gel electrophoresis, a single band corresponding to the monomer, with an apparent weight of ca. 65 kDa, was found; the molecular weight of AP under native conditions was estimated by measuring the sedimentation coefficient: A value of about 6.5S was obtained, indicating that native AP was dimeric [87] with a molecular weight of 130 kDa. Plasma emission spectroscopy (Service central d'Analyse, CNRS, Vernaison, France) was used to determine the Zn^{2+} content in the AP. There were about two Zn^{2+} ions per dimer of AP. A FTIR study describing the great thermal and pH stability of AP is also found in [87].

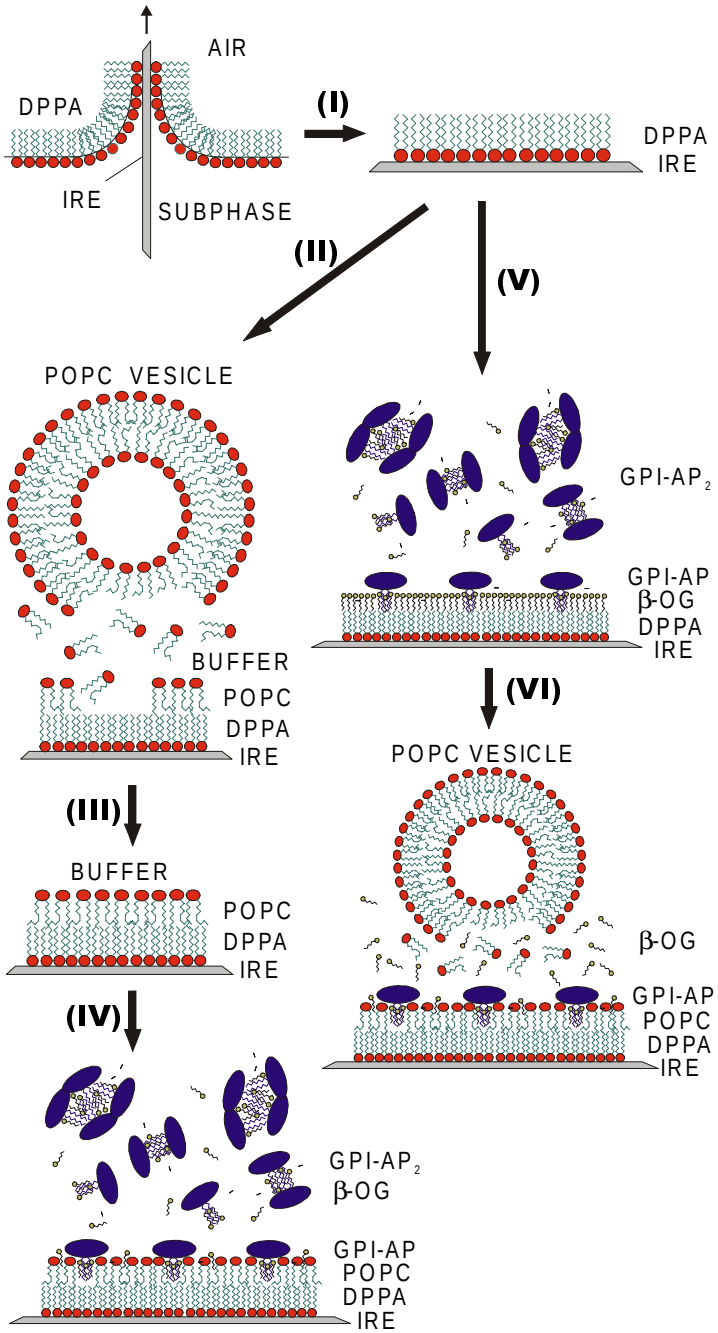

Fig. 14. Schematic description of two pathways for immobilizing GPI-AP on lipid model membranes attached to an IRE-plate. **Path 1**: *Immobilization on a DPPA/POPC bilayer*. (I) Transfer of the inner IRE-attached DPPA monolayer from the air/water interface of a film balance to an internal reflection element (IRE) by the Langmuir-Blodgett (LB) technique; (II) spontaneous adsorption of POPC lipid molecules from vesicles energetically driven by the reduction of the unfavorable high energy of the hydrophobic surface of the DPPA monolayer in contact with the aqueous environment; (III) completed asymmetric DPPA/POPC bilayer; (IV) adsorption of GPI-AP (solubilized by β-OG) to the bilayer.
Path 2: *Immobilization of GPI-AP on a DPPA monolayer*. (I) as described above; (V) spontaneous adsorption of GPI-AP (solubilized by β-OG) to the DPPA monolayer; (VI) reconstitution of a bilayer-like system by passing POPC vesicles over the GPI- AP/DPPA-assembly.

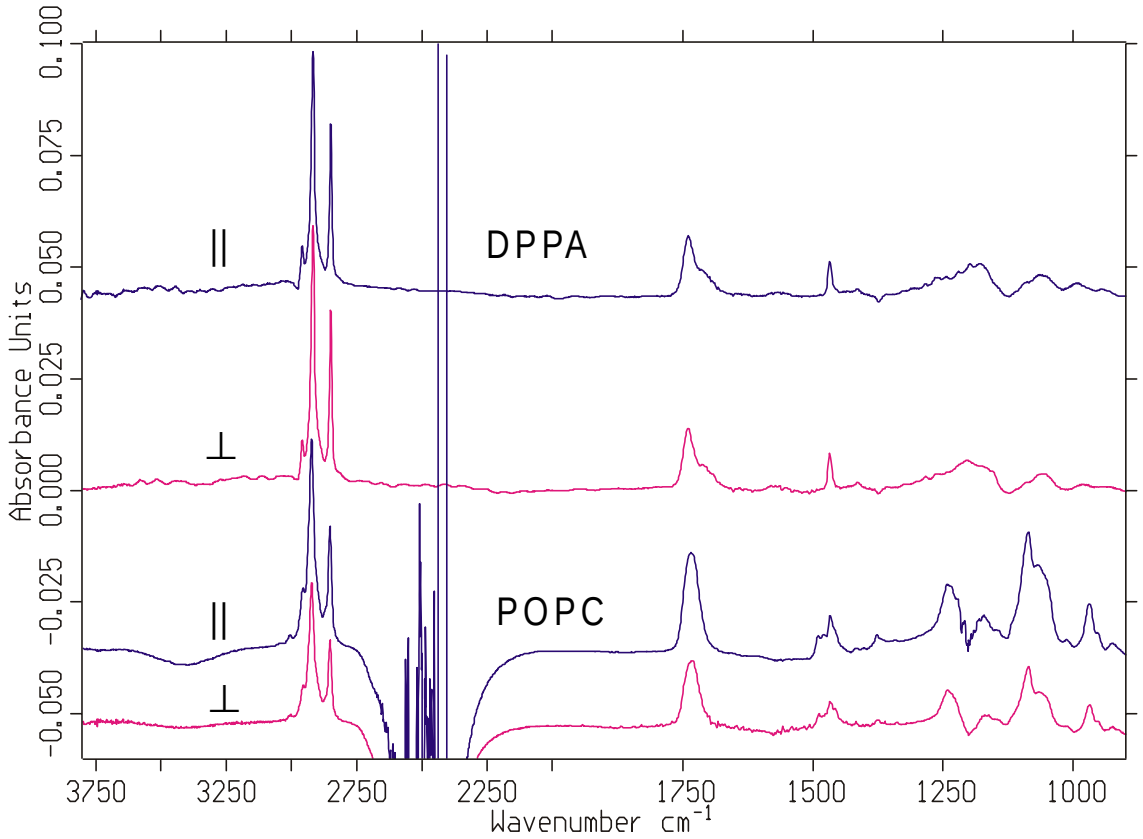

Fig. 15. Parallel (‖) and vertical (⊥) polarized absorbance spectra of DPPA and POPC. **Top**: DPPA transferred at 30 mN/m from aqueous subphase (10^{-4} M $CaCl_2$) to a germanium ATR plate. Spectra were measured against air. Surface concentration was calculated with the thin film approximation: surface concentration $\Gamma = 3.80 \cdot 10^{-10}$ mol cm^{-2}; dichroic ratio R ($A_{\parallel}/A_{\perp}$) = 0.93 (at 2850 cm^{-1}); angle of light incidence θ, 45°; number of active internal reflections N, 39.0. **Bottom**: Polarized IR ATR absorbance spectra of POPC adsorbed on a DPPA monolayer; T, 25°C; reference DPPA monolayer in D_2O Tris buffer; surface concentration $\Gamma = 2.59 \cdot 10^{-10}$ mol cm^{-2}; dichroic ratio R, 1.46; angle of light incidence q, 45°; number of active internal reflections N, 36.6.

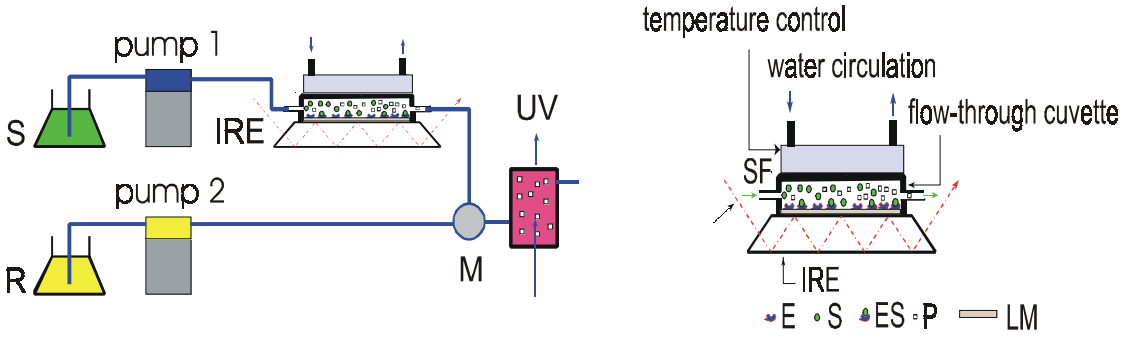

Fig. 16. Schematic setup for IR ATR in situ enzyme activity measurements. **Left**: The substrate (S) is pumped over the enzyme immobilized on the internal reflection element (IRE) and is detected by reaction with reagent (R) to a UV light absorbing product. The temperature is controlled by a thermostatization plate. **Right**: Flow-through cell in detail (E: enzyme, S: substrate, ES: enzyme-substrate complex, SF: substrate flow-through, P: product, LM: lipid membrane).

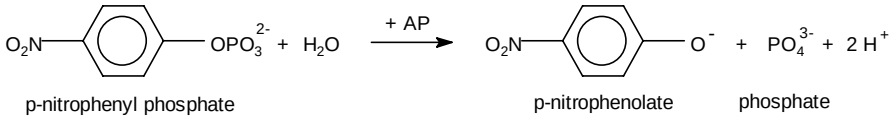

Fig. 17. AP-catalyzed hydrolysis of p-nitrophenyl phosphate (p-NPP) into p-nitrophenolate (p-NP) and phosphate under alkaline conditions.

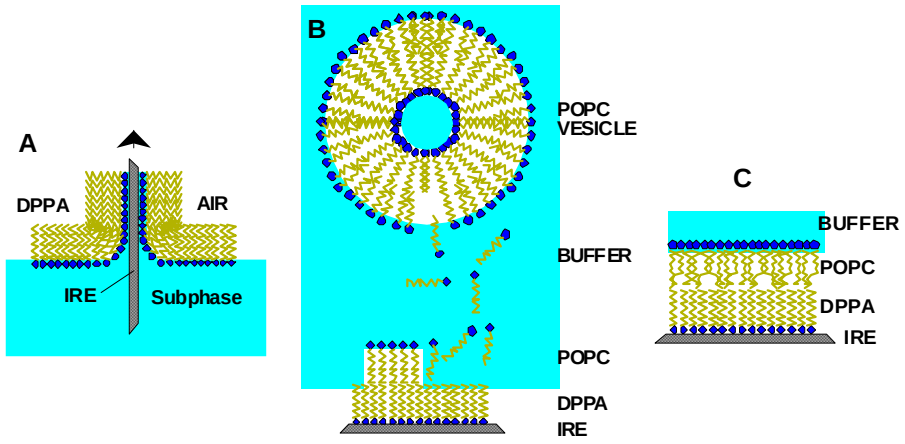

Fig. 18. Supported lipid membrane prepared by the LB/vesicle technique. A: The solid support (IRE) is coated by a lipid monolayer (e.g. DPPA) transferred in the compressed state ($\pi = 30$ mN/m) from the air-water interface of a film balance by means of the Langmuir-Blodgett technique. B: Spontaneous lipid transfer from vesicles (e.g. POPC) to the hydrophobic surface of the LB monolayer occurs by forming a supported bilayer. C: Completed asymmetric bilayer (e.g. DPPA/POPC) in contact with buffer solution.

2.3.4 Membrane bound creatine kinase

Mitochondrial creatine kinase (CK) is a highly ordered octamer. It has nearly cubic shape with an edge of 93 Å [54] and features an accumulation of positive charges at two opposite sides of the cube. Probably one of these sides binds to the membrane surface, predominantly by electrostatic interaction. Therefore, a supported DPPA/CL membrane (CL: cardiolipin) prepared by the LB/Vesicle Method [6]. was used as model membrane where CL formed the outer negatively charged layer of the supported bilayer. With the help of a film balance, the first layer consisting of dipalmitoyl phosphatidic acid (DPPA) (Fig. 15,top) was transferred to the surface of a clean germanium plate. The second layer consisting of negatively charged cardiolipin (CL) was produced by spontaneous adsorption to the hydrophobic DPPA film from a vesicular solution (Fig. 20, III, and Fig. 21,top). Pumping CK through the ATR flow-through cuvette (Fig. 19) lead to a spontaneous adsorption of CK(Fig. 20, IV, and Fig. 21,bottom), also in the case of the DPPA/DPPA bilayer (Fig. 20, II and Fig. 22). The observed surface coverage of 60 % and the kinetics of CK adsorption were in accordance with results obtained by a plasmon resonance study [55].

With the set up shown in Fig. 7 it is possible to observe interactions between reagents and components of the membrane *in situ*. Furthermore, a chopper behind the cuvette splits the beam and allows one to measure sample and reference spectra quasi simultaneously (SBSR-technique).

Fig. 20 visualizes the stepwise preparation of CK membrane assemblies, whereby step by step spectra like Fig. 15 (top, DPPA monolayer) Fig. 22 (DPPA bilayer) and Fig. 21 (top, cardiolipin) can be used to characterize and quantify the results.

Activity measurements: The activity was verified *in situ* by observing the decrease of typical phosphocreatine (PCr) and ADP IR signals when a substrate solution with 20mM PCr and 4mM ADP is pumped through the cuvette. The SBSR absorbance spectra (S-R) display directly the amount of turnover to Cr and ATP.

Interaction with MgADP. 10mM MgADP in 20mM D_2O phosphate buffer pD 7.0 was flushed through both compartments of the cuvette. The SBSR technique records the enzyme-MgADP complex and compensates the MgADP signal (Fig. 31).

Adsorption of Mi-CK on bilayers and Ge. The clean Ge plate resp. the bilayers were exposed to 0.6 mg enzyme /ml solution and the adsorption process was monitored. Afterwards the solution was replaced by buffer and spectra of the immobilized enzyme were measured.

HD exchange of Mi-CK adsorbed on bilayers. D_2O phosphate buffer was pumped into the cuvette and the shift from amide II to amide II´ was observed for several hours. HDO compensation was achieved through the SBSR arrangement (Fig. 32).

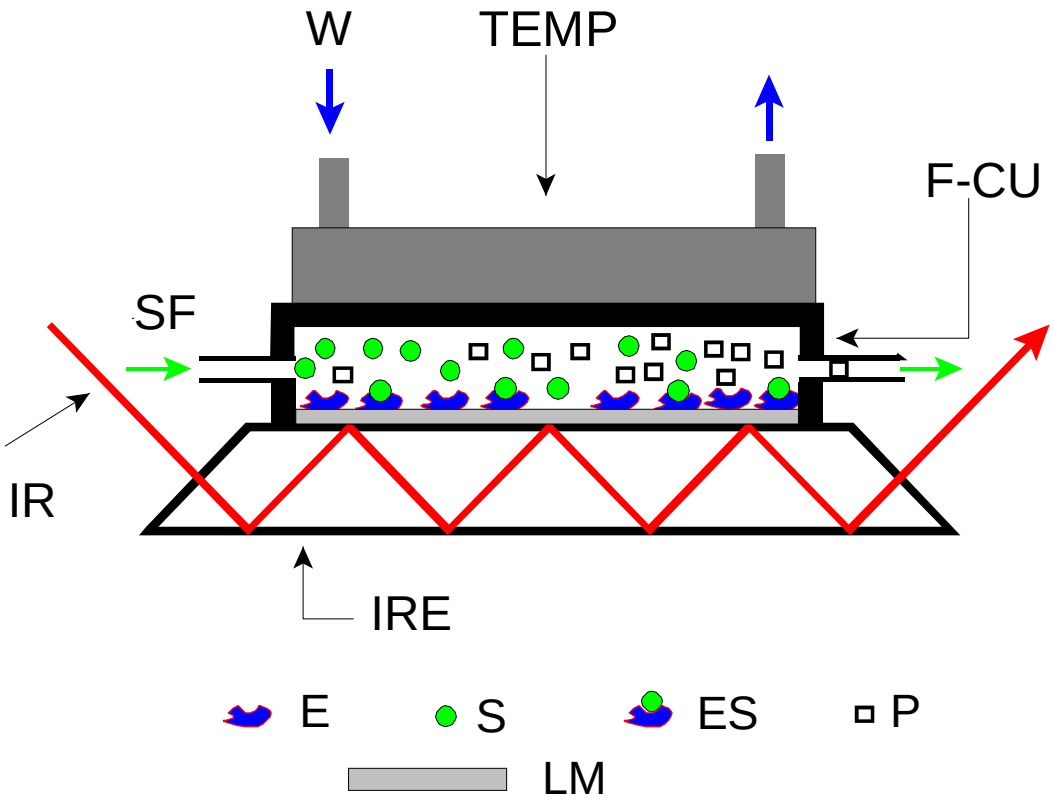

Fig. 19. Flow through cuvette (F-CU) for *in situ* FTIR ATR spectroscopy. The IRE is coated by a supported bilayer (LM) to whom the enzyme (E) is immobilized. The substrate (S) flowing through the cuvette (SF) is enzymatically converted into the product (P).

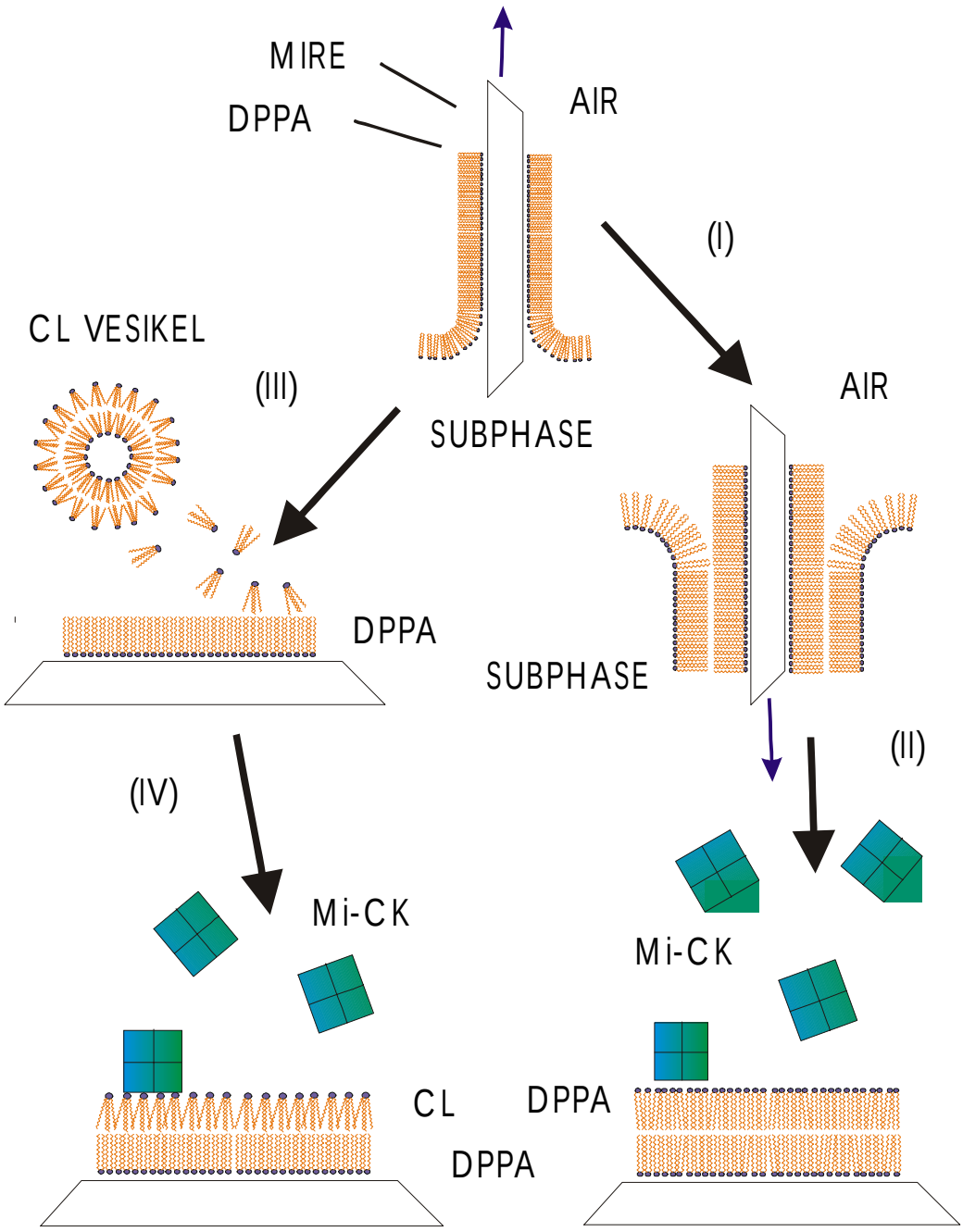

Fig. 20. Schematic description of the two pathways to build up the bilayers used for immobilization of Mi-CK. Both paths start with the transfer of a DPPA monolayer from the air/water interface of a film balance to the Ge plate by the Langmuir-Blodgett (LB) technique. Path 1: The second leaflet is deposited by dipping the plate into the subphase again (I). During every step of further handling contact to air was avoided to assure an intact bilayer for protein adsorption (II). Path 2: (III) Due to hydrophobic interactions CL adsorption occurred from a vesicle solution, spontaneously resulting in an asymmetric bilayer mimicking the mitochondrial membrane. This bilayer was offered to the Mi-CK (IV).

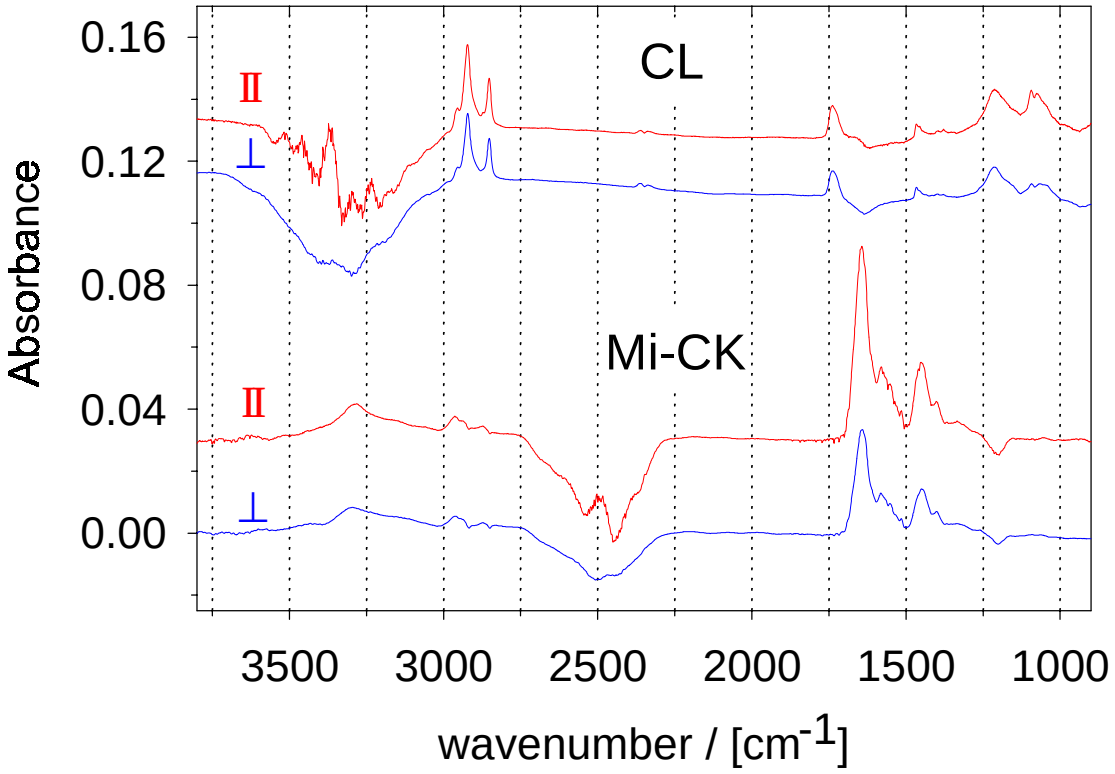

Fig. 21. Polarized IR ATR absorbance spectra of CL and immobilized Mi-CK **Top**: Cardiolipin (CL) from E. Coli assembled from a vesicle solution (0.67 mg CL/ml) on a DPPA-layer. This bilayer was in contact with 20 mM phosphate buffer pH, 7.0; T 18°C; reference, DPPA in phosphate buffer; dichroic ratio R, 1.16; surface concentration $\Gamma = 1.68 \cdot 10^{-10}$ mol·cm^{-2}. **Bottom**: Polarized IR ATR absorbance spectra of Mi-CK immobilized on a DPPA/CL-bilayer in 10 mM D_2O phosphate buffer solution pD 7.0; T, 25°C; reference DPPA/CL-bilayer in D_2O buffer; dichroic ratio R, 1.85; surface concentration $\Gamma = 9.6 \cdot 10^{-13}$ mol·cm^{-2}; Both surface concentrations were estimated with the thin film approximation: angle of light incidence θ, 45°; number of active internal reflections N, 16.

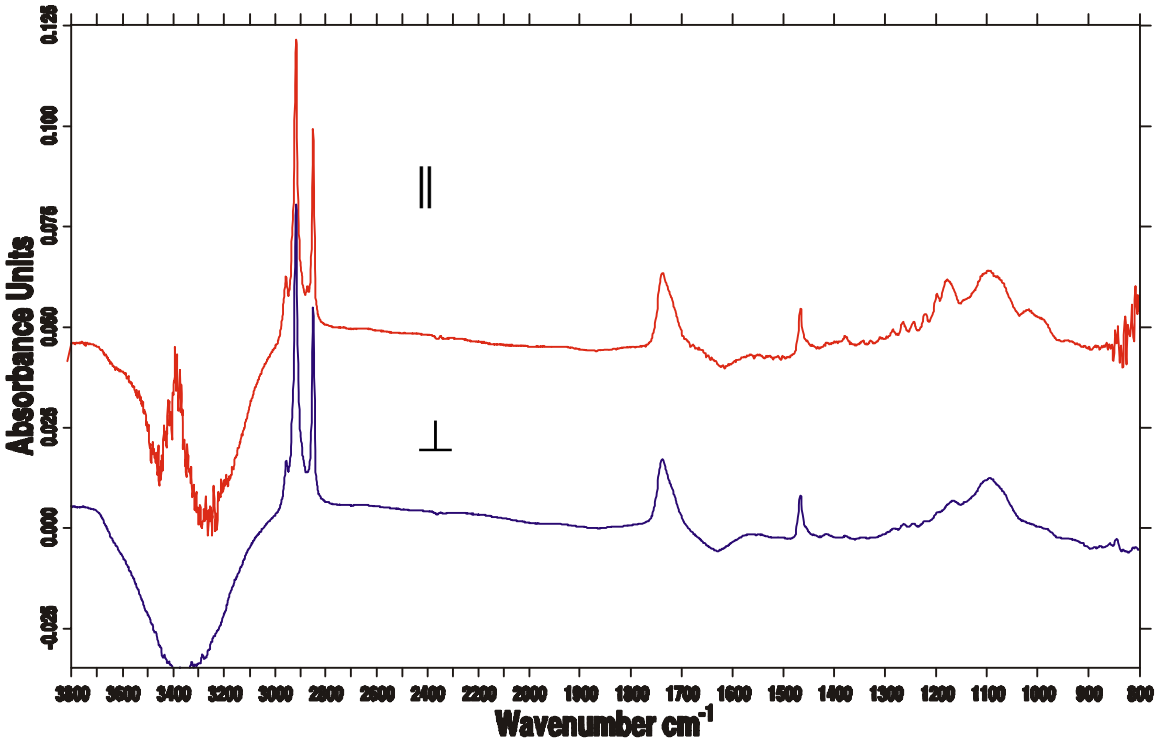

Fig. 22. Parallel (∥) and vertical (⊥) polarized IR ATR absorbance spectra of a DPPA bilayer. DPPA bilayer transferred from an aqueous subphase (10^{-4} M $CaCl_2$) to a germanium plate at 30mN/m with 2 mm/min; 20 mM phosphate buffer pH 7.0, T 25°C; reference: Ge plate and 20 mM phosphate buffer pH 7.0, T 25°C; $\Gamma = 3.5 \cdot 10^{-10}$ mol·cm^{-2}; dichroic ratio R ($A_{\parallel}/A_{\perp}$) = 0.92; angle of incidence θ, 45°; number of active internal reflections N = 28.0.

2.4 ME Spectroscopy

External modulation of a thermodynamic parameter may have a selective influence on the state of a system. In this case those absorption bands of the spectrum which result from stimulated molecules or parts of them are marked with the same frequency. Therefore, the selective response of the system can be detected separately from the unstimulated background. Moreover, if the kinetics of the stimulated process is in the same time range as the external stimulation, phase-lag measurements of modulated absorbances give information about the kinetics of the process and about the sequence of the corresponding reacting species in the reaction scheme.

There are several well-documented kinds of modulation, e.g.:

- Chemical Modulation (modulation of hydration, pH or a relevant substance): e.g. determination of hydration sites of lipids [70].

- Temperature Modulation: study of structural and kinetic details of lipid and peptide phase transitions on a molecular level [69,88].

- Electric Field Modulation: study of electric field induced effects in molecules, such as reorientation, conformational changes and field dissociation effects[72,74].

The principle set up for a modulated excitation (ME) experiment is depicted by Fig. 23. In contrast to relaxation experiments where step-excitation (SE) is used ME technique is based on a periodic stimulation. Both techniques give access to the characteristic dynamic quantities of a system, the relaxation constants. The response of SE is a superposition of exponentials, $\exp(-t/\tau_i)$, where τ_i denotes the i-th relaxation time of the system. ME on the other hand results in a superposition of sine waves, $\sin(\omega t + \Phi_i)$ where the phase lag Φ_i is given by $\Phi_i = \arctan(-\omega\tau_i)$, see eqn. (33).

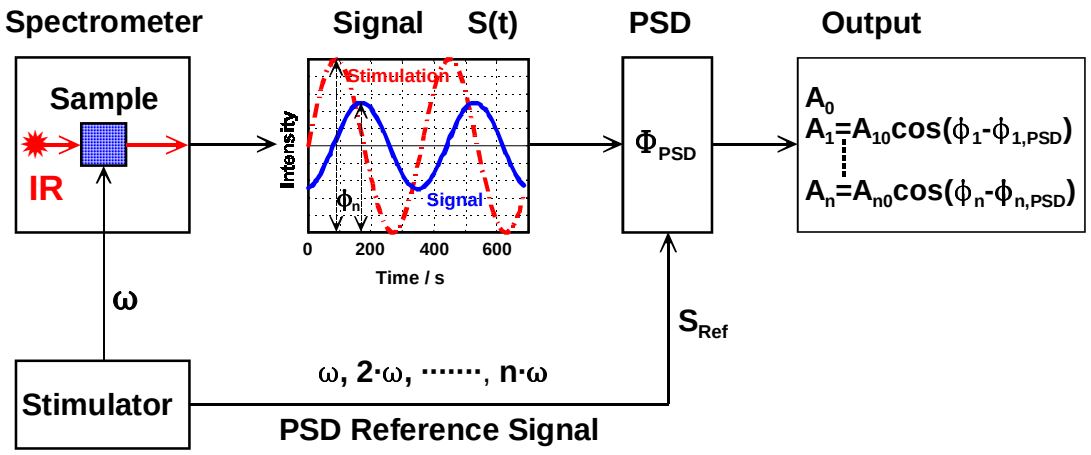

Fig. 23. Schematic set up for modulated excitation (ME) experiments. A periodic excitation is exerted on the sample with frequency ω. The sample response S(t), as sensed by IR radiation, contains the frequency ω and higher harmonics at wavelengths that are significant for those parts of the sample that have been affected by the stimulation. Selective detection of the periodic sample responses is performed by phase sensitive detection (PSD), resulting in the DC output A_n of fundamentals ω (n = 1) and their harmonics nω (n = 2, 3, ...), as well as the phase shifts Φ_n between the n-th harmonic and the stimulation. This phase shift is indicative of the kinetics of the stimulated process and of the underlying chemical reaction scheme. Since the PSD output A_n (n = 1,2,...,n; frequency n·ω) is proportional to $\cos(\Phi_n - \Phi_{n,PSD})$, absorption bands featuring the same phase shift Φ_n are considered to be correlated, i.e. to be representative of a population consisting of distinct molecules or molecular parts. $\Phi_{n,PSD}$ is the operator controlled PSD phase setting. Because of the cosine dependence, different populations will have their absorbance maxima at different $\Phi_{n,PSD}$ settings, thus enabling selective detection. Moreover, since in the case that $0.1 < \omega\tau_i < 10$ (τ_i denotes the i-th relaxation time of the system and is a function of the rate constants involved in the stimulated process), Φ_n becomes ω dependent, $\Phi_n = \Phi_n(\omega)$. The spectral information can then be spread in the $\Phi_{n,PSD}$-ω-plane resulting in a significantly enhancement of resolution with respect to standard difference spectroscopy and time resolved spectroscopy.

3 Results and Discussion

3.1 DPPA monolayer

3.1.1 Sensitivity of stationary ATR measurements

Commercial multiple internal reflection elements MIRE enable up to 50 internal reflections. This is generally enough for thin layer spectroscopy in the nanometer or even sub-nanometer region. As an example, Fig. 24 shows a dipalmitoyl phosphatidic acid (DPPA) monolayer, i.e. a lipid monolayer of about 2.5 nanometer thickness which has been transferred from the air-water interface to a germanium MIRE by means of the Langmuir-Blodgett technique.

The dominant bands in Fig. 24 result from the stretching vibrations of 28 CH_2-groups of the two saturated hydrocarbon chains of the DPPA molecule. Looking at three resolved weaker bands in order to get an impression of the absorbance to be expected from a monomolecular coverage by functional groups of medium or weak molar absorption. The first is the terminal methyl group of the hydrocarbon chains. The antisymmetric stretching vibration, $\nu_{as}(CH_3)$ absorbs at $\approx$ 2960 cm^{-1}. As concluded from Fig. 24, this monolayer results in an absorbance of about 6 mAU. A weaker band is observed near 1420 cm^{-1} and may be assigned to the bending vibration of the α-methylene groups of the hydrocarbon chains, $\delta(\alpha\text{-CH2})$. Thus an approximate monolayer of α-CH2 groups results in an absorbance of only about 1 mAU. Thirdly, a monolayer of phosphate headgroups results in more intense absorption bands because of the larger transition dipole moment of the polar group. The corresponding absorbancies of PO_3-stretching vibrations in the range 1000-1250 cm^{-1} are within 5 and 10 mAU. Concluding that conventional ATR measurements may enable significant access to bands of about 0.2 to 0.5 mAU which corresponds to 20 to 50 percent of a monolayer of weak absorbers. With 20-40 internal reflections, the detection limit of an immobilized protein lies within 10^{-11} to 10^{-10} mol amino acid residues per cm^2, depending upon the intensity of the chosen marker absorption band.

3.1.2 Quantitative analysis of stationary ATR spectra

The DPPA monolayer spectra shown in Fig. 24 are now used to demonstrate the ease of application of the formalism for quantitative analysis of ATR spectra presented in 1.3.2.

3.1.2.1 Dichroic ratio of symmetric CH_2-stretching

The dichroic ratio according to eqn. (18) was calculated from the integrated absorbancies of the symmetric CH_2-stretching bands, $\nu_s(CH_2)$, using linear baselines as marked in Fig. 24 with lower and upper limits at 2828 cm^{-1} and 2871 cm^{-1}, respectively. The corresponding integrals were found to be $\int A_{\parallel} d\tilde{\nu} = 0.381\,cm^{-1}$ and $\int A_{\perp} d\tilde{\nu} = 0.413\,cm^{-1}$, resulting in $R_{ATR} = 0.923$. This is the relevant experimental quantity.

3.1.2.2 Mean orientation of hydrocarbon chains

Uniaxial orientation, i.e. isotropic distribution of DPPA around the z-axis is assumed. The mean square cosine of the angle between the transition dipole moments of $\nu_s(CH_2)$ of the whole population of CH_2-groups of the molecule (28 groups in hydrocarbon chains, 2 in the glycerol part, slightly shifted in frequency) can be calculated from eqn.(19).

The squares of relative electric field components at the interface (z=0) in medium 2 as calculated from eqn. (9) for $\theta = 45$ degrees, $n_1 = 4.0$ (germanium), $n_2 = 1.5$ (DPPA monolayer) and $n_3 = 1.0$ (dry air) result in $E^2_{0x,2} = 1.991$, $E^2_{0y,2} = 2.133$ and $E^2_{0z,2} = 0.450$. It follows, $E^2_{0\parallel,2} = E^2_{0x,2} + E^2_{0z,2} = 2.441$ and $E^2_{0\perp,2} = E^2_{0y,2} = 2.133$. The dichroic ratio for an isotropic film under these conditions would result in, according to eqn. (17), $R^{ATR}_{iso,2} = 1.144$. Explicit formulae of relative electric field components calculated by means of Harrick's weak absorber approximation are summarized in eqn. (9).

Introducing the experimental value of R^{ATR} and the calculated squares of relative electric field components into eqn. (19), one obtains for the mean square cosine of the angle between transition moment of $\nu_s(CH_2)$ and the z-axis $\langle \cos^2 \alpha \rangle = -0.025$. This value should not be negative because its minimum is zero, however, since it is small, we consider it as to be within experimental and predominately systematic errors. Therefore, we set $\langle \cos^2 \alpha \rangle = 0$, resulting in $\alpha = 90$ degrees. This result requires that all methylene groups of the hydrocarbon chains assume all-trans conformation and moreover, all hydrocarbon chains are aligned normal to the MIRE, i.e. parallel to the z-axis (tilt angle zero degrees). The exact wavenumbers of the symmetric stretching vibration of the 2 CH_2-groups in glycerol are not known. However, overlapping with $\nu_s(CH_2)$ of the hydrocarbon chains is probable. Consequently, also the bisectrice of the glycerol CH2 groups may be concluded to be predominately parallel to the x,y-plane.

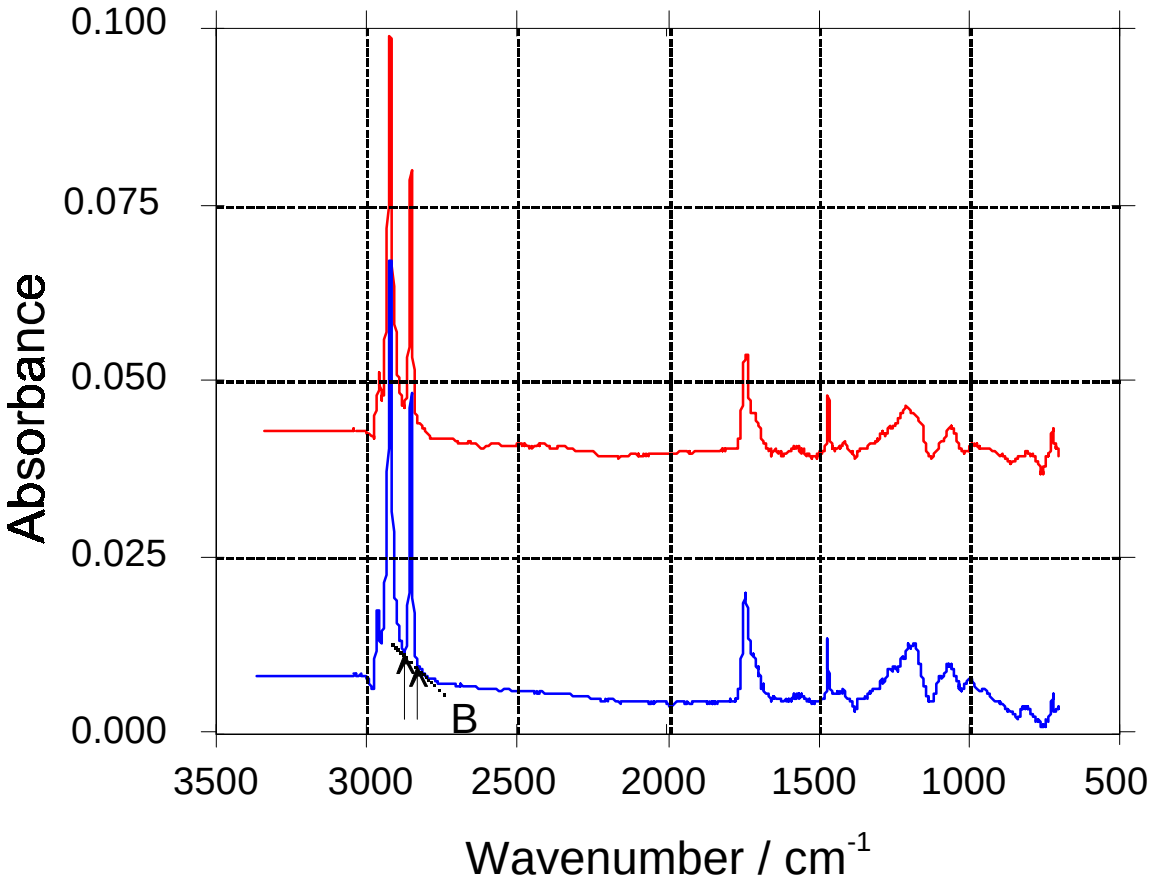

Fig. 24. Parallel (||) and perpendicular (⊥) polarized ATR absorbance spectra of a dipalmitoyl phosphatidic acid (DPPA) monolayer transferred at 30 mN/m from the aqueous subphase (10^{-4} M $CaCl_2$) to a germanium multiple internal reflection element (MIRE). Spectra were obtained from the dry monolayer in contact with dry air. A surface concentration of $\Gamma = 3.60 \cdot 10^{-10}$ mol/cm^2 was calculated by means of eqn. (24) using the dichroic ratio of the symmetric CH_2-stretching vibration at 2850 cm^{-1} with respect to a linear baseline (B), resulting R^{ATR} ($\nu_s(CH_2)$) = 0.923. Angle of incidence $\theta_i = 45°$, number of equal functional groups $\nu = 30$, number of active internal reflections N = 39.0, details see 3.1.2.

3.1.2.3 Mean order parameter of CH_2 groups

The mean segmental order parameter resulting from eqn. (20) is found to be $\overline{S}_{seg}\left(\nu_s\left(CH_2\right)\right) = -1/2$. This value is representative of a perfectly ordered molecular entity with isotropic arrangement of transition dipole moments around the z-axis and perfect parallel alignment to the interface (x,y-plane). It should be noted, that for $\left\langle \cos^2 \alpha \right\rangle = 1$, i.e. transition moments perfectly aligned normal to the interface (z-axis), eqn. (20) results in the upper limit $\overline{S}_{seg} = 1$. Lipids in natural biomembranes consist of a considerable amount of unsaturated hydrocarbon chains. Double bonds cause unavoidably gauche defects in elongated hydrocarbon chains leading to a reduced chain ordering. $\overline{S}_{seg}\left(\nu_s\left(CH_2\right)\right)$ is increased reaching zero for isotropic chain arrangement, since $\left\langle \cos^2 \alpha \right\rangle = 1/3$ in this case.

It should be noted, that the determination of order parameters of individual methylene groups in the hydrocarbon chains requires generally selective deuteration. In this respect comprehensive deuterium NMR work should be mentioned [89].

A more general case of sample geometry is that of a transition moment m being inclined by an angle Θ with respect to the molecular axis a and isotropically distributed around a. Furthermore, the molecular axis a forming an angle γ with respect to the tilt axis t, and being isotropically distributed around it, and finally, the axis t forming a tilt angle δ with the z-axis and being isotropically distributed around it (Fig. 25). In this case, the segmental order parameter, e.g. $S_{seg,i}\left(\nu_s\left(CH_2\right)\right)$, may be expressed as superposition of three uniaxial orientations [6] according to

$$S_{seg} = \left(\frac{3}{2}\left\langle \cos^2 \delta \right\rangle - \frac{1}{2}\right) \cdot \left(\frac{3}{2}\left\langle \cos^2 \gamma \right\rangle - \frac{1}{2}\right) \cdot \left(\frac{3}{2}\left\langle \cos^2 \Theta \right\rangle - \frac{1}{2}\right) \qquad (36)$$

$$= S_\delta \cdot S_\gamma \cdot S_\Theta$$

The angles δ, γ and Θ may be distinct or fluctuating (partly or all), describing a microcrystalline ultrastructure (MCU) and a liquid crystalline ultrastructure (LCU), respectively [4]. S_γ is referred to as molecular order parameter S_{mol}.

Applying eqn. (36) to the DPPA monolayer under discussion, one obtains: $S_\delta = 1$, $S_\gamma = 1$, $S_\Theta = -1/2$, meaning no tilt ($\delta = 0°$), molecular axis (hydrocarbon chain) normal to the interface ($\gamma = 0°$), and transition dipole moment normal to the molecular axis ($\Theta = 90°$).

3.1.2.4 Surface concentration and area per molecule

The surface concentration may be calculated using eqn. (24). The following additional information is required: (i) the integrated molar absorption coefficient related to a linear baseline from 2828-2871 cm^{-1} (Fig. 24) was $\int \varepsilon \, d\tilde{\nu} = 5.7 \cdot 10^5$ $cm \cdot mol^{-1}$, (ii) the real thickness of the layer was assumed to be d = 2.5 nm, (iii) the number of equal functional groups $\nu = 30$, and (iv) the effective thickness d_e for parallel or perpendicular polarized incident light, which have been calculated from eqn. (5) and (21), resulted in $d_{e,\parallel} = 3.97$ nm, and $d_{e,\perp} = 4.30$ nm. The mean surface concentration was found to be $3.60 \cdot 10^{-10}$ mol/cm^2, corresponding to a molecular cross section of 0.462 nm^2/molecule (46.2 $Å^2$/molecule). This value leads to the conclusion that the two hydrocarbon chains of a DPPA molecule predominantly determine the molecular area, since the cross section of an elongated hydrocarbon chain is 20 $Å^2$ [90].

3.1.2.5 Concluding remarks

Quantitative analysis, inclusive orientation measurements has been shown to be straightforward when the formalism based on Harrick's weak absorber approximation (see 1.3.2.3) is applied. For thin adsorbed layers, such as the DPPA monolayer under discussion, the results are quite good. Application to bulk materials may introduce systematic errors. If the weak absorber approximation is still to be applied one should take care to work with an angle of incidence which is at least 15 degrees larger than the critical angle in order to avoid significant band distortions. In many cases it is possible to use quantitative data from transmission experiments to check the validity of the formalism applied to ATR data.

A general critical aspect concerning the baseline selection should be mentioned. A linear tangential baseline has been used for quantitative analysis of the symmetric CH_2-stretching vibration of DPPA (see Fig. 24). Obviously the correct baseline is lower, i.e. the integrated absorbancies used for analysis are systematically too small. The reason for this proceeding is only to enable a well reproduction. While the determination of the dichroic ratio is rather indifferent with respect to the choice of the baseline, it is mandatory to use integrated or peak molar absorption coefficients which have been determined under the same conditions. Even then deviations in the range of several percents may occur among different operators. Finally, it should be noted, that ATR spectroscopy enables very good background compensation, when adequate equipment is used.

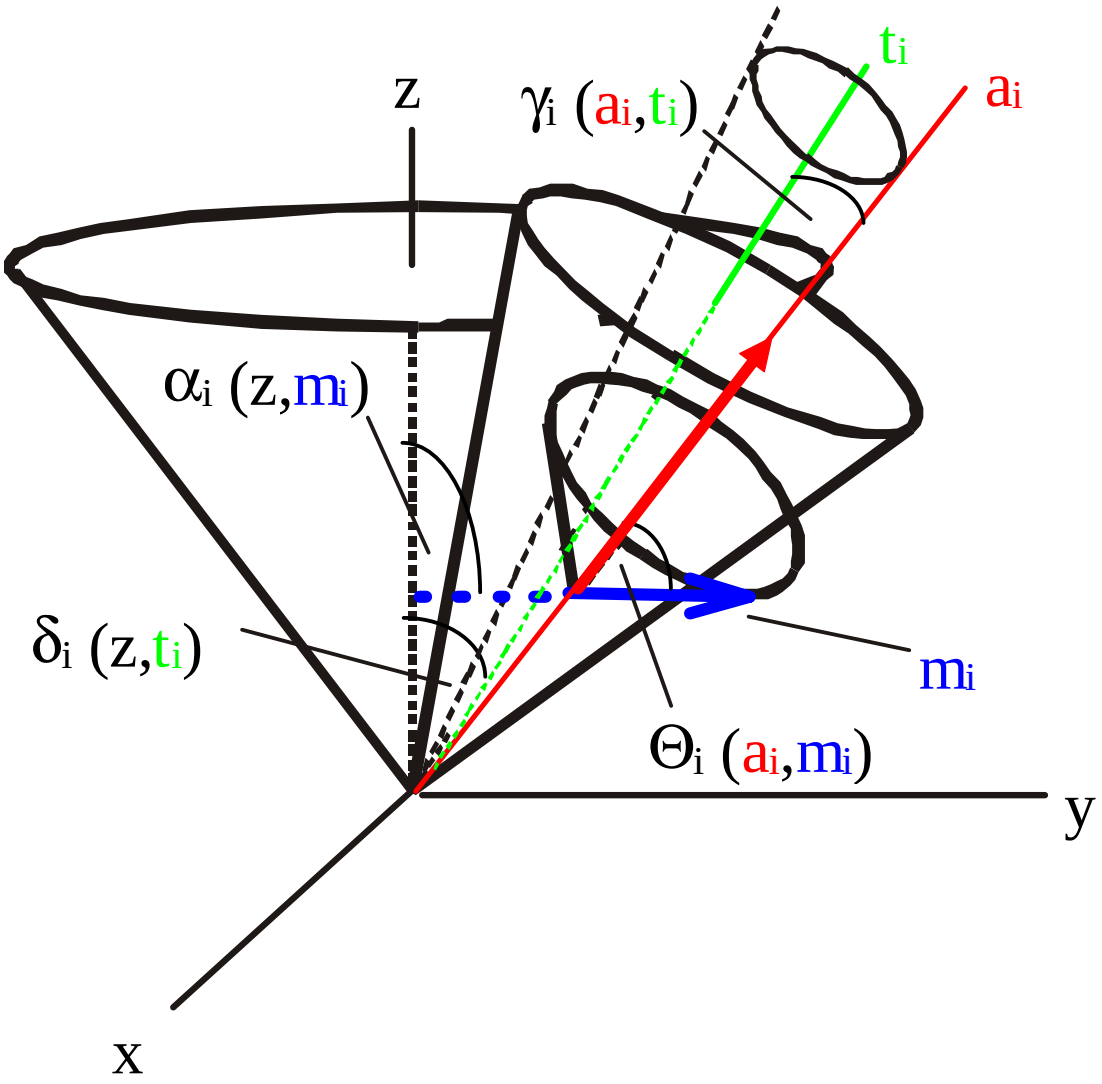

Fig. 25. Superposition of three uniaxial distributions. m_i: instantaneous orientation of the unit vector of the transition moment. a_i: instantaneous orientation of the segmental molecular axis. t_i: tilted average orientation of the molecular axis. Angles: δ_i: tilt angle between z axis and t_i; γ_i: angle between the tilt axis t_i and a_i; Θ_i: angle between a_i and the transition moment m_i; α_i: angle between z axis and the transition moment m_i. By means of polarized ATR spectra the mean angle α between *m* and the z-axis is measured.

3.2 Alkaline phosphatase

Well-ordered assemblies of lipid or lipidlike molecules are important for the success of our binding studies of AP. Therefore, IR ATR absorbance spectra of DPPA (DPPA monolayer, Fig. 14, step I) and POPC adsorbed to DPPA (DPPA/POPC bilayer, Fig. 14, steps II and III) are shown in Fig. 15. The values of the surface concentrations Γ indicate quite tightly packed films and the dichroic ratios R give information about the orientation of the hydrocarbon chains which are more ordered in the case of DPPA.
However, in the case of the enzyme GPI-AP there has to be taken care about the amount of tenside (ß-OG, Fig. 26) present in the original protein sample: If it is too large, GPI-AP will remain solubilized and will not adsorb to a model membrane; if it is too small, GPI-AP will aggregate from the beginning.

3.2.1 Interaction of GPI-AP with a monolayer and with a bilayer

Enzyme adsorption to a DPPA monolayer (Fig. 14, step V) and a DPPA/POPC bilayer (Fig. 14, step IV and Fig. 28, bottom) from a 50 µg GPI-AP/ml 20 mM Tris buffer solution pH 7.4 (catalytic specific activity: 30 U/mg) was performed until saturation was achieved after about 8 hours. The AP adsorption spectra in case of DPPA and DPPA/POPC are depicted in Fig. 27, top, and Fig. 28, bottom, respectively. In contrast to Mi-CK adsorbing to the negatively charged bilayer, GPI-AP exhibits a much slower adsorption process because the lipid-protein-interaction is not of electrostatic nature. It is evident that more enzyme is attached to the monolayer, however, an increase of the ν(CH) bands is seen during GPI-AP adsorption to the bilayer indicating strong interaction with the lipids presumably mediated by the tenside β-OG (for explanation see 3.2.2.2).
The GPI-AP/DPPA-assembly can be completed with POPC molecules (Fig. 14, step VI) yielding a "bilayer"-like structure. Fig. 29 (bottom) shows that the POPC adsorbed to this assembly exhibits the same properties as a pure outer POPC layer on DPPA, except for a less degree of order indicated by the higher dichroic ratio (compare with Fig. 15, bottom). The adsorbed POPC showed a surface concentration of $\Gamma = 1.54 \cdot 10^{-10}$ mol·cm^{-2} which is about 60% of the value of the pure, tightly packed POPC layer in Fig. 15. The quantification of the amide I´-band (1650 cm^{-1})[10] revealed an enzyme surface concentration of $1.74 \cdot 10^{-12}$ mol·cm^{-2} (Fig. 29,top), corresponding to a density of coverage of 46% (see 2.3.3.4).
Both types of immobilization according to Fig. 14 yield catalytically active assemblies for at least three days at room temperature (about 30 U/mg). All these experiments were also carried out with anchorless AP with the same results.

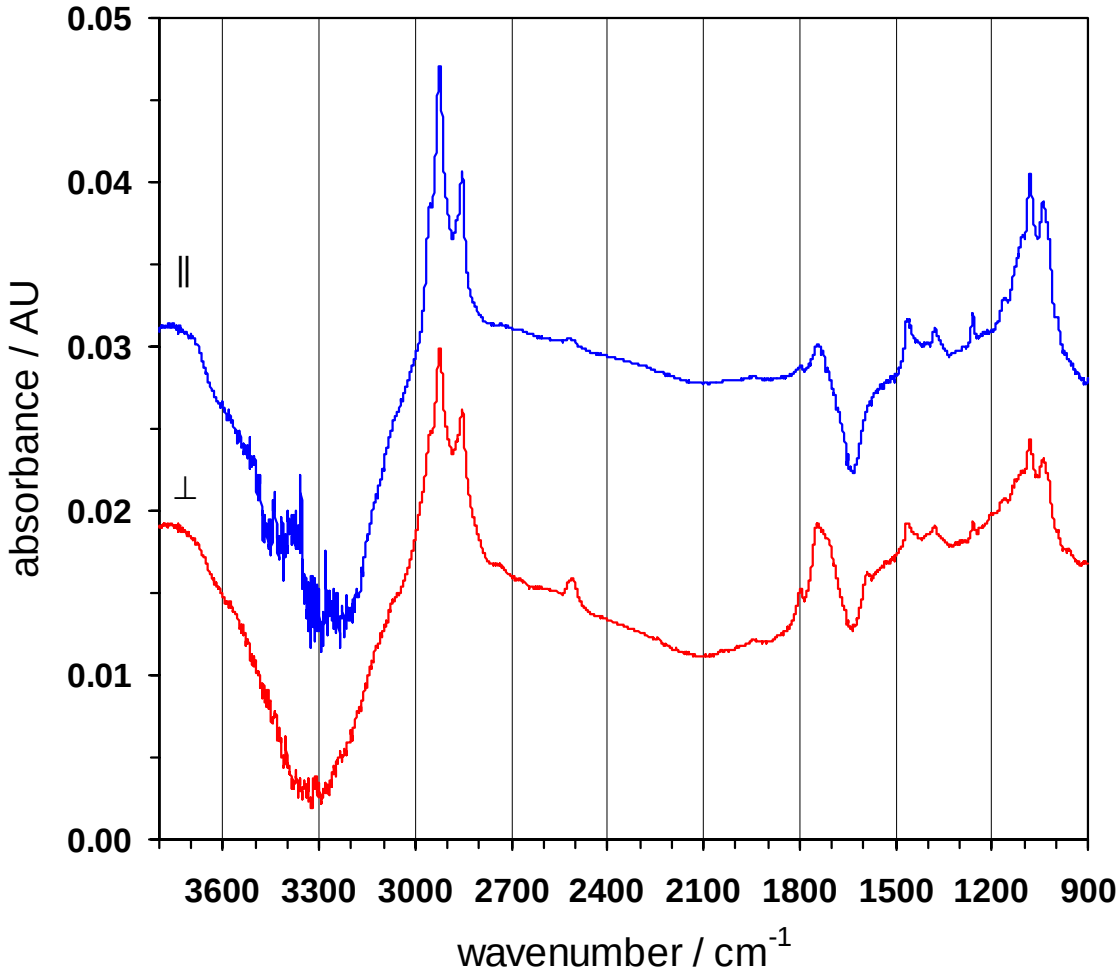

Fig. 26. Parallel (||) and vertical (⊥) polarized absorbance spectra of 11 mM β-octylglucoside in 20mM phosphate buffer pH 7.0, 100 mM NaCl; T 18°C; reference, clean germanium plate in phosphate buffer; angle of light incidence θ, 45°; number of active internal reflections N, 15.5.

3.2.2 Comparison of APs with and without anchor

The native enzyme with GPI anchor is represented by the abbreviation „GPI-AP“, whereas the commercially available enzyme without GPI anchor is termed as „AP“.

3.2.2.1 Interaction of GPI-AP and AP with a DPPA monolayer

As shown in Fig. 27, there is almost no difference concerning the binding of the two enzymes of interest to a DPPA monolayer. This means that the GPI anchor plays no significant role in the attachment of alkaline phosphatase to this hydrophobic monofilm. However, in the case of GPI-AP, additional bands at 3000-2800 cm^{-1} and 1050 cm^{-1} are seen, indicating unambiguously that a considerable amount of β-OG has adsorbed to the DPPA LB layer, too. Anchorless AP interaction (without β-OG) with DPPA exhibits a structural effect of the hydrocarbon chains of DPPA induced by AP binding. The C-H stretching vibrations of the methylene groups at 2850 cm^{-1} (symmetric stretching, $\nu_s(CH_2)$) and near 2920 cm^{-1} (antisymmetric stretching, $\nu_{as}(CH_2)$) exhibit negative bands in the vertical (⊥) polarized spectrum (Fig. 27, bottom, lower trace). However, loss of DPPA should cause negative corresponding bands in the parallel (||) polarized spectrum (Fig. 27, bottom, upper trace), too. This is not the case, but one can observe weak positive bands at slightly higher wavenumbers than those in absorbance spectra of pure DPPA (Fig. 15, top). This effect is indicative of hydrocarbon chains exhibiting gauche defects [91] occurring partly in DPPA chains. Therefore, most probably the reason for all that is not a loss of DPPA molecules, but rather disturbance of the originally very high order [6] in the monolayer evoked by AP binding.

3.2.2.2 Interaction of GPI-AP and AP with a DPPA/POPC bilayer

AP was adsorbed to the DPPA/POPC bilayer from a 150 µg enzyme/ml solution, GPI-AP was adsorbed from a 50 µg enzyme/ml solution, explaining the difference by a factor of 3 concerning the bound amount of enzyme (Fig. 28). Therefore, both enzymes seem to interact similarly with the bilayer. This means that the absence of the GPI anchor does not affect the binding to the DPPA/POPC bilayer. This result corresponds to that obtained in 3.2.2.1. Moreover, as to the interaction of enzyme with the outer layer POPC, analyzing the spectral range 3000-2800 cm^{-1}, essentially the same effects are seen as discussed in 3.2.2.1: Anchorless AP (Fig. 28, top) induces a disturbance of the POPC outer layer upon binding, whereas GPI-AP adsorbs together with β-OG (additional bands at 3000-2800 cm^{-1} and 1050 cm^{-1}). The great signal in the C-H range 3000-2800 cm^{-1} shows that not only β-OG, but also POPC has additionally adsorbed to the GPI-AP-DPPA/POPC assembly. This can be explained by the following supposition: POPC particles had adsorbed onto the flowthrough cell surfaces during bilayer preparation, and β-OG mediated by resolubilization the adsorption of these particles to the enzyme-membrane assembly.

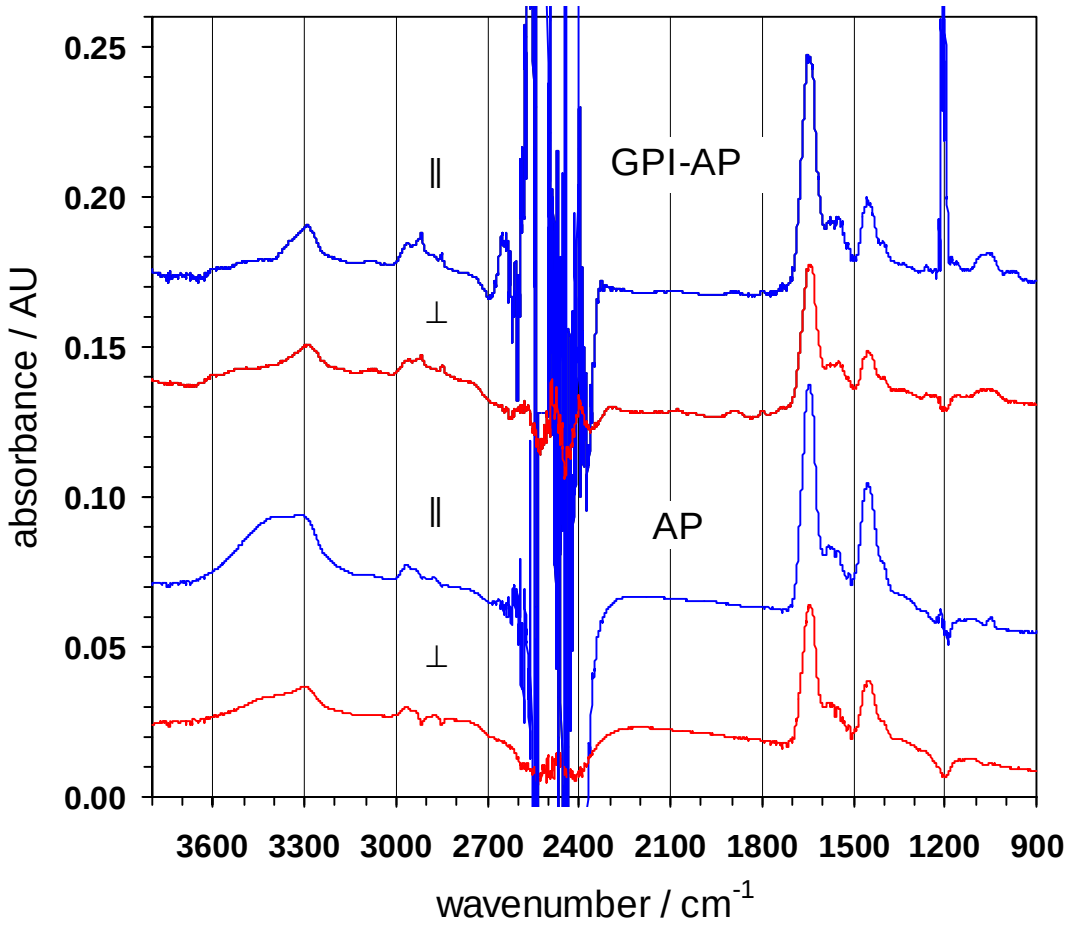

Fig. 27. Parallel (∥) and vertical (⊥) polarized absorbance spectra of GPI-AP and of the anchorless AP immobilized on a DPPA monolayer. **Top**: GPI-AP immobilized on a DPPA monolayer; 20 mM D_2O Tris buffer pH* 7.0 (pD 7.4); T 25°C; reference, DPPA monolayer in D_2O Tris buffer; dichroic ratio R, 1.62 (at 1650 cm^{-1}); surface concentration $\Gamma = 1.74 \cdot 10^{-12}$ $mol \cdot cm^{-2}$; angle of light incidence θ, 45°; number of active internal reflections N, 36.6. **Bottom**: Anchorless AP immobilized on a DPPA monolayer; 20 mM D_2O Tris buffer pH* 7.0 (pD 7.4); T 25°C; reference, DPPA monolayer in D_2O Tris buffer; dichroic ratio R, 1.62 (at 1650 cm^{-1}); surface concentration $\Gamma = 1.65 \cdot 10^{-12}$ $mol \cdot cm^{-2}$; angle of light incidence θ, 45°; number of active internal reflections N, 36.6.

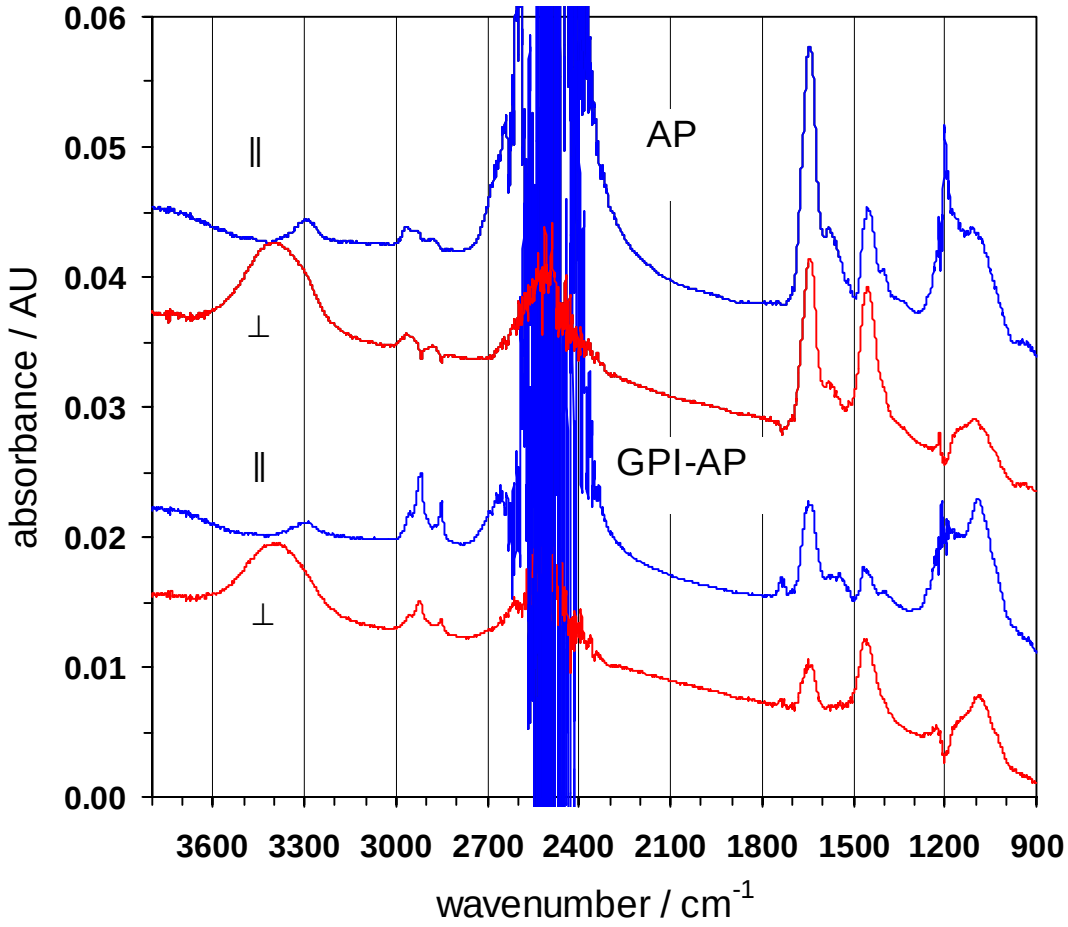

Fig. 28. Parallel (‖) and vertical (⊥) polarized absorbance spectra of GPI-AP and of the anchorless AP immobilized on a DPPA/POPC bilayer **Top**: Anchorless AP immobilized on a DPPA/POPC bilayer from a 150 µg AP/ml solution; 20 mM D_2O Tris buffer pD 7.4; T 25°C; reference, DPPA/POPC bilayer in D_2O Tris buffer; dichroic ratio R, 1.60 (at 1650 cm^{-1}); surface concentration $\Gamma = 4.69 \cdot 10^{-13}$ $mol \cdot cm^{-2}$; angle of light incidence θ, 45°; number of active internal reflections N, 36.6. **Bottom**: GPI-AP immobilized on a DPPA/POPC bilayer from a 50 µg AP/ml solution; 20 mM D_2O Tris buffer pD 7.4; T 25°C; reference, DPPA/POPC bilayer in D_2O Tris buffer; dichroic ratio R, 1.67 (at 1650 cm^{-1});surface concentration $\Gamma = 1.68 \cdot 10^{-13}$ $mol \cdot cm^{-2}$; angle of light incidence θ, 45°; number of active internal reflections N, 36.6.

3.2.2.3 In situ activity measurements

With UV/VIS spectroscopy and p-NPP it is possible to monitor the catalytic activity of the immobilized enzyme (see 2.3.3.2b). The germanium plate with the AP or GPI-AP immobilisate was built into another clean flowthrough cell in order to avoid contamination of enzyme not being attached directly to the germanium. 10 mM p-NPP substrate solution in Tris buffer pH 7.4 was pumped continously over the immobilisate and measured at 420 nm, and in each experiment activity of about 30 U/mg immobilisate was found to be maintained for about three days; this is approximately the same specific activity as in solution before adsorption (see also 3.2.2.4 and Tab. 1).

In order to investigate activity by FTIR ATR, GPI-AP was immobilized in an SBSR cell on the S part of a DPPA monolayer while the R part remained in contact with buffer. Afterwards the S and R compartment were simultaneously filled with substrate solution (250 mM p-NPP). The SBSR spectrum shows the activity of the enzyme, i.e. the conversion of p-NPP into p-NP (Fig. 30). After this maximal conversion which only results in a small IR signal, activity stops because of product inhibition. The substrate solution was exchanged 10 times (1 time per hour), and GPI-AP showed almost the same activity again. Therefore, the immobilisate is quite stable in that time.

3.2.2.4 Summary of results

A summary of the results of the experiments is given in Tab. 1.

Firstly, the DPPA monolayer and the POPC leaflet of the DPPA/POPC bilayer which were used for the experiment, were quite closely packed (surface coverage of about 100%) and stable.

Secondly, the reconstitution experiment of GPI-AP, where GPI-AP was adsorbed to a DPPA monolayer and POPC was added to the GPI-AP/DPPA assembly to yield a bilayer-like structure, showed that the sum of the surface coverages of GPI-AP (line 3 in Tab. 1) and adsorbed POPC (line 4 in Tab. 1) is 105% [= (46 + 59)%]. Within the experimental error-which should not be larger than ± 7 %-this is in good agreement with a complete coverage of the accessible flow through cell area with enzyme and lipid.

Thirdly, there is no significant effect of the GPI anchor detectable concerning the binding of enzyme to the model membrane. Concerning the interaction with DPPA, both enzymes exhibit about the same surface concentrations after adsorption under the same conditions, namely $1.74 \cdot 10^{-12}$ mol/cm^2 for GPI-AP and $1.65 \cdot 10^{-12}$ mol/cm^2 for the anchorless AP (see line 3 and 5 in Tab. 1). Concerning the interaction with a DPPA/POPC bilayer, preliminary experiments showed that the interaction of enzyme with this type of bilayer is considerably weaker than with the DPPA monolayer. Therefore, I started with the 3fold enzyme concentration in the case of commercial anchorless AP (150µg/ml), whereas I did not change the concentration of the GPI-AP fraction (50µg/ml). Because of that, the surface concentrations of the proteins differed by a factor of ca. 3 (0.469/0.168 = 2.8, see lines 6 and 7 of Tab. 1); both enzymes showed only about 10 % surface coverage compared with the corresponding Γ values of the DPPA experiments [GPI-AP: 4.5/46 ≈ 0.1 and AP: (12.5/3)/44 ≈ 0.1, see Tab. 1].

The concentration of the enzyme in solution before and after adsorption was also determined in each experiment, showing that, regardless of the type of model membrane, the loss of protein was about 25% owing to enzyme adsorption not only to the IRE, but also to the other surfaces of the flowthrough system with its cover walls and tubings. The loss of specific activity after adsorption in each experiment was also ca. 25% after 14 hours recirculation of the enzyme solution in order to absorb the protein onto the model membranes.

Tab. 1. Summary of data of the experiments with GPI-AP (with anchor) and AP (without anchor). The surface concentrations and coverages of the lipid model systems DPPA and POPC-being the basis for the enzyme experiments-are also given. For further explanation and interpretation of these data see 3.2.2.4.

				before adsorption			**after adsorption**		
	Sample	surface conc. Γ [10^{-12} mol/cm^2]	cove-rage [%]	enzyme conc. [µg/ml]	act. [U/ml]	spec. act. [U/mg]	enzyme conc. [µg/ml]	act. [U/ml]	spec. act. [U/mg]
1	DPPA monolayer	380	≈ 100	-	-	-	-	-	-
2	POPC of a DPPA/POPC bilayer	259	≈ 100	-	-	-	-	-	-
3	GPI-AP on DPPA monolayer	1.74	46	50	1.5	30	39	0.90	23
4	POPC adsorbed on GPI-AP/DPPA assembly	154	59	-	-	-	-	-	-
5	AP on DPPA monolayer	1.65	44	50	1.3	26	37	0.68	18
6	GPI-AP on DPPA/POPC bilayer	0.168	4.5	50	1.6	32	38	0.92	24
7	AP on DPPA/POPC bilayer	0.469	12.5	150	4.0	27	116	2.4	21

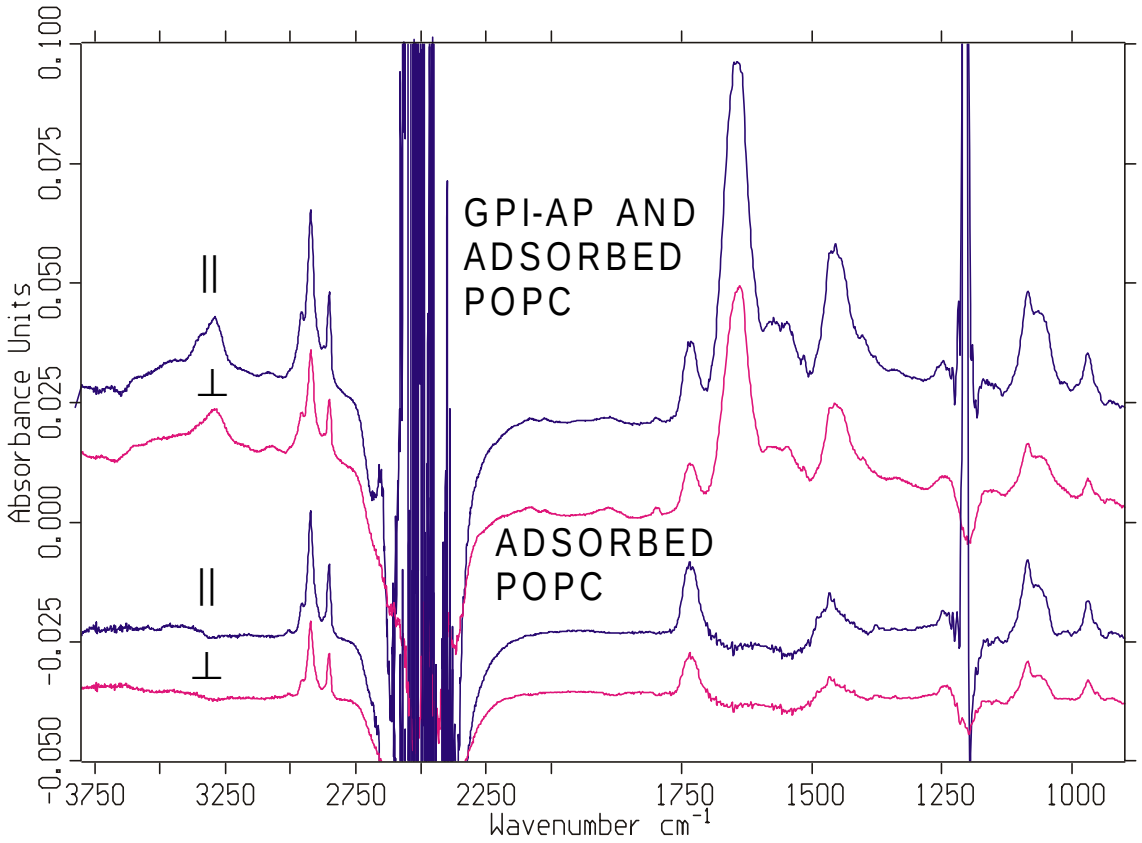

Fig. 29. Polarized IR ATR absorbance spectra of AP after adsorption of POPC and spectra of the adsorbed POPC (cf. Fig. 14, path 2, step VI). **Top**: POPC and AP assembled from a vesicular POPC-solution (0.67 mg/ml POPC) on a DPPA-layer with immobilized AP; 20 mM D_2O Tris buffer pD 7.4; T 25°C; reference, DPPA in D_2O Tris buffer; surface concentration $\Gamma = 1.74 \cdot 10^{-12}$ mol·cm^{-2}; dichroic ratio R, 1.62; angle of light incidence θ, 45°; number of active internal reflections N, 36.6. **Bottom**: Polarized IR ATR absorbance spectra of POPC adsorbed on a AP/DPPA-assembly; T, 25°C; reference AP/DPPA-assembly in D_2O Tris buffer; surface concentration $\Gamma = 1.54 \cdot 10^{-10}$ mol·cm^{-2}; dichroic ratio R, 1.59; angle of light incidence θ, 45°; number of active internal reflections N, 36.6 (cf. Fig. 15 bottom).

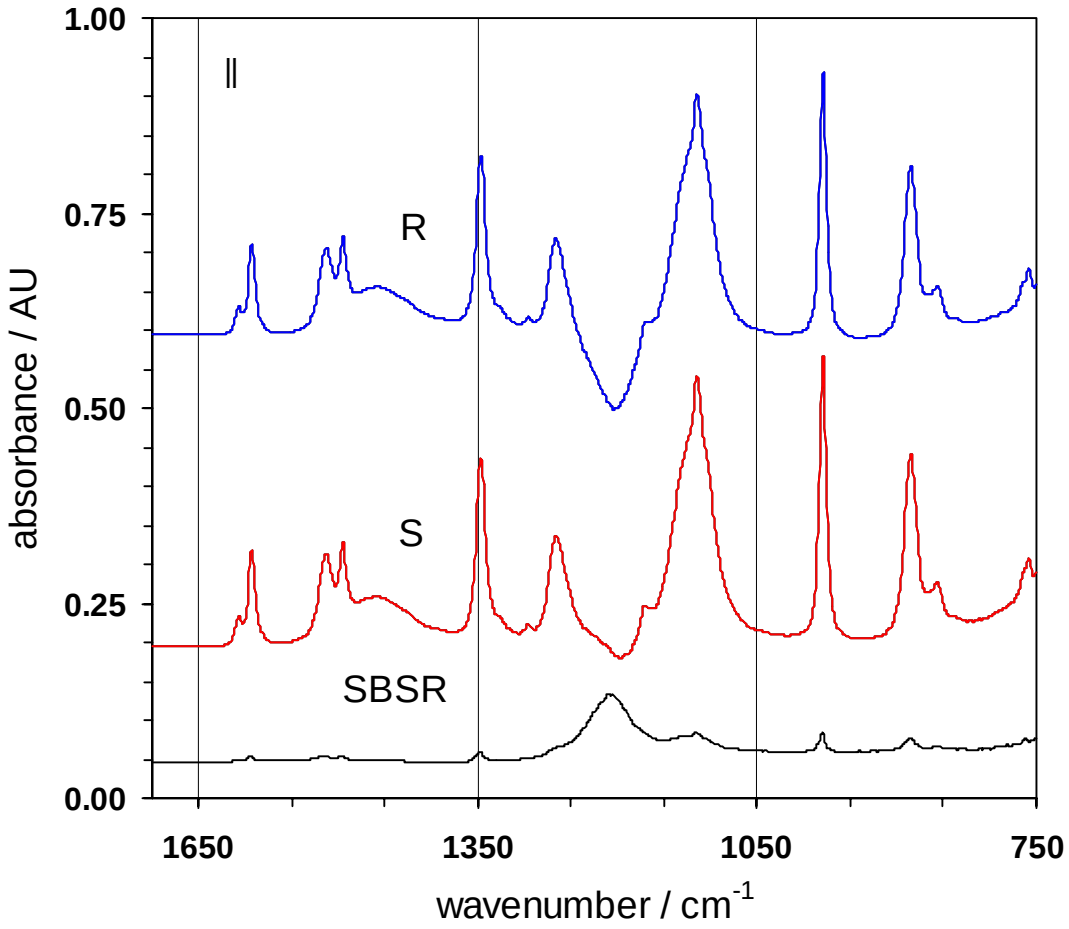

Fig. 30. Polarized IR ATR absorbance spectra of activity measurements of GPI-AP immobilized on a DPPA monolayer. R: Reference part of the cell. IR signal of 250 mM p-NPP in contact with the DPPA monolayer. S: Sample part of the cell. IR signal of 250 mM p-NPP in contact with the GPI-AP immobilized on the DPPA monolayer. SBSR: Difference of the S and R signal resulting in the SBSR trace which represents the enzymatic activity.

3.2.2.5 Concluding remarks

As shown by FTIR ATR spectra and by enzymatic activity data, catalytically active GPI-AP and AP can be immobilized on planar model membranes.

In contrast to the conclusion drawn in [77], there could not be detected any significant difference between the binding of GPI-AP and anchorless AP to supported model membranes. The experiments described in [77] were carried out with POPC liposomes (not with planar model membranes), and about 3% of the liposomal surface were estimated to be covered with GPI-AP after incubation of the protein, being in good accordance with the 5 % in the case of DPPA/POPC bilayer adsorption, but in the case of anchorless AP, no activity was found in the liposome experiments in contrast to the DPPA/POPC bilayer investigations. The protein concentration in the liposome experiment was estimated only by activity measurements owing to the very low enzyme concentrations involved. Because of lack of activity in the case of anchorless AP, it was concluded that this enzyme type exhibited no interaction with the liposomes. In contrast, with the help of FTIR ATR the absorbance signals of both enzymes immobilized on a POPC/DPPA bilayer have been received. Due to that fact one cannot exclude that AP without anchor was also actually attaching to the liposomes in [77] but was for any reason not detected by activity measurements. However, in this study, the presence of the GPI anchor had no influence on the binding and activity of alkaline phosphatase immobilized to model membranes.

Finally, in order to receive more detailed results of structure-function-relationships of AP in lipidic environment, e.g. ME spectroscopy may be an appropriate tool for further investigations.

3.3 Mitochondrial creatine kinase

For the immobilization of Mi-CK a 0.55 mg enzyme/ml solution in phosphate buffer (pH 7.0) was slowly pumped over the DPPA/CL bilayer at 25°C. The process could be monitored *in situ* because replacement occurred in the aligned cell in the sample compartment of the spectrometer by means of a peristaltic pump. As one would expect for an adsorption, driven by electrostatic forces, we found the Mi-CK rapidly binding to the membrane: within 30 min 99% of the process took place. After 1 hour the medium was changed to D_2O (pH* 6.6 ≈ pD 7.0) and the H-D-exchange was monitored. Analysing the amide II and amide II´-bands indicates that Mi-CK is a rather stiff protein. The quantification of the amide I-band (1650 cm^{-1}) [10] revealed a surface concentration of about $1 \cdot 10^{-12}$ $mol \cdot cm^{-2}$, corresponding to a density of coverage of 50-60%. Fig. 21 shows FTIR ATR spectra of the Mi-CK and the outer leaflet of the bilayer consisting of CL. A weak dichroism of the amide I´ band points to a slight distorsion of the Mi-CK structure as determined by X-ray crystallography (point group 422)[54].

Adsorption of Mi-CK on bilayers and Ge. Beside the immobilization of Mi-CK to the negatively charged bilayers, adsorption to Ge was found, too. Evidently from data of Tab. 2, adsorption to the DPPA bilayer ends up in the greatest density of coverage and with the smallest dichroic ratio R for the protein. Compared to the CL/DPPA bilayer, the DPPA bilayer opposes a higher charge density, as can be revealed by a smaller R evolving from a higher order within the DPPA bilayer. This results in a higher protein coverage with better order strongly supporting electrostatic attraction between Lys and Arg and the lipid headgroups as driving force for the adsorption process. Adsorption of Mi-CK to the DPPA bilayers does not change their dichroic ratio for ν(CH) stretch indicating that the enzyme is not penetrating and disturbing the DPPA leaflet. Dichroic ratios for ν(CH) stretch of the CL layer increase after adsorption of Mi-CK. The enzyme seems to sink into the more elastic CL leaflet.

Activity control measurements revealed activity loss but proved the preservation of 50% of the initial activity after 115 hours.

HD exchange of the system. The amide II (1550 cm^{-1}), the amide II´ (1450 cm^{-1}) and the NH stretching (3300 cm^{-1}) bands can be used to analyse the flexibility of the protein. The octameric 645 kD Mi-CK is a rather stiff protein and/or possesses inaccessible regions. About 30% of the amide protons are hardly exchanged at all within the duration of experiment of 17 hours (Fig. 32) being in agreement with 33% α-helices observed in X-ray diffraction [54].

Interaction with MgADP. The difference SBSR absorbance spectra shown in Fig. 31 reflect the alterations through binding of MgADP to Mi-CK in protein structure and give an idea of the amino acid side chains involved. The prominent peaks at 1652 cm^{-1} (α-helix) and 1637 cm^{-1} (β-pleated sheet) can be assigned to changes of the secondary

structure, whereas the peaks at 1607 cm^{-1}, 1586 cm^{-1}, 1569 cm^{-1} and 1518 cm^{-1} can be related to side chain absorption of Arg, Asp, Glu and Tyr. The peak at 1627 cm^{-1} reflects changing H-bridges of Asp and Glu [92]. Polarization for the band at 1652 cm^{-1} indicates that an α-helix, with the transition moment rather parallel to the bilayer surface, takes part in the binding of the Mi-CK/MgADP-complex. Data from Lit. [92] are derived from FTIR difference spectra produced with the help of caged substrates. Their photoproducts may interact with the enzyme and it can be sophisticated to separate these effects from the substrate-enzyme binding. Anyway, FTIR ATR and the SBSR technique provide an elegant access to investigation of structure-function relationships like the binding studies of MgADP to Mi-CK.

Tab. 2. Results of Mi-CK adsorption from a 0.55 mg/ml solution to three types of surfaces. The bilayers and the protein layer are characterized by the surface concentration (Γ) and the dichroic ratio R. Surface concentration was calculated with the thin film approximation (angle of incidence $\theta = 45°$). For the lipids the mean head group area (A) and for the protein the mean side length (a) is listed.

surface	**surface characterization**			**characterization of immobilized Mib-CK**			
	Γ [10^{-10} mol cm^{-2}]	R	A [$Å^2$/molecule]	Γ [10^{-12} mol cm^{-2}]	R	a [Å/molecule]	protein coverage [%]
Ge	-	-	-	1.01	1.72	128	53
DPPA bilayer	3.5	0.92	48	1.40	1.63	109	73
DPPA/CL bilayer:				1.05	1.65	126	55
DPPA	3.6	0.93	46				
CL	1.9	1.16	87				

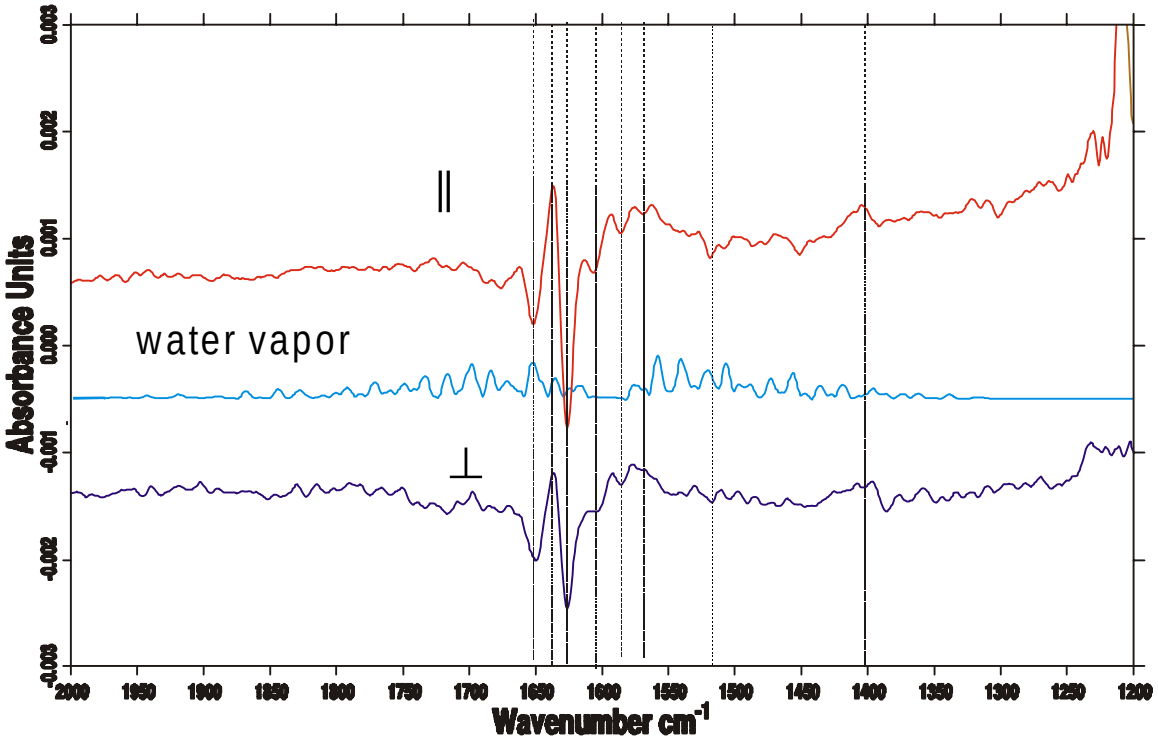

Fig. 31. Difference of SBSR absorbance spectra [Mi-CK/MgADP]-[Mi-CK] parallel (||) and vertical (⊥) polarized. S: Mi-CK on DPPA bilayer; $\Gamma = 0.7 \cdot 10^{-12}$ mol·cm^{-2}; R: DPPA bilayer; for both compartments the bulk was 10 mM MgADP in D_2O phosphate buffer pH* 6.6 (pD 7.0). The lines mark peaks at 1652 cm^{-1},1637 cm^{-1},1627 cm^{-1}, 1607 cm^{-1}, 1586 cm^{-1}, 1569 cm^{-1}, 1518 cm^{-1} and 1403 cm^{-1}, and relate them to the water vapor spectra in the middle.

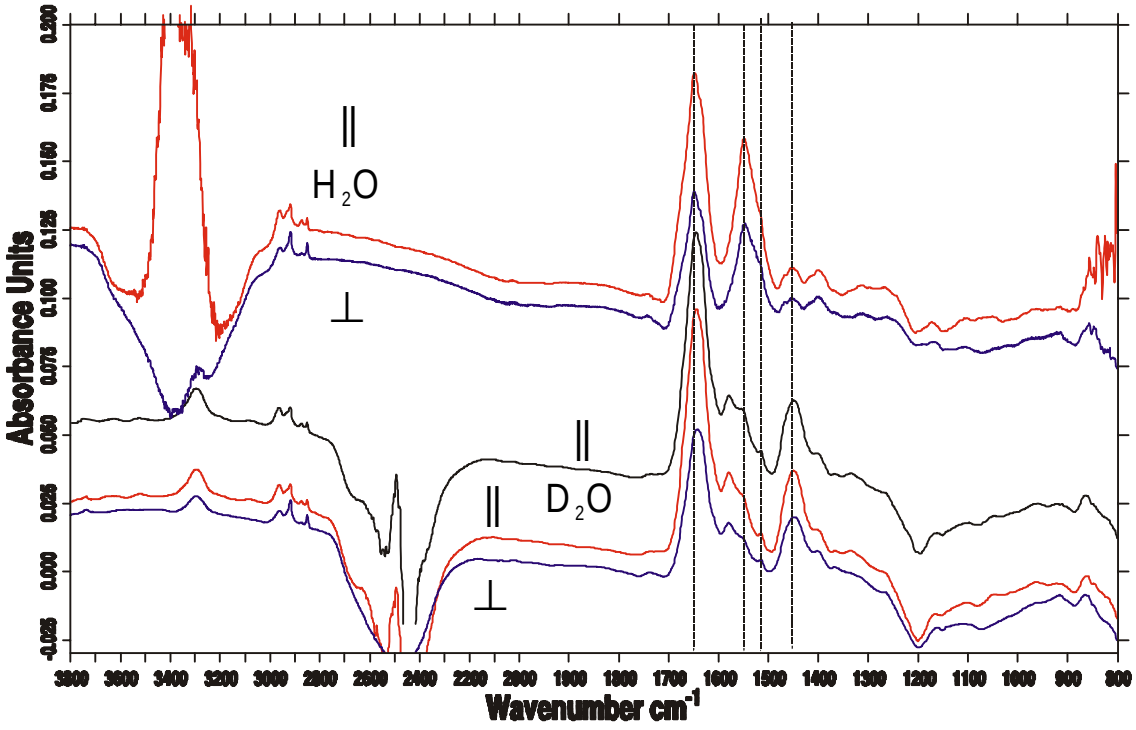

Fig. 32. Polarized IR ATR absorbance spectra of immobilized Mi-CK during the HD exchange. Protein adsorbed from 0.6 mg enzyme /ml solution to a DPPA bilayer. **Top**: H_2O SBSR absorbance spectra (S-R). S: Mi-CK on DPPA bilayer; R: DPPA bilayer; both in 20 mM phosphate buffer pH 7.0, T 25°C; **Middle**: D_2O SBSR absorbance spectrum (S-R) after 2h; **Bottom**: D2O SBSR absorbance spectra (S-R) after 17 h; both compartments with 20 mM phosphate buffer pH* 6.6 (pD 7.0), T 25°C; $\Gamma = 1 \cdot 10^{-12}$ mol·cm^{-2}; dichroic ratio R ($A_{\parallel}/A_{\perp}$) = 1.7; angle of incidence θ, 45°; number of active internal reflections N = 24.5; amide I, amide II, tyrosine (ν C-C ring) and amide II´ band are marked with lines.

3.4 Temperature modulated excitation (T-ME) experiments

3.4.1 The α helix to β pleated sheet conversion of poly-L-lysine

A poly-(L)-lysine (PLL) film cast on an ATR plate and hydrated with D_2O (80% rel. humidity, 28°C) was exposed to a periodic temperature variation of $\Delta T/2 = \pm 2°C$ at the mean value of $\overline{T} = 28°C$. The results obtained after phase sensitive detection (PSD) are shown in Fig. 33. Part (A) shows the stationary spectrum and part (B) phase resolved spectra of the system response with the fundamental frequency ω. The numbers indicated on the spectra denote phase difference between the modulated excitation and phase setting at the phase sensitive detector (PSD). The ME spectra shown in Fig. 33B may be expressed by eqn. (37) [60,61].

$$\Delta A\left(\tilde{\nu}.\Phi_{PSD}\right) = \kappa \cdot \sum_{i=1}^{N} \Delta A_{0i}(\tilde{\nu}) \cos\left(\Phi_i - \Phi_{PSD}\right) \qquad (37)$$

$\Delta A_{0i}(\tilde{\nu})$ is the i-th component-spectrum in which each band has the same phase angle Φ_i. Consequently, this set of bands may be considered to be correlated, i.e. to belong to a population of molecules or functional groups featuring the same kinetic response to the external stimulation. In such a population all absorbance bands exhibit a periodic dependence on the PSD phase setting Φ_{PSD}. The amplitudes become maximum for $(\Phi_i - \Phi_{PSD}) = 0°$, minimum (negative) for $(\Phi_i - \Phi_{PSD}) = 180°$, and zero for $(\Phi_i - \Phi_{PSD}) = 90°$ or 270°. Obviously, Φ_{PSD} can be used to sense the phase angle Φ_i of a population of absorption bands, because Φ_{PSD} is a parameter under experimental control. The most accurate determination of Φ_i is got by performing a line shape analysis of the phase resolved spectra shown in Fig. 33B, followed by fitting each component according to eqn.(37), see ref.[61].

The first impression on comparing Fig. 33A with Fig. 33B is that modulation spectra are significantly better resolved. The spectral resolution was 4 cm^{-1} for both, stationary and modulation spectra. However, overlap is drastically reduced in the latter, because they contain only absorption bands from species that have been affected by the external stimulation. Furthermore, Fig. 33B shows that not only the intensity but also the shape of phase-resolved spectra is changing with Φ_{PSD}-setting. This is an unambiguous indication of the existence of populations of conformational states featuring different phase angles Φ_i. Extraction of these populations according to eqn. (37) enabled the assignment of transient species in the amide I' and amide II' regions. For details the reader is referred to ref. [61]. Attention should be drawn to a correlation between CH_2 stretching and the secondary structure of PLL which has not been reported so far. The weak absorption bands at 2865 cm^{-1} and 2935 cm^{-1} result from symmetric and antisymmetric stretching of the CH_2 groups of the lysine side chains. They displaced by approximately 3 cm^{-1} towards lower wavenumbers with respect to the corresponding bands in the stationary state (Fig. 33A). This finding is indicative for a conformational change of a hydrocarbon

chain from gauche defects into trans conformations [93], since these bands are correlated with the formation of antiparallel β-pleated sheet structure (amide I' bands at 1614 cm^{-1} and 1685 cm^{-1}). We conclude therefore, that the conversion of PLL from α helix to β sheet is paralleled by a conformational change of the side chain from a bent to an extended structure.

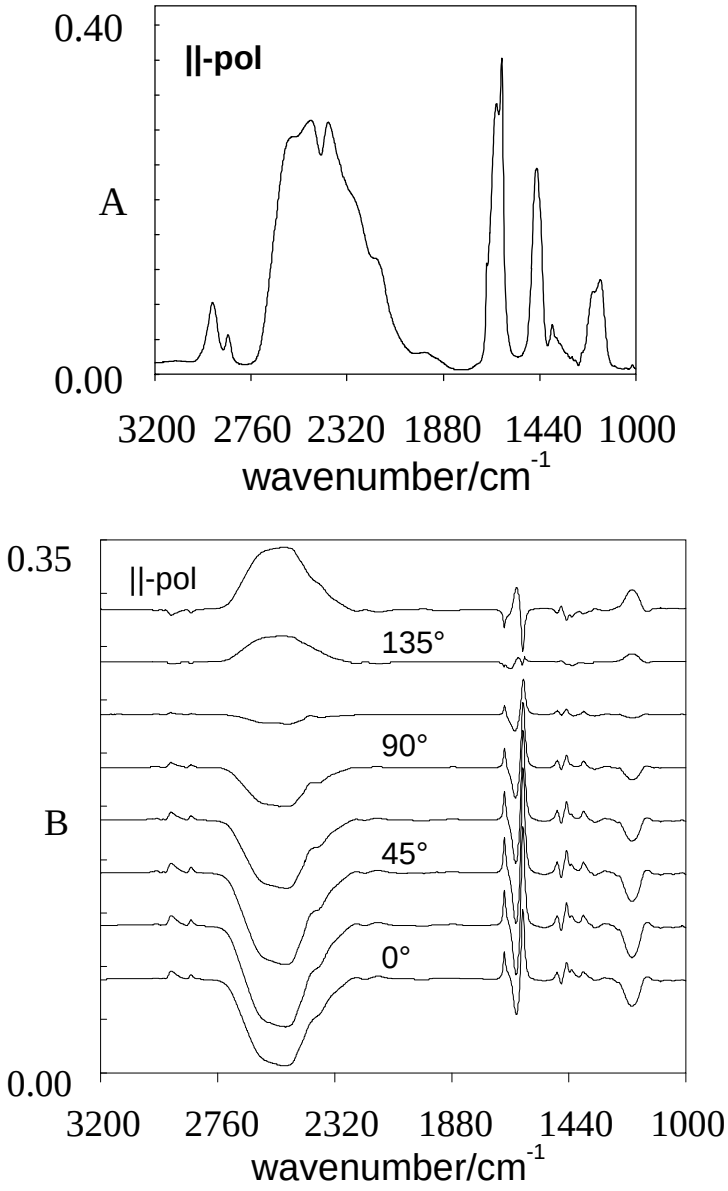

Fig. 33. Parallel polarized T-ME FTIR spectra of a poly-(L)-lysine deuterobromide film hydrated with D_2O (80% rel. hum., 28°C). The film was deposited on a CdTe ATR plate. A rectangular temperature stimulation was applied with a period of 14.7 min ($\omega = 0.427$ min^{-1}) at $\overline{T} = 28°C \pm 2°C$. Angle of incidence: $\theta = 45°$, mean number of internal reflections: N = 9-10. (A) Stationary part of the T-MEIR spectrum of PLL. (B) Set of phase-resolved T-MEIR spectra after phase sensitive detection (PSD) at phase settings $\Phi_{PSD} = 0°$-157.5° (phase resolution 22.5°) with respect to the T-stimulation. $\Phi_{PSD} = 0°$ means in-phase with temperature switching from 26°C to 30°C. Heat transfer from the thermostats to the sample resulted in an additional phase lag of $\Phi_T = 25°$. (From ref. [61]).

3.4.2 Reversible unfolding/folding of RNAse A

Understanding of the molecular mechanism of protein folding and unfolding is of increasing interest not least because of molecular biological approaches to protein synthesis and modifications. RNAse A is an enzyme that may be unfolded/denatured by heating and refolded/renatured upon cooling. Kinetic FTIR measurements have been reported recently using temperature jump techniques [62,94]. The T-ME experiments were performed in solution. The stimulation amplitude was $\Delta T/2 = 5°C$ at $\overline{T} = 64°C$ with a period of $\tau_m = 25$ s. A sequence of time resolved spectra is shown in Fig. 34. Like in case of PLL there are drastic differences between the modulation spectra and the stationary spectrum (upper trace). As mentioned above modulation spectra suppress any absorbance which is not labelled by the stimulation frequency. Two interesting observations should be mentioned. (i) the corresponding isosbestic points in the amide I' band at 1667 cm^{-1} and in the amide II' at 1435 cm^{-1}, and (ii) the response of a distinct tyrosine population to T-ME. In the modulation spectrum, the tyrosine band appears at 1517 cm^{-1}, whereas in the stationary spectrum the corresponding band is found to be considerably broader with the peak maximum shifted to lower wavenumbers.

As in the case of PLL the shapes of modulation spectra alter with PSD phase setting Φ_{PSD}, indicating that some phase resolution is achieved. The effect, however is less distinct than with PLL. Most probably higher modulation frequencies are required in order to get larger differences in the phase angles Φ_i of different conformational populations. T-ME-experiments at higher frequencies are in progress.

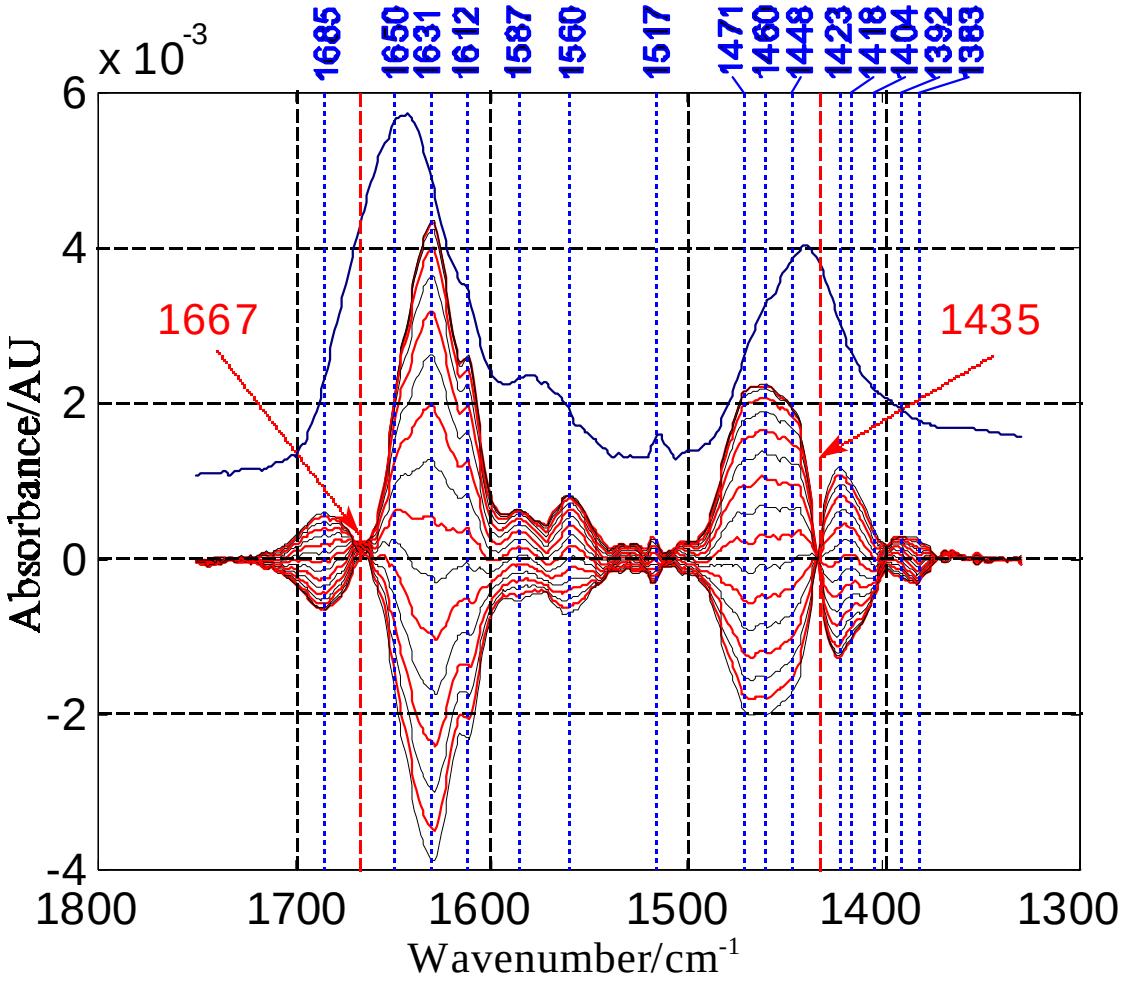

Fig. 34. Stationary (upper trace) and phase resolved (9°) FTIR ATR modulation spectra of temperature modulated excitation of RNAse A dissolved in D_2O buffer, pD 7. Mean temperature $\overline{T}$ = 64°C, modulation amplitude $\Delta T/2$ = 5°C. Note tyrosine response T-ME is selective, because the responding population absorbs at 2-3 cm^{-1} higher than the superposition of all tyrosines of RNAse. Secondary structural conversion results in isosbestic points in the amide I' and amide II' regions.

3.5 Conclusion

Fourier Transform Infrared Attenuated Total Reflection (FTIR ATR) spectroscopy provides an appropriate tool to investigate interactions between membrane proteins and lipid bilayers mimicking a biological membrane. Its great advantages are a high sensitivity even in aqueous systems and, using polarized light, the access to informations about the structural order within the membranes. Regardless whether the interactions between enzymes and lipid membranes are of electrostatic or hydrophobic nature, the results in this study show that it is possible to build up well defined and stable protein-lipid assemblies. The simultaneous application of FTIR ATR measurements with methods for determining the native enzymatic activity, combined with the powerful tool of time resolved modulated excitation (ME) spectroscopy, will surely give new insights into the mechanisms of interactions between different types of membrane proteins and their lipidic matrices.

4 Bibliography

[1] Tamm, L.K., and McConnell, H.M., *Biophys. J.* **47**, 105-113 (1985).
[2] Brian, A., and McConnell, H.M., *Proceedings of the National Academy of Sciences USA* **81**, 6159-6163 (1984).
[3] Fringeli, U.P. in Schlunegger, U.P. (Ed.), *Biologically Active Molecules*; Springer: Berlin, **1989**; pp. 241-252.
[4] Fringeli, U.P. in Mirabella, F.M. (Ed.), *Internal Reflection Spectroscopy, Theory and Applications*, Marcel Dekker **1992**, Chpt. 10, 255-324.
[5] Kalb, E., Frey, S., and Tamm, L., *Biochim. Biophys. Acta* **1103**, 307-316 (1992).
[6] Wenzl, P., Fringeli, M., Goette, J. and Fringeli, U.P., „Supported Phospholipid Bilayers Prepared by the 'LB/Vesicle Method': A Fourier Transform Infrared Attenuated Total Reflection Spectroscopic Study on Structure and Stability" *Langmuir* **10**, 4253-4264 (1994).
[7] Schöpflin, M., Perlia, X., and Fringeli, U.P., *J. Am. Chem. Soc.* **109**, 2375-2380 (1987).
[8] Jeannette Goette, ATR-IR-spektroskopische Untersuchungen der Lokalanästhetika-Modellmembran-Interaktion und dampfdruckosmometrische Bestimmung der Assoziation von Lokalanästhetika in wässriger Lösung. Zürich: PhD Thesis Nr. 9721, Swiss Federal Institute of Technology (ETH), 1992.
[9] Goette, J., Fahr, A., and Fringeli, U. P., *Langmuir*, in preparation.
[10] Fringeli, U.P., Apell, H.-J., Fringeli, M., and Läuger, P., *Biochim. Biophys. Acta* **984**, 301-312 (1989).
[11] Frey, S., and Tamm, L.K., *Biophys. J.* **60**, 922-930 (1991).
[12] Fringeli, U.P., and Fringeli, M., *Proc. Natl. Acad. Sci. USA* **76**, 3852-3856 (1979).
[13] Stephens, S.M., and Dluhy, R., *Thin Solid Films* **284-285**, 381-386 (1996).
[14] MacComb, R.B. Bowers, G.N. and Posen, S., *Alkaline Phosphatases*, New York: Plenum 1979.
[15] Coleman, J.E., and Gettins, P., *Adv. Enzymol.* **55**, 381-452 (1983).
[16] Fernley, H.N., in *The Enzymes*, Boyer, P.D. ed., 1971 pp., 417-447.
[17] Otvos, J.D., and Armitage, I.M., *Biochemistry* **19**, 4021-4030 (1980).
[18] Kim, E.E., and Wyckoff, H.W., *J. Mol. Biol.* **218**, 449-464 (1991).
[19] Gettins, P., and Coleman, J.E., *J. Biol. Chem.* **258**, 396-407 (1983).
[20]Gettins, P., and Coleman, J.E., *J. Biol. Chem.* **258**, 408-416 (1983).
[21] Coleman, J.E., in *Phosphate Mechanism and Cellular Regulation in Microorganisms*, Washington, DC: American Society for Microbiology, 1987, 127-138.
[22] Wong, P.T.T., and Armstrong, D.W., *Biochim. Biophys. Acta* **1159**, 237-242 (1992).
[23] Mersol, J.V., Steel, D.G., and Gafni, A., *Biophys. Chem.* **43**, 281-291 (1993).
[24] Culp, J.S., Hermodson, M., and Butler, L.G., *Biochim. Biophys. Acta* **831**, 330-334 (1985).
[25] Weissig, H., Schildge, A., Hoylaerts, M.F., Iqbal, M. and Millan, J.L., *Biochem. J.* **290**, 503-508 (1993).

[26] Kim, E.E., and Wyckoff, H.W., *Clin Chim. Acta* **186**, 175-188 (1989).
[27] Moss., D.W., *Clin. Chem.* **38**, 2486-2492 (1992).
[28] McConville, M.J., and Ferguson, M.A.J., *Biochem. J.* **294**, 305 (1993).
[29] Ferguson, M.A.J., *Curr. Op. Struct. Biol.* **1**, 522-529 (1991).
[30] Low, M.G., and Zilversmit, D.B., *Biochemistry* **19**, 3913-3918 (1980).
[31] Blobel, G., *Methods Enzymol* **96**, 663-682 (1983).
[32] Gerber, D.L., Kodukula, K., and Udenfriend, S., *J. Biol. Chem.* **267**, 12168-12173.
[33] Ferguson, M.A.J., and Williams, A.F., *Annu. Rev. Biochem.* **57**, 285-320 (1988).
[34] Low, M. G., *Biochim. Biophys. Acta* **988**, 427-454 (1989).
[35] Cross, G.A.M., *Annu. Rev. Cell. Biol.* **6**, 1-39 (1990).
[36] Udenfriend, S., Micanovic, R., and Kodukula, K., *Cell. Biol. Int. Rep.* **15**, 739-759 (1991).
[37] Bingham, E.W., and Edyth, L.M., *Comp. Biochem. Physiol.* **102**, 213-218 (1992).
[38] Malik, A.-S., and Low, M.G., *Biochem. J.* **240**, 519-527 (1986).
[39] Romero, G., *Cell. Biol. Int. Rep.* **15**, 827-851 (1991).
[40] Thomas, J.R., Dwek. R.A., and Rademacher, *Biochemistry* **29**, 5413-5422 (1990).
[41] Ferguson, M.A.J., *Biochem. Soc. Trans.* **20**, 243-256 (1992).
[42] Sanchez-Arias, J.A., Sanchez-Gutierrez, J.C., Guadano, A., Alvarez, J.F., Samper, B., Mato, J..M., and Feliu, J.E., *Endocrinology* **131**, 1727-1733 (1992).
[43] Zoppini, G., and Kahn, C.R., *Diabetologia* **35**, 109-115 (1992).
[44] Misek, D.E., and Saltiel, A.R., *J. Biol. Chem.* **267**, 16266-16273 (1992).
[45] Redman, C.A., Thomas-Oates, J.E., Ogata, S., Ikehara, Y., and Ferguson, M.A.J. *Biochem. J.* **302**, 861-865 (1994).
[46] Armesto, J., Hannappel, E., Leopold, K., Fischer, W., Bublitz, R., Langer, L., Cumme G.A., and Horn, A., *Eur. J. Biochem.* **238**, 259-269 (1996).
[47] Hoffmann-Blume, E., Garcia Marenco, M.B., Ehle, H., Bublitz, R. Schulze, M. and Horn, A., *Eur. J. Biochem.* **199**, 305-312 (1991).
[48] Sebesta, D.G., Bradshaw, F.J., and Prockop D.J., *Gastroenterology* **47**, 166-170 (1964).
[49] Kaplan, M.M., and Rigetti, A., *Biochim. Biophys. Acta* **184**, 667-669 (1969).
[50] Brydon, W.G., Crofton, P.M., Smith, A.F., Barr, D.G.D., and Harkness, R.A., *Biochem. Soc. Trans.* **3**, 927-929 (1975).
[51] Lange, P.H., Millan, J.L., Stigbrand, T., Vessella, R.L., Ruoslahti, E., and Fishman, W.H., *Cancer Res.* **42**, 3244-3247 (1982).
[52] Wallimann,T., Wyss, M., Bridiczka, D., Nicolay, K. and Eppenberger, H.M., *Biochem. J.* **281**, 21-40 (1992).
[53] Rojo, M., Hovius, R., Demel, R., and Wallimann T., *FEBS Letters* **281**, 123 (1991).
[54] Fritz-Wolf, K., Schnyder, Th., Wallimann, Th, and Kapsch, W., *Nature* **381**, 341-345 (1996).
[55] Stachowiak, O., Dolder, M., and Wallimann, Th., *Biochemistry*, **35**, 15522-15528 (1996).
[56] Siam, M., Reiter, G., Schwarzott, M., Baurecht, D., and Fringeli, U.P., *„Interaction of two different types of membrane proteins with model membranes investigated with*

FTIR-ATR spectroscopy“, presented at the 11th International Conference on Fourier Transform Spectroscopy (ICOFTS-11), Athens, Georgia, U.S.A., August 10-15, 1997.
[57] Siam, M., Stachowiak, O., Schlattner, U., Wallimann, Th., and Fringeli, U.P., in preparation.
[58] Miyazawa, T., Shimanouchi, T., and Mizushima, S., *J. Phys. Chem.* **29**, 611-616 (1958).
[59] Mendelsohn, R., and Mantsch, H.H. in Watts, A., de Pont, J.J.H.H.M. (Eds.), *Progress in Protein-Lipid Interactions*, Elsevier: Amsterdam **1986**, 103.
[60] Fringeli, U.P., *Simultaneous phase-sensitive digital detection process for time-resolved, quasi-simultaneously captured data arrays of a periodically stimulated system*, PCT international patent application, WO97/08598, 1997.
[61] Müller, M., Buchet, R., and Fringeli, U.P., *J. Phys. Chem.* **100**, 10810-10825 (1996).
[62] Reinstädler, D., Fabian, H., Backmann, J., and Naumann, D., *Biochemistry* **35**, 15822-15830 (1996).
[63] Bellamy, L.J., *The Infrared Spectra of Complex Molecules*, London: Methuen, 1975.
[64] Griffiths, P.R., *Chemical Infrared Fourier Transform Spectroscopy*, New York: John Wiley & Sons, 1975.
[65] Jakobsen, R.J., Wasacz, F.M., and Smith, K.B., *Chemical, Biological and Industrial Applications of Infrared Spectroscopy*, J.R. Durig ed., New York: John Wiley & Sons, 1985.
[66] Lieberman, R.A., and Wlodarczyk, M.T., *Chemical, Biochemical and Environmental Sensors*, SPIE, 1989, 1172 ff.
[67] Born, M., and Wolf, E., *Principles of Optics*, Oxford: Pergamon Press, 1983, 6th ed. Ch. 1, pp. 47-51.
[68] Harrick, N.J., *Internal Reflection Spectroscopy*, New York: Interscience Publisher, 1967.
[69] Fringeli, U.P., *Chimia* **46**, 200-214 (1992).
[70] Fringeli, U.P., and Günthard, Hs. H., *Biochim. Biophys. Acta* **450**, 101-106 (1976).
[71] Fringeli, U.P., and Günthard, Hs. H., „Infrared Membrane Spectroscopy“, in: „Membrane Spectroscopy“, E. Grell ed., Springer 1981, pp. 270-332.
[72] Fringeli, U.P., and Hofer, P., *Neurochemistry International* **2**, 185-192 (1980).
[73] Roberts, *Thin Isolating Films on Semi-Conductors*, Springer Heidelberg, 1981.
[74] Fringeli, U.P., Schadt, M., Rihak, P., and Günthard, Hs. H., *Z.Naturforsch*. **31a**, 1098-1107 (1976).
[75] Baurecht, D., Neuhäusser, W., and Fringeli, U.P., „Modification of Time-Resolved Step-Scan and Rapid-Scan FTIR Spectroscopy for Modulation Spectroscopy in the Frequency Range from Hz to kHz“, *AIP Conference Proceedings no. 430*, pp 367-370, ©1998.
[76] Forster, M., Loth, K., Andrist, M., Fringeli, U.P., and Günthard, Hs. H., *Chemical Physics* **17**, 59-85 (1976).

[77] Muriel, A., *Etude d'incorporation d'une protéine possédant un pied d'ancrage GPI dans des membranes biomimétiques. Exemple de la phospatase alcaline.* Thèse de 3eme cycle. Université Claude Bernard, Lyon I, 1997.
[78] Blodgett, K.B., and Langmuir, I., *Phys. Rev.* **51**, 964ff. (1937).
[79] Kuhn, H., Möbius, D., and Bücher, H. In *Techniques of Chemistry Vol. I, Part III,*. A. Weinberger and B. Rossiter eds, New York: John Wiley & Sons,1972,577 ff.
[80] Puu, G., Gustafson, I., Artursson, E., and Ohlsson, P.-Å., "Retained Activities of some Membrane Proteins in Stable Lipid Bilayers on a Solid Support", *Biosensors & Bioelectronics* **10**, 463-476 (1995).
[81] Ohlsson, P.-Å., Tjärnhage, T., Herbai, E., Löflås, S., and Puu, G., "Liposome and Proteoliposome Fusion onto Solid Substrates, Studied Using Atomic Force Microscopy, Quartz Crystal Microbalance and Surface Plasmon Resonance. Biological Actvities of Incorporated Components". *Bioelectrochemistry and Bioenergetics* **38**, 137-148 (1995).
[82] Sellström, Å., Gustafson, I., Ohlsson, P.-Å., Olofsson, G., and Puu, G., „On the Deposition of Phospholipids onto Planar Supports with the Langmuir-Blodgett Technique Using Factorial Experimental Design. 1. Screening of Various Factors and Supports." *Colloids and Surfaces* **64**, 275-287 (1992). 2. „Optimizing Lipid Composition for Maximal Adhesion to Platinum Substrates." *Colloids and Surfaces* **64**, 289-298 (1992).
[83] Garen, A., and Levinthal, C., *Biochim. Biophys. Acta* **38**, 470-483 (1960).
[84] Bradford, M.M., *Anal. Biochem.* **72**, 248-254 (1976).
[85] Read, S.M., and Northcote, D.H., *Anal. Biochem.* **116**, 53-64 (1981).
[86] Fringeli, U.P., „Distribution and Diffusion of Alamethicin in a Lecithin/Water Model Membrane System", *J. Membrane Biol.* **54**, 203-212 (1980).
[87] de La Fournière, L., Nosjean, O., Buchet, R., and Roux, B., *Biochim. Biophys. Acta* **1248**, 186-192 (1995).
[88] Müller, M., Buchet, R., and Fringeli, U.P., „2D-FTIR ATR Spectroscopy of Thermo-Induced Periodic Secondary Structural Changes of Poly-L-Lysine: A Cross-Correlation Analysis of Phase-Resolved Temperature Modulation Spectra." *J. Phys. Chem.* **100** (25), 10810-25 (1996).
[89] Seelig, J. and Seelig, A., *Quart. Rev. Biophysics*. **13**, 19-61 (1980).
[90] Ries, H.E., *Sci. Am.* **244**, 152 (1961).
[91] Casal, H.L. and Mantsch, H.H., *Biochim. Biophys. Acta* **779**, 381-401 (1984).
[92] Raimbault, C., Buchet, R. and Vial, C., *Eur. J. Biochem.* **240**, 134-142 (1996).
[93] Mantsch, H.H., and McElhaney, R.N., *Chem. Phys. Lipids* **57**, 213-226 (1991).
[94] RNAse A project: Collaboration with Dieter Naumann and Diane Reinstädler, Robert Koch Institut, Berlin, Germany.